

53

THE TRANSMISSION OF ELECTRONS BY GASES

HAMISH PORTER

THESIS SUBMITTED FOR THE DEGREE OF

DOCTOR OF PHILOSOPHY

UNIVERSITY OF STIRLING

APRIL, 1973

ELECTRON TRANSMISSION IN GASES

Abstract

This thesis is concerned with the measurement of total electron-atom and electron-molecule collision cross-sections and their interpretation, and the observation of fine structure in the transmitted current due to resonance processes.

The definitions of total cross-section and related observable parameters are discussed. We then review the methods that have been used to observe electron transmission in gases and the cross-sections that have been reported in the literature. The interpretation of the features of the total cross-section function is discussed in terms of theoretical models. We consider classical mechanical models, wave mechanical models, and correlations based upon the similarity of chemical structures. Fine structure is considered in terms of modern resonance theory.

From these considerations we outline the design requirements of an electron transmission spectrometer. A practicable design procedure using computer calculations of electron optical parameters is described. This is then used to construct a spectrometer which will operate in the electron energy range 2-100 eV with a nearly constant background current, and with an energy resolution of about 0.050 eV.

The operating characteristics of the apparatus are described and an investigation of helium reported. We

present total cross-section data for helium in the region 2-30 eV and compare them with published data. Our results, the first total cross-sections recorded in a non-magnetic electron spectrometer, deviate somewhat at higher energies from previously published cross-sections.

We also record the resonances at 19.3 eV in helium and 1.8-5.0 eV in nitrogen.

CONTENTS

	Page
I.	<u>THE QUANTITATIVE STUDY OF ELECTRON TRANSMISSION IN GASES</u>
I.1.	Introduction 1
I.2.	The quantitative study of the collisions of electrons with gases. 13
I.3	The observed total cross-section functions. 38
I.4	Theoretical models and the interpretation of the total cross-section functions. 52
	Classical models. 53
	Wave mechanical models. 62
	Resonance fine structure. 74
	Chemical models. 78
II.	<u>THE DESIGN OF AN ELECTRON TRANSMISSION SPECTROMETER</u>
II.1	Electron transmission spectrometry. 82
II.2	Electron optics design. 87
	Principles of electron optics. 87
	Phase space restrictions. 95
	Electron lens design. 101
II.3	The spectrometer design. 121
	The electron gun. 122
	The deceleration stage. 126
	The matching condenser lens. 128
	The monochromator. 130
	The beam forming lens. 133
II.4	Miscellaneous design details. 135
	Mechanical details. 135
	Electrical system. 137
	Vacuum system. 140
	Cancellation of the earth's magnetic field. 141

III. THE OPERATION OF THE ELECTRON TRANSMISSION SPECTROMETER

III.1	The operational characteristics of the spectrometer.	143
III.2	The transmission spectrum of helium.	146
III.3	The transmission spectrum of nitrogen.	148
III.4	Conclusions.	148

REFERENCES

CHAPTER I. THE QUANTITATIVE STUDY OF ELECTRON
TRANSMISSION IN GASES.

I.1 Introduction

Since the discovery of the electron at the end of the nineteenth century, the study of the collision of electrons with atoms and molecules has led to major developments in our understanding of the structure of these complex systems of particles. This thesis is concerned with an investigation of one particular experimental technique which permits an estimate to be made of the number of electrons in an electron beam, of varying mean energy, which are not scattered by gas atoms or molecules as the beam passes through the gas. This technique I have termed "Electron Transmission Spectrometry", but before considering the details of this technique we will first classify the various phenomena which can occur when electrons are scattered by atoms or molecules in a gas.

The scattering of electrons by other particles is dependant on a "collision" of some form having first occurred. The concept of a collision between particles of sub-atomic and atomic dimensions with their implied wave-particle dualities, mutually exclusive certainties in position and momentum and so on, is not as simple as it may at first seem in a mental "billiard ball" model. A satisfactory but rather general definition, sufficient for our present purposes, is: "An electron-atom or electron-molecule collision can be said to have taken place if any physical change can be detected in the system after the distance between the electron and the target particle has first decreased and then increased." Let

us consider these physical changes. The only physical change possible for the incident electron is a change in kinetic energy. For energy to be conserved this can only occur if the target particle either gains or loses energy in the collision. The target particle has internal structure, so the physical changes possible for it are much more varied. One possibility is that it can conserve its internal energy and change only its kinetic energy. This is called an ELASTIC COLLISION. The total fractional change in the kinetic energy of the incident electron can be shown classically to be $2m/M$, where m is the mass of the electron and M is the mass of the target. This fraction is approximately 1×10^{-4} for a simple molecular target. For many purposes, then, we can regard an electron scattered elastically as not having lost kinetic energy in the collision but merely having changed its direction of motion. Hence the term "elastic". The other possibility for the target particle is a change in internal energy. For an atom, this requires a transition from one electronic energy state to another, whereas for a molecule electronic, vibrational and rotational states are involved, and the number of possible excitation transitions is very much increased. If the target gains internal energy we have a COLLISION OF THE FIRST KIND or INELASTIC COLLISION; and if it gives up internal energy to the kinetic energy of the incident electron we have a COLLISION OF THE SECOND KIND or SUPER-ELASTIC COLLISION. The third kind of collision involving a change in internal energy is an IONISING COLLISION and here the target has a net gain, or loss, of bound electrons after the collision. If one electron is gained, the maximum observed, the target becomes a NEGATIVE ION, and if one or more electrons are lost it becomes a POSITIVE ION.

For any particular value of the incident electron kinetic energy, each of these possible processes has a finite probability of

occurring. Which process we observe at any particular energy will depend upon their relative probabilities. The probability of any particular physical change will thus be a function of the incident electron kinetic energy.

Having introduced probabilities, our discussion of collision can now become quantitative. We define the probability of scattering, S , as the number of electrons scattered (ie. having undergone a collision as previously defined), per unit incident electron current, per unit path length, per unit gas pressure at some specified temperature, per unit solid angle in the polar direction, θ , with respect to the original beam. This probability of scattering can be further divided into: probability of elastic scattering, S_E ; probability of inelastic scattering, S_1 ; probability of superelastic scattering, S_2 ; probability of ionising scattering, S_I . The probability of inelastic scattering must be specified as the probability of excitation to a particular energy state; and the probability of ionisation must specify the nature of the ion. The probability of collision, P_c , is related to the scattering probability, S , by the following equation:

$$P_c = \int_{\delta}^{\pi} S_E \cdot 2\pi \cdot \sin \theta \cdot d\theta + \int_0^{\pi} (S_1 + S_2 + S_I) \cdot 2\pi \sin \theta d\theta \quad (\text{I.1.1})$$

The meaning of delta, δ , as a limit of integration will be considered when we have completed the definitions. The probability of excitation, P_x , is related to the probability of scattering inelastically by:

$$P_x = \int_0^{\pi} S_1 \cdot 2\pi \cdot \sin \theta \cdot d\theta \quad (\text{I.1.2})$$

and the probability of ionisation, P_I , is:

$$P_I = \int_0^{\pi} S_I \cdot 2\pi \cdot \sin \theta \cdot d\theta \quad (\text{I.1.3})$$

The lower limit of the first integral in equation (I.1.1) cannot be zero as then the incident beam of electrons which have passed through

the gas without collision would be included with those which have collided and P_c , the probability of a collision, would be unity! Theoretically this difficulty is rationalised by the fact that as the polar angle, θ , approaches zero, so too does $S_E \sin\theta$ and so the value of the integral can be extrapolated, as $\delta \rightarrow 0$, without including the original beam.

The probability of a collision by an electron in a beam travelling a distance, dx , in a gas at a pressure, p , is $P_c \cdot p \cdot dx$. Thus a current of electrons of initial strength, I , passing through the layer, dx , is decreased by dI , where,

$$dI = -I \cdot P_c \cdot dx. \quad (\text{I.1.4})$$

If we now integrate this expression over a finite distance x with a finite change in electron current of $(I_0 - I)$, where I_0 is the initial current and I is the current after the beam has travelled a distance x in the gas, we get an expression:

$$\int_{I_0}^I (dI/I) = -P_c \cdot p \cdot \int_0^x dx \quad (\text{I.1.5})$$

which on integration gives,

$$\ln(I/I_0) = -P_c \cdot p \cdot x \quad (\text{I.1.6})$$

or,

$$I = I_0 \cdot \exp(-P_c \cdot p \cdot x) \quad (\text{I.1.7})$$

The average distance that an electron travels in a gas before a collision involving it occurs is called the mean free path, λ , and is defined by:

$$p \cdot \lambda = 1/P_c \quad (\text{I.1.8})$$

The dimensions of P_c are $[L]^{-1} \cdot [p]^{-1}$ or $[L]^2 \cdot [L]^{-3} \cdot [p]^{-1}$ i.e. area, per unit volume, per unit pressure. P_c can therefore be considered as the effective area for collision of all the atoms in a unit volume, at unit pressure. In equation (I.1.7) the probability of

collision occurs in exactly the same way that an absorption coefficient occurs in the decrease in intensity of X-rays or of light in passing through matter. One of the first investigators in this topic P. Lenard (1903) called the coefficient, P_c , the "absorbing power" and many later investigators have used the terms absorption coefficient or attenuation coefficient, where this coefficient, α , is defined by the equation:

$$I = I_0 \cdot \exp(-\alpha \cdot x) \quad (\text{I.1.9})$$

However, electrons are for the most part scattered, so true absorption or attachment is a process seldom observed. To avoid this Darrow, in 1932, suggested the term "likelihood of interception", in place of absorption coefficient. (K.K. Darrow, 1932). In order to discuss the probability of a particular atom undergoing collision, the term "effective cross-section for collision" was used by many European workers. The effective area or cross-section of a single atom, Q , (from the German word for cross-section, Querschnitt) can be expressed as the probability of collision, divided by the number of gas particles per unit volume, per unit pressure (Loschmidt's number). If the unit of pressure is one Torr (1 mm. Hg at 0 °C) and the unit of volume is 1 cm³ then,

$$Q = 0.281 \times 10^{-16} P_c \text{ [cm}^2\text{]} \quad (\text{I.1.10})$$

The effective radius, r , of an atom with an effective cross-section Q , is,

$$r = (Q/\pi)^{\frac{1}{2}} = 0.3(P_c)^{\frac{1}{2}} \times 10^8 \text{ [cm]} \quad (\text{I.1.11})$$

but most authors use the cross-section rather than the effective radius in their publications.

Comparison of this cross-section with the gas kinetic cross-section, calculated from the mean radius of the atom or molecule obtained from diffusion, or similar, experiments was very popular at

one time. One way in which this was done was to plot the ratio of the probability of collision, P_c , to the reference probability, calculated from gas kinetic considerations, P_{KT} , versus the electron energy. Not surprisingly, this ratio was very different from unity. A parameter, which is very convenient in practice is the "target parameter", π , where:

$$\pi = nx = px/kT \quad (\text{I.1.12})$$

and n , is the gas number density; p , the gas pressure; k , the Boltzman constant and T , the absolute temperature.

Nowadays, only the term cross-section is used. The TOTAL CROSS-SECTION, Q_T , is composed of the cross-sections for all possible processes.

$$Q_T = Q_0 + \sum_{N=1}^N Q_N + \sum_{I=1}^I Q_I \quad (\text{I.1.13})$$

where Q_0 is the cross-section for elastic scattering,

Q_N is the inelastic cross-section for the inelastic process N .

Q_I is the ionisation cross-section for the ionising process I .

The concept of a differential cross-section is found to be very useful in the comparison of experimental results and theoretical models. The DIFFERENTIAL CROSS-SECTION for a particular process is the cross-section for an electron being scattered into a solid angle $d\Omega$ after undergoing this process. If θ is the polar angle and ϕ , the azimuthal angle, then $d\Omega$, the solid angle, is $\sin \theta \cdot d\theta \cdot d\phi$.

Thus, any cross-section, Q , can be expressed in terms of its differential cross-section, $\sigma(\theta)$, as follows,

$$Q = \int_0^\pi \int_0^{2\pi} \sigma(\theta) \cdot \sin \theta \cdot d\theta \cdot d\phi \quad (\text{I.1.14})$$

In theory, we can design experiments to measure any of these cross-sections such as the differential elastic cross-section, total

inelastic cross-section and so on.

Our concern, in this thesis, is the measurement of the total cross-section, Q_T . In terms of electron currents, as already defined, we can write,

$$I = I_0 \cdot \exp(-n \cdot Q_T \cdot x) \quad (\text{I.1.15})$$

where n is the number density of the gas.

We can now devise an experimental method to measure Q_T . The basic requirements will be: a source of electrons; some system to form these electrons into a beam of the required current density and energy; a gas cell to contain the gas at the required pressure, with an entrance aperture large enough to allow the electron beam to enter but not large enough to let a significant proportion of the gas escape, and an exit aperture large to allow the unscattered beam to leave the cell but small enough to limit the escape of electrons which have been scattered at small angles and which if allowed to leave the cell would be mistaken for unscattered electrons; and an electron collector to record the transmitted beam current. It must be pointed out that electrons scattered inelastically at zero degrees to the beam path will always be included with the unscattered electrons in this type of experiment. The distance between the entrance and exit apertures of the gas cell we will regard, at the moment, as the path length, x , defined in equation (I.1.15).

This defines, to a first order, what is meant by "Electron Transmission Spectrometry". An electron transmission spectrum is a graph of the total cross-section (derived from equation I.1.15) versus the mean energy of the electron beam. As the beam energy is varied and different scattering processes occur, such as elastic, inelastic, superelastic and ionising collisions, the transmission of the gas will decrease indicating an increase in scattering.

Electron transmission spectrometry is not the only technique that can be used to measure total electron-atom or electron-molecule collision cross-sections. We shall treat these other techniques in detail later in this chapter. At this stage, however, we must introduce another cross-section which is closely related to the total cross-section, and therefore useful for comparison purposes. This is the MOMENTUM TRANSFER or DIFFUSION CROSS-SECTION. We stated earlier, without proof, that the total fractional kinetic energy change of an electron undergoing an elastic collision was approximately $2m/M$ where m , is the mass of the electron and M , is the mass of the target particle. Using the same classical model we find that the fractional kinetic energy loss, per electron scattered through a polar angle θ , is approximately $2m(1 - \cos \theta)/M$. Now, if $P(\theta)\sin \theta.d\theta.d\phi$ is the probability that the electron is scattered into the solid angle of Ω about the polar angle, θ , the mean fractional kinetic energy loss per collision will be

$$2(m/M) \int_0^\pi \int_0^{2\pi} (1 - \cos \theta).P(\theta).\sin \theta.d\theta.d\phi \quad (\text{I.1.16})$$

If we compare this equation with equation (I.1.14) we can define the momentum transfer cross-section by this equation:

$$Q_m = \int_0^\pi \int_0^{2\pi} \sigma(\theta).(1 - \cos \theta).\sin \theta.d\theta.d\phi \quad (\text{I.1.17})$$

In this cross section, forward scattering is weighted most heavily. A similar cross-section is the viscosity cross-section, Q_η , but it is very seldom encountered in the literature. It is defined by this equation:

$$Q_\eta = 2\pi \int_0^\pi \sigma(\theta)\sin^3 \theta.d\theta \quad (\text{I.1.18})$$

Here the scattering perpendicular to the beam path is weighted most heavily.

If the scattering is isotropic, ie. $\sigma(\theta)$ is not a function of θ , the total and momentum cross-sections become the same, as follows:

$$\begin{aligned} \text{from (I.1.14),} \\ Q_T &= \sigma \int_0^\pi \sin\theta \cdot d\theta \cdot \int_0^{2\pi} d\phi \\ &= 4\pi \cdot \sigma \end{aligned} \quad (\text{I.1.19})$$

$$\begin{aligned} \text{from (I.1.17),} \\ Q_m &= \sigma \int_0^\pi (\sin\theta - \sin\theta \cdot \cos\theta) d\theta \int_0^{2\pi} d\phi \\ &= 4\pi \cdot \sigma \end{aligned} \quad (\text{I.1.20})$$

If the scattering is anisotropic, the total and momentum transfer cross-sections are related by the expression for the mean fractional energy loss per collision, $\overline{\Delta E}/E$:

$$(\overline{\Delta E}/E) = (2m/M)(Q_m/Q_T)$$

Cross-sections are expressed in units of $[\text{cm}]^2$ $[\text{atom or molecule}]^{-1}$, or as multiples of $\pi a_0^2 [\text{cm}]^2$, where a_0 is the radius of the first Bohr orbit of the hydrogen atom; absorption coefficients in units of $[\text{cm}]^2 [\text{cm}]^{-3} [\text{Torr}]^{-1}$; and, probabilities of collision in units of $[\text{cm}]^{-1} [\text{Torr}]^{-1}$.

We have only made two assumptions in our discussion so far, and these we can justify by considering a simple classical model. We consider both the incident electron and the target molecule to be impenetrable elastic spheres ("billiard balls"). This model is limited, but does represent reasonably well the exponential short-range repulsion of a low energy ("slow") electron and a spherically-symmetric atom. To justify this statement Figure 1a. shows the

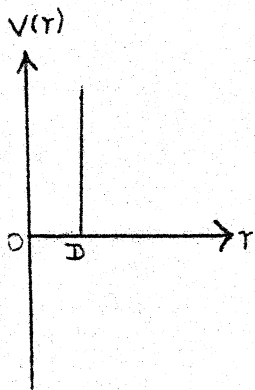


FIGURE 1a.
Hard Sphere Potential.

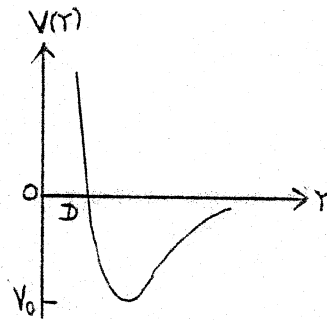


FIGURE 1b.
Lennard-Jones Potential.

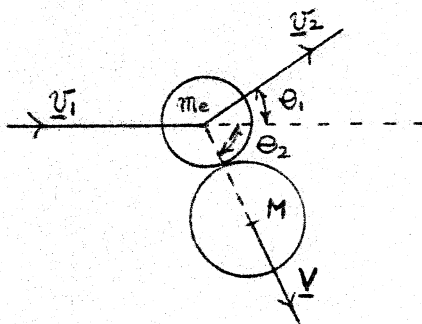


FIGURE 2.

COLLISION OF ELASTIC SPHERES

potential function for smooth elastic spheres and Figure 1b. shows the Lennard-Jones potential which is accepted as a reasonable approximation to the spherically-symmetric potential function of an atom. We further assume that, in a laboratory system of coordinates, we can regard the target as stationary before collision with respect to the electron. Some figures will justify this assumption. A ten electron-volt electron has a speed of 1.9×10^8 cm.sec.⁻¹, and the root mean square velocity of the hydrogen molecule at room temperature is approximately 2×10^5 cm.sec.⁻¹ ie. a ratio of 10^3 . A two dimensional representation of a collision in this model is shown in Figure 2.

Let,

v_1 = incident electron velocity before collision.

v_2 = incident electron velocity after collision.

V = velocity of the target after the collision.

m_e = mass of the electron.

M = mass of the target.

E = kinetic energy of the incident electron.

The fractional kinetic energy loss of the incident electron is,

$$(\Delta E/E) = (\frac{1}{2} m_e v_1^2 - \frac{1}{2} m_e v_2^2) / \frac{1}{2} m_e v_1^2 \quad (\text{I.1.21})$$

$$\text{where } E = \frac{1}{2} m_e v_1^2$$

In this model the target has no internal structure, so we can rewrite equation (I.1.21) as,

$$(\Delta E/E) = \frac{1}{2} M V^2 / \frac{1}{2} m_e v_1^2 \quad (\text{I.1.22})$$

From the conservation of kinetic energy,

$$\frac{1}{2} m_e v_1^2 = \frac{1}{2} m_e v_2^2 + \frac{1}{2} M V^2 \quad (\text{I.1.23})$$

and from the conservation of linear momentum,

$$m_e v_1 = m_e v_2 \cos \theta_1 + MV \cos \theta_2 \quad (\text{I.1.24})$$

in the direction of the beam trajectory, and

$$0 = m_e v_2 \sin \theta_1 - MV \sin \theta_2 \quad (\text{I.1.25})$$

perpendicular to the direction of the beam trajectory.

Solving for V, we get:

$$V = 2v_1 (m_e / m + M) \cos \theta_2 \quad (\text{I.1.26})$$

and so,

$$(\Delta E/E) = ((4m_e M / (m_e + M)^2) \cos^2 \theta_2) \quad (\text{I.1.27})$$

The average fractional energy loss, $(\overline{\Delta E}/E)$ will be given by,

$$(\overline{\Delta E}/E) = \int_0^{\pi} ((4m_e M) / (m_e + M)^2) \cos^2 \theta_2 \cdot P(\theta_2) \cdot d\theta_2 \quad (\text{I.1.28})$$

where $P(\theta_2) \cdot d\theta_2$ is the probability that θ_2 lies between θ_2 and $\theta_2 + d\theta_2$.

From simple geometrical considerations,

$$P(\theta_2) \cdot d(\theta_2) = \begin{cases} \sin 2\theta_2 d\theta_2 & (0 \leq \theta_2 \leq \pi/2) \\ 0 & (\pi/2 < \theta_2 \leq \pi) \end{cases} \quad (\text{I.1.29})$$

Thus,

$$\begin{aligned} (\overline{\Delta E}/E) &= ((4m_e \cdot M) / (m_e + M)^2) \int_0^{\pi/2} \cos^2 \theta_2 \cdot \sin 2\theta_2 \cdot d\theta_2 \\ &= ((4m_e \cdot M) / (m_e + M)^2) \int_0^{\pi/2} -2 \cos^3 \theta_2 \cdot d \cos \theta_2 \\ &= ((2m_e \cdot M) / (m_e + M)^2) \cdot \end{aligned} \quad (\text{I.1.30})$$

Considering the relative masses of an electron and a molecule, we can let $(m_e + M) \simeq M$ and so,

$$(\overline{\Delta E}/E) \simeq 2 \cdot (m_e / M) \quad (\text{I.1.31})$$

As $\theta_2 = (\pi/2) - (\theta_1/2)$, then:

$$V \simeq (2 m_e/M) \cdot v_1 \cdot \cos\theta_2, \quad (\text{I.1.32})$$

and,

$$(\Delta E/E) (\theta_1) \simeq (2m_e/M) \cdot (1 - \cos\theta_1). \quad (\text{I.1.33})$$

Equations (I.1.31) and (I.1.33) justify our approximations. It is worth noting that, in this model, backward scattering (θ_1 or $\theta_2 > (\pi/2)$) has zero probability.

We shall firstly consider the techniques that have been employed to observe the variations of total cross-sections and, where appropriate, some related cross-sections. Then review the total cross-sections that have been reported in the literature and, finally, consider some of the simpler theoretical models that are of use in interpreting the cross-section functions.

I.2 The Quantitative Study of the Collisions of Electrons with Gases.

The first quantitative study of the interaction of electrons with gases was that of Lenard, in 1903, who measured the absorbing power of some gases and solids. The gases which he studied were helium, argon, molecular hydrogen and carbon dioxide. He concluded that the absorption at higher incident electron velocities was proportional to the gas density; and, as the velocity was reduced, the absorption increased reaching a constant value at zero velocity. This constant value was found to have good agreement with that expected from gas kinetic considerations. He also noted an absorption maximum at lower electron energies (< 80 eV) in argon. Earlier, in 1895, he suggested, from the results of preliminary experiments, that the effective cross-section for the collision of molecules with high energy electrons (> 100 eV) was proportional to the sum of the cross-sections of all the atoms in the molecule.

Lenard's apparatus is shown diagrammatically in figure 3. The electrons coming from a photocathode of zinc, Z, are accelerated by a grid, G1, and then drift through field-free space to another grid, G2, at the same potential as G1. The aperture, A, permits some of the electrons to pass through to the Faraday cup collector, C. The current flowing from the cathode to the collector is measured by a

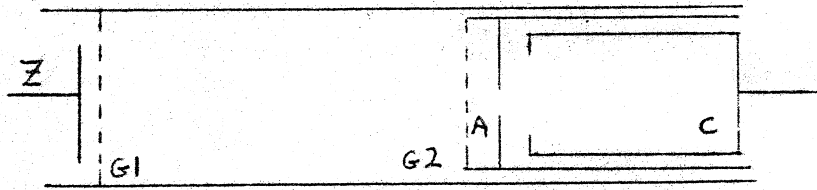


FIGURE 3. Lenard's Apparatus.

FIGURE 4a.
Ramsauer's
Apparatus.

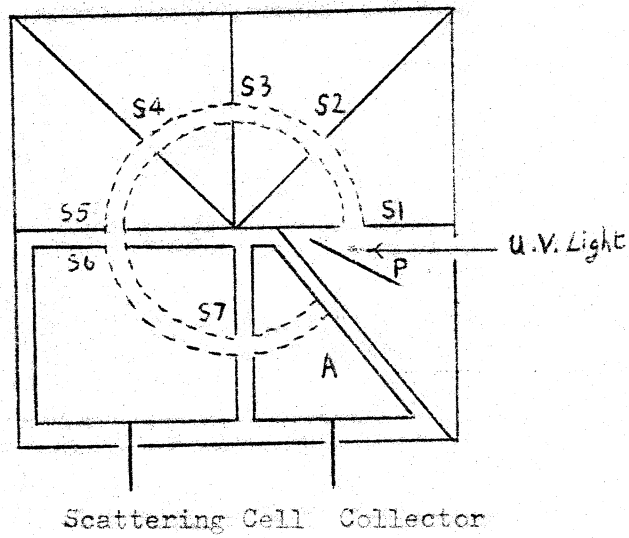


FIGURE 4b.

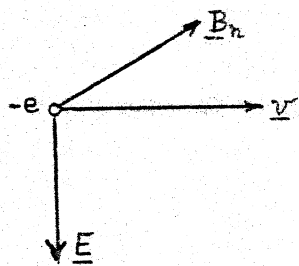
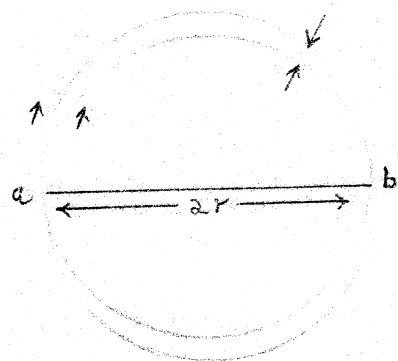


FIGURE 4c.



Focussing in a plane perpendicular
to the magnetic field vector.

galvanometer. If the total cathode current, i , and the collected current, C , are recorded at a residual gas pressure, p_0 , and then at a sample gas pressure of p_1 , the probability of collision, P_c , will be given by;

$$P_c = [(p_1 - p_0)/x] \cdot [\log(i_0/c_0) - \log(i_1/c_1)] \quad (I.2.1)$$

where x is the path length defined in the figure. From this equation we can see that if the electron current to the collector decreases then the observed probability of collision will increase. The aperture, A , is considerably larger than the beam diameter, so some electrons that have been scattered will be collected with the unscattered electron beam. This will add a collector resolution background to the observed probability. Now, the electrons in a beam repel each other causing the beam diameter to increase. This phenomenon is called "space charge spreading". In general, the lower the mean energy of a beam (hence the lower the electron velocity), the greater the amount of space charge spreading. This could well account for the increase in scattered current at low energies. This we will call an electron optical background, for reasons which will be discussed later. His interpretation of the higher energy cross-sections, by summing the constituent atomic cross-sections to give a molecular cross-section, was coincidental. Later data does not support this interpretation; but does show that above about 50 eV the cross-section is roughly proportional to the atomic or molecular weight of the gas. It is not difficult to imagine that with limited, inaccurate data this could be confused with Lenard's theory. The maximum in argon does exist, but it is doubted

whether Lenard really observed this, as his value for the energy of this feature is in error with accepted data, by about seventy volts! Even the limited equipment available for measuring voltage at that time could not account for this discrepancy.

I have dealt in detail with Lenard's two papers for two reasons. Firstly, they were the initial, pioneering investigations in this topic and showed that the amount of scattering depended upon the nature and pressure of the gas. Secondly, Lenard's apparatus can be regarded as the basic practical electron transmission spectrometer, and the interpretation of its failings can help us to develop design criteria for improved versions.

Lenard's results were confirmed in 1905 by Becker and in 1910 by Silbermann. Only six years later Akesson, with an almost identical apparatus, observed a very much different set of curves. (Akesson, 1916). The word "curve" can be somewhat misleading, as all results produced before second world war technology involved the plotting of individual points and the curves being drawn by interpolation. Modern data either involves recording enough data points to give a continuous line without interpolation, or the use of a recorder to draw a continuous data line. To emphasise this point, Lenard's published curve for argon is based upon eight data points between zero and three thousand volts. Akesson found that the probability of collision did not increase uniformly to a limit at low velocities. He observed distinct maxima and minima in the cross-section function. He achieved this by plotting the ratio of collected current to total cathode current versus

electron energy. If Akesson had recorded background spectra in the absence of gas, he could have calculated the probability of collision. He studied methane, propylene, carbon monoxide, carbon dioxide, nitrous oxide, nitrogen, oxygen, air and water. In nearly all these gases, the maxima observed have been confirmed by later experiments, although the energy calibration has had to be changed. In particular, the 3 eV maximum in nitrogen and the 7 eV maximum in methane have been confirmed and in these examples the energy calibration was good. He also produced the first evidence of a phenomenon which was to lead to considerable investigation at a later stage. This was the low energy transparency to electrons of certain gases; in his words: "the slower electrons were more penetrating than the faster". H.F. Mayer at the Radiological Institute at Heidelberg repeated these experiments and got results that agreed with Lenard rather than Akesson (Mayer, 1921). The only basic difference between Mayer's apparatus and that of Lenard was the introduction of a heated filament instead of a photocathode.

A colleague of Mayer, Carl Ramsauer, who was working in the same laboratory on the investigation of the velocity distribution of photoelectrons emitted by a zinc surface, decided to check Mayer's results employing the apparatus he had designed for his photoelectron studies (Ramsauer, 1914). This apparatus consists of a photocathode as a source of electrons; and a magnetic field which focusses the electrons into two circular paths, where the beams are collimated by a series of slits. The two beams then pass through two scattering cells to be collected by two Faraday

cups. He added gases (He, Ar, H₂, N₂ and air) to this system and performed attenuation measurements. (Ramsauer, 1921a). He only measured energies close to one electron volt. We will take argon, as an example, to show the nature of his results. He found the remarkably small values of $P_c = 2.6$ for 0.75 eV electrons and $P_c = 5.5$ for 1.1 eV electrons. These results caused Mayer to check his results and this time he confirmed the results of Ramsauer and Akesson. Mayer also noted a maximum of $P_c = 73$ at 12 eV in argon. These results are substantially those accepted nowadays. The extremely small probability of collision for electrons less than one electron volt, which Ramsauer found in argon (and later in krypton and xenon) is known as the Ramsauer effect.

The success of this experiment led Ramsauer to devise an improved apparatus which was to become one of the classic experiments in atomic physics. (Ramsauer, 1921b). With this apparatus, between 1921 and 1930, he measured the total cross-sections of many atomic and simple molecular systems. Several other researchers copied this design, making only minor alterations. The main research schools based on this technique were those of E. Brüche, a physical chemist at Danzig, and of R.B. Brode at the University of California. The literature shows that approximately 85% of all presently available total cross-sections were measured by this technique.

Ramsauer's first apparatus did not produce electron beams of variable energy. Only two energies, 0.75 eV and 1.1 eV were possible. He decided that this had to be changed to give beams of variable energy, and that two

electron beams were unnecessary. The magnetic field, perpendicular to the beam path, was kept as it provided energy selection for the incident beam and the scattered electrons. A diagram of the apparatus is shown in figure 4a.

Now, electrons moving at right angles to a constant magnetic field describe a circle. If \underline{B} is the magnetic induction vector of the magnetic field, and \underline{v} is the velocity vector of the electrons; then, the force of deflection on the electrons is \underline{F} , where:

$$\underline{F} = -e \cdot \underline{v} \wedge \underline{B} \quad (\text{I.2.2})$$

The direction of the vector is shown in figure 4b. As the electron moves, the force will remain constant but change in direction. The force and velocity vectors must remain mutually perpendicular to the magnetic field vector. Thus the electron motion is circular with the force vector acting radially and the velocity vector acting tangentially. Figure 4c shows this result for electrons starting at the same point but with different starting angles. It can be shown (Pierce, 1954) that if V is the voltage of the apparatus with respect to the cathode, the radius of the circular trajectory is,

$$r = (3.37 \times 10^{-6}) \cdot V^{1/2} / B \quad [\text{metres}] \quad (\text{I.2.3})$$

If we now consider the apparatus again we can see how this principle is applied. The electrons leave the photocathode, P, with different angles, are accelerated to voltage V and then describe the circle defined in equation (I.2.3), through the slits S_1 to S_5 with the beam being

energy-selected by the width of the slits. This energy selecting action is shown by noting that equation (I.2.3) defines different circles for different initial electron velocities and directions. The radius in Ramsauer's apparatus was 10 mm. and the slit widths were 1 mm. The beam then enters the 90° scattering chamber through slit S₆ and leaves through S₇ to be collected in the Faraday cup, A. Electrons scattered elastically or inelastically will change their velocity (either in magnitude or direction) and so depart from the mean apparatus circle and therefore not reach the collector. This gives reasonably good post-collision angular resolution. I can find no detailed analysis of this resolution in the literature.

The experimental procedure is as follows. The whole apparatus is set at V volts, in a magnetic field of B webers, and a sample gas introduced at a pressure p₁ torr. The current, i₁, to the collector alone and the current, j₁, to the scattering cell and collector together are measured with an electrometer. The scattering path length, x, is taken as the distance between S₆ and S₇, and is given by:

$$x = \frac{1}{2} \cdot \pi \cdot r \quad (\text{I.2.4})$$

where r is given by substituting for V and B in (I.2.3). From equation (I.1.9);

$$i_1 = j_1 \cdot e^{-p_1 \cdot \alpha \cdot x} \quad (\text{I.2.5})$$

If we now repeat this experiment with the same voltage and magnetic field and a different gas pressure, p₂ torr, we get a similar expression;

$$i_2 = j_2 \cdot e^{-p_2 \cdot \alpha \cdot x} \quad (\text{I.2.6})$$

Subtracting (I.2.5) and (I.2.6);

$$(P_1 - P_2) = \ln(j_1 \cdot i_2 / j_2 \cdot i_1) / \alpha \cdot x \quad (\text{I.2.7})$$

The total cross-section, Q_T , can now be calculated from the attenuation coefficient, α ;

$$Q_T = \alpha/n = 2.8 \times 10^{-17} \cdot \alpha/p \quad [\text{cm}^2] \quad (\text{I.2.8})$$

where n is the gas number density and p is the pressure.

The energy, E , of a monochromatic electron beam moving in a circle of fixed radius, R , in a uniform magnetic field, B , is given by,

$$E = (B \cdot e \cdot R)^2 / 2m \quad (\text{I.2.9})$$

So,

$$\Delta E \simeq (B \cdot e)^2 \cdot 2R \cdot \Delta R / 2m \quad (\text{I.2.10})$$

and from these two equations,

$$\Delta E/E \simeq 2 \cdot (\Delta R/R) \quad (\text{I.2.11})$$

where ΔE is the energy spread (base full width) of the beam, $\Delta E/E$ is the energy resolution of the magnetic selector and ΔR is the slit width. For Ramsauer's apparatus, $R = 10$ mm. and $\Delta R = 1$ mm and so the energy resolution is approximately 20% ie. approximately 0.2 eV full width at half maximum for a 2.0 eV beam. For sufficiently large values of E , the energy spread, ΔE , will become independent of E as the value of ΔE which slits will accept will be larger than the energy spread leaving the cathode. If, in equation (I.2.9) we substitute for R from equation (I.2.3) we find that the energy of the electron beam is a function of the applied voltage and the magnetic field.

FIGURE 5.

Brode's Apparatus.

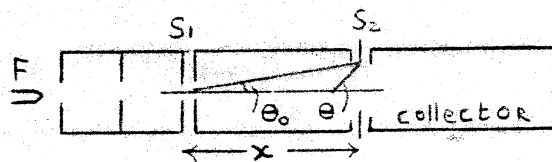
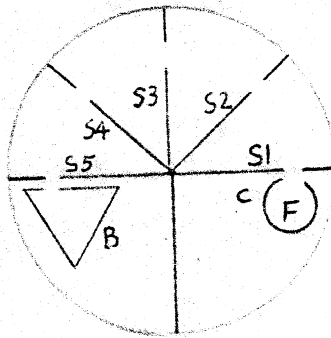
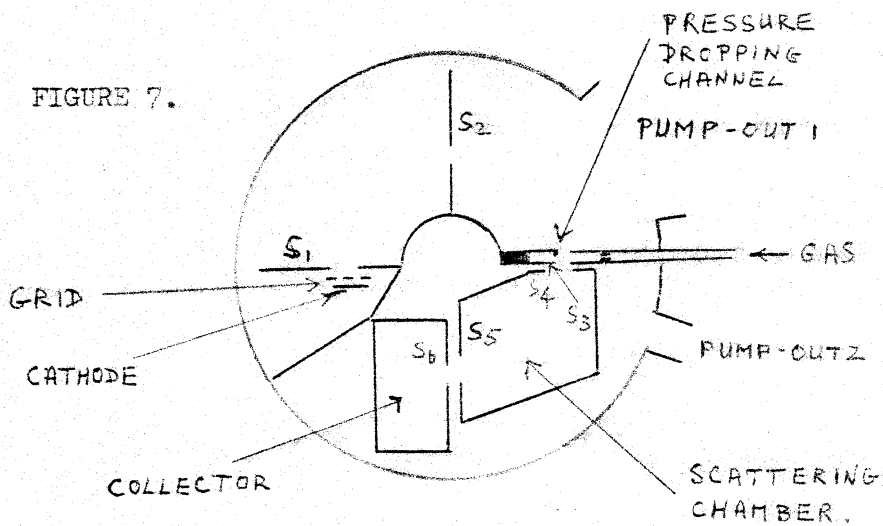


FIGURE 6.

Palmer's Apparatus.

(Magnetic field vector perpendicular to plane of paper).

FIGURE 7.



Golden's apparatus. (Magnetic field vector perpendicular to plane of paper.)

The Ramsauer type of experiment requires a lot of work to get one point on the total cross-section versus electron energy curve. One major drawback is that gas is everywhere in the apparatus and this must mean that the electron energy distribution from the cathode is a function of gas pressure.

Brode adapted this apparatus design in order to measure cross-sections for metal vapours. The Brode apparatus uses no separate energy selector, instead the scattering cage occupies 180° of the electron trajectory and so serves as the energy selector. (Brode, 1929). A diagram of this apparatus is shown in figure 5. Electrons from the thermionic filament, F, are accelerated to the cylinder, C, and some of these electrons go through the slit S_c . The electrons are then deflected by the magnetic field through slits S_1 to S_5 , then into the collector B. The initial current, I_0 , is assumed to be proportional to the current leaving the slit S_c . If the constant of proportionality is k , then the equation for attenuation is:

$$I = k \cdot I_0 \cdot e^{-P_c \cdot x \cdot p} \quad (\text{I.2.12})$$

where x is the path length; and, in this case $x = \pi r$, where r is the radius of curvature of the beam, I is the collector current and p is the gas pressure. We can rewrite equation (I.2.12) as,

$$\log (I/I_0) + \log k = P_c \cdot x \cdot p \quad (\text{I.2.13})$$

So a plot of $\log (I/I_0)$ as a function of the path length, x , times the pressure, p , will give a straight line of slope, P_c . The pressure of the metal vapour can be varied by changing the temperature of the apparatus. (Brode, 1930).

The value of the cross-section in these experiments is influenced by the size of the defining apertures. This effect was first investigated by Green (1930) who found no variation but, later, Palmer (1931) showed that Green's results were unreliable. Figure 6 shows Palmer's apparatus. The distance between S_1 and S_2 is x , the path length. The radius of the circular aperture, S_2 , is a . The limiting angle for a deflection along the axis is given by $\tan \theta = a/x$. If I_0 is the current entering S_1 , I is the current entering S_2 and $\Delta I = I_0 - I$, then at low pressures;

$$P'_c \cdot x \cdot p = \Delta I / I_0 \quad (\text{I.2.14})$$

where P'_c is the observed probability of collision.

The number of electrons scattered to the collector is,

$$\Delta I = I_0 \int_{\theta_0}^{\pi} 2\pi \cdot (x - a/\tan\theta) \cdot S \cdot \sin\theta \cdot d\theta - x \cdot E_i \quad (\text{I.2.15})$$

where S is the probability of scattering, defined in the introduction, and $(-xE_i)$ is the contribution of positive ions formed in the gas and assumes that the number of positive ions leaving the scattering chamber for the collector is the same as the number of positive ions leaving the collector for the scattering chamber. However, this will not be true if there is a retarding potential between collector and chamber. It is found that P'_c is a function of θ_0 (which, as is seen in figure 6 is proportional to the size of the slit in S_2). He observed that as θ_0 goes from 2° to 10° the probability of collision, as observed, is doubled.

A modern version of the "Ramsauer" apparatus is that of D.E. Golden at Lockheed Research Laboratories, California. (Golden and Bandel, 1965a). The apparatus is

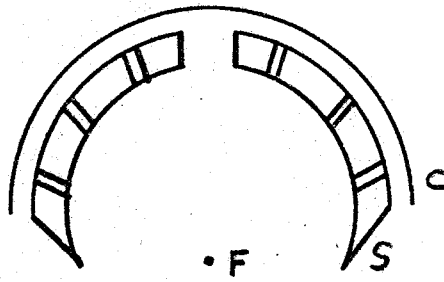
shown in figure 7. It has a high vacuum system, capable of 10^{-9} torr, after baking; is of all-metal construction and metal surfaces seen by the electron beam are coated with colloidal graphite to reduce the contact potential differences experienced by the beam. (Parker and Warren, 1962). The electrons, from an indirectly heated cathode, at a potential negative with respect to earth, are accelerated through a control grid to a slit S_1 which, like the rest of the apparatus, is at ground potential. The electrons at slit S_1 are focussed through 180° to slit S_3 as shown in figure 4c. Momentum selection is achieved by slits S_1 , S_2 and S_3 . After leaving S_3 , the electrons pass through a 90° scattering region and then into a collector. The cathode and momentum selection region are differentially pumped, and the gas is introduced to the scattering chamber only. The gas pressure was measured to an accuracy of $\pm 3\%$ with a Schulz-Phelps high pressure ion gauge (Schulz and Phelps, 1957). The currents to the scattering chamber and electron collector were measured with vibrating-reed electrometers and all voltages measured with a precision differential d.c. voltmeter. The beam energy is controlled by varying the grid to cathode voltage, not the magnetic field. This technique was discussed previously. Golden estimated the full width at half maximum of his electron energy distribution to be 3.5% of the mean electron beam energy. He also performed a rough calculation of the geometric angular detection efficiency. The angular resolution for forward scattering is 8° , and 2° for backward scattering. From these considerations, the best estimate

of the probable error in the cross-section measurement due to detection error is about $\pm 1\%$ for the energy range studied.

All types of "Ramsauer" experiment suffer from the following problems. Firstly, the electron energy cannot be scanned. This means that cross section functions have to be recorded point by point, so the apparatus stabilities, in particular, cathode emission and electron optics, have to be controlled for extended periods. Secondly, the measurement of the electron energy leads to difficulties as it requires a very uniform magnetic field, and if retarding potential difference methods are used then, the magnetic field introduces an uncertainty which has never been analysed.

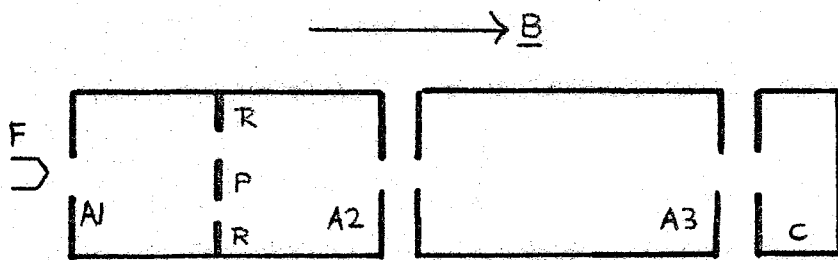
Golden carried out measurements down to 0.3 eV but this energy was not low enough to investigate the low energy structure in helium. To overcome this, a new version of the apparatus has been constructed by the United Aircraft Research Laboratories at Connecticut (Bullis et al, 1967). This employs an electroformed collision chamber to eliminate contact potential effects. It has been estimated that contact potential differences of as much as 1.4 eV can exist in common experimental configurations. The influence of the earth's magnetic field is minimised using magnetic shielding and Helmholtz coils. The resolution of the apparatus is estimated to be 6% and the beam can be controlled down to 0.09 eV. However no subsequent reports from this group have been published.

FIGURE 8.



Rusch's Sector Apparatus.

FIGURE 9.



Rusch's longitudinal magnetic field apparatus.

Two other designs from the early German school, both by Martin Rusch of Tubingen are worth consideration. The first was produced in 1925 and is shown in figure 8. (Rusch, 1925).

Electrons from a hot filament, F, are emitted radially, accelerated towards the sector, S, then pass through the narrow collimating shafts to the collecting plates, C. No analysis has been performed on this apparatus but one can instinctively see that the angular resolution, which will depend upon the width and length of the radial shafts, must be reasonably good. The method for recording the data points was slightly different to the previous techniques which have involved continuous changes in the gas pressure. With only residual gas present, the current to the collector, C, is recorded for different accelerating voltages (in fact, 0.3 volts to 2.0 volts in 0.1 volt intervals) then, with sample gas present, this procedure is repeated. This gives two curves which, when subtracted, and corrected for path length and gas pressure produce the cross-section function. To emphasise the vacuum problems which all the workers at this time experienced, we point out that Rusch with a brass apparatus worked with a residual gas background of 1.4×10^{-3} torr and with gas sample pressures of between 1.0×10^{-2} torr and 9×10^{-3} torr. Despite the simplicity of the apparatus and the lack of energy selection of the beam before collision, Rusch studied the low energy (<2.0 eV) behaviour of argon, krypton, neon and hydrogen. He reproduced the Ramsauer-Townsend minima of argon and krypton well but the energy calibration is out by 0.2 volt.

FIGURE 10. Schulz's transmission spectrometer. (First Version).

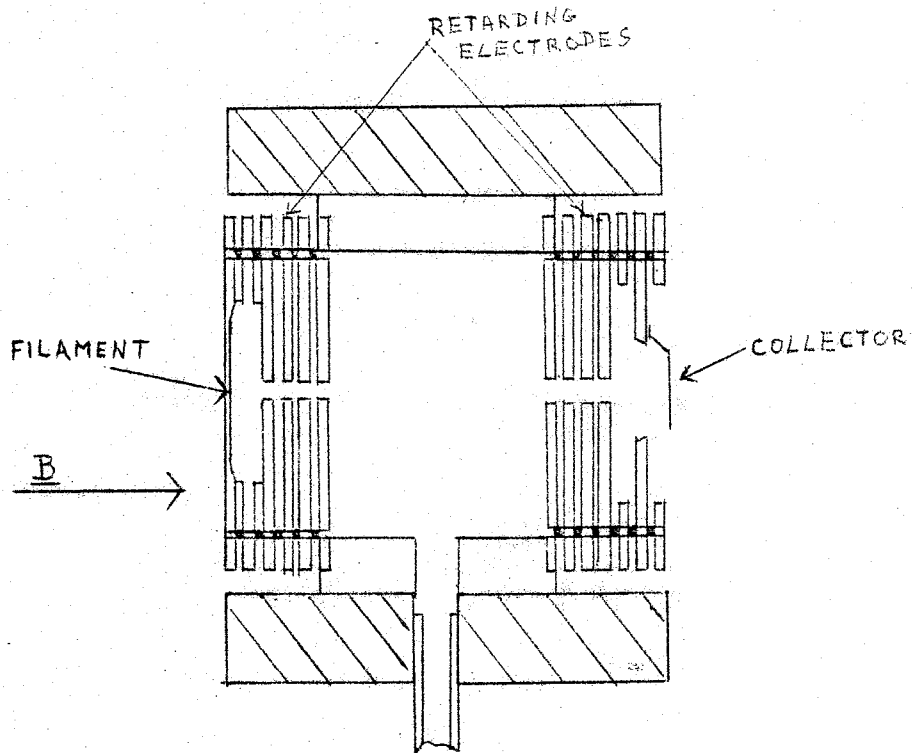
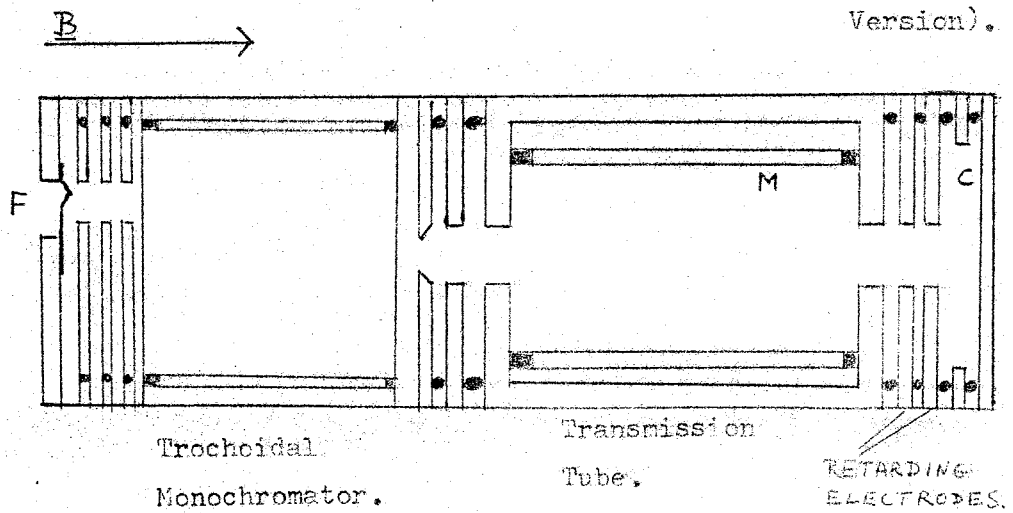


FIGURE 11. Schulz's transmission spectrometer. (Later Version).



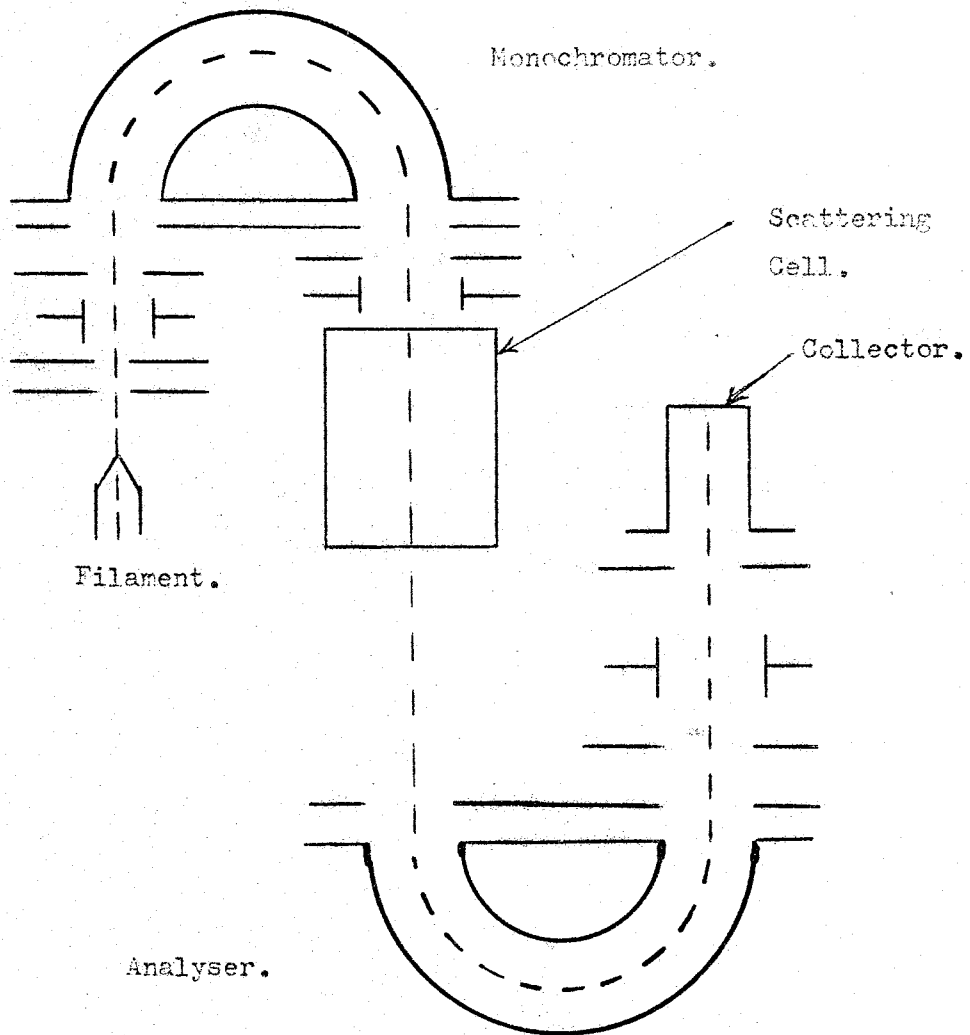
The second apparatus is the longitudinal magnetic field spectrometer. (Rusch, 1926). This is shown in figure 9. Electrons leave a hot filament, F, pass through a small aperture, A1, and enter the monochromator. Unlike Ramsauer's apparatus, the magnetic field vector and the electron velocity vector, in this case, are parallel, not perpendicular, so the electron motion is helical with the helix axis going from A1 to A2. The radius of the helix followed by a particular electron will depend upon its velocity and hence its energy. Thus energy selection can be achieved by impeding the helical path of unwanted electrons. Rusch inserted the ring, R, and the disc P to do this. Because the monochromator and scattering cell are the same length A1 and A3 are focal points of the beam. The procedure is similar to that for the Ramsauer experiment. The currents to the collector and to the collector and scattering chamber together are recorded at different pressures and the argument explained in (I.2.5) through (I.2.8) is followed to give the cross-section. The apparatus may be regarded as the forerunner of the series of longitudinal magnetic field spectrometers designed by Schulz at Yale in recent years, two of which we now consider.

Figure 10 shows the Schulz transmission apparatus (Schulz, 1964). The monochromator operates on the retarding potential difference technique. The principle of this is as follows. The energy of the electrons entering the gas cell is defined by the voltage difference between the last electrode in the monochromator and the cathode. Let this voltage be V_1 . If the electrodes intermediate between the cathode and this electrode are at the voltage V_2 , where

$V_2 < V_1$, then only electrons of energy greater than $e(V_1 - V_2)$ can reach the electrode at voltage V_1 to enter the scattering chamber with energy eV_1 . If V_1 remains unchanged and the unscattered electron beam is measured at the collector for voltages of V_2 and $V_2 - \Delta V$ on the intermediate electrodes, then the difference between these currents represents the transmission of electrons coming from the filament with energies between $e(V_1 - V_2)$ and $e(V_1 - V_2 + \Delta V)$, or an energy spread of $e \cdot \Delta V$. The voltage ΔV can be applied as a square wave a.c. voltage and the resultant modulated collector current synchronously detected. A longitudinal magnetic field is used to align the electrons. The electrodes are gold plated to minimise the contact potentials and the whole apparatus is bakeable and operated under high vacuum conditions of cleanliness. This apparatus has been used mainly for fine structure studies with beam energies larger than 10 eV. One problem that might exist with this type of apparatus is a varying electron optical background at low energies. There is no reference to this in the literature.

Figure 11 shows a later refinement of this technique (Schulz and Sanche, 1971). Electrons from the filament, F, are aligned by the magnetic field, B, then pass through a trochoidal monochromator, collision chamber and retarding electrodes (which provide a potential barrier for scattered electrons) until they reach the collector. The trochoidal monochromator operates as follows. As discussed in the Rusch experiment, electrons with their velocity vectors parallel to a magnetic field vector move in helices, the radius of which depends upon the electron velocity. In the trochoidal monochromator (Stamatovic and Schulz, 1968) electrons, aligned

FIGURE 12. Simpson's Apparatus.



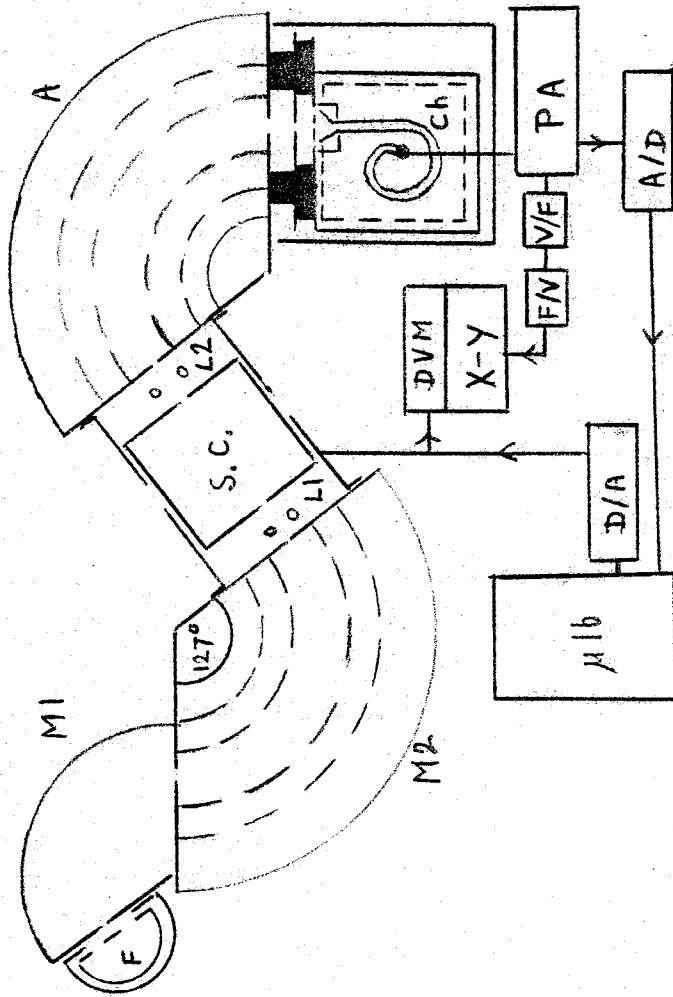
by the axial magnetic field, enter the monochromator region off-centre. An electric field is applied at right angles to the electron beam. In this cross-field region, the electron trajectories describe a trochoidal motion and the electrons are dispersed according to their axial velocities and those electrons which reach the centre of the tube are transmitted through the axial exit hole of the monochromator. This system can produce a beam of 5×10^{-9} amp with an energy spread of 40 meV (full width at half-maximum). Unlike the conventional transmission experiment, which measures directly the transmitted current, this technique is used to measure the derivative of the transmitted current. A sine-wave modulation voltage is applied between the collision chamber and an insulated cylinder, M, inside the collision chamber. The resulting modulation in the transmitted current collected at C is measured in phase with the modulating signal by a phase-sensitive detector. By observing the derivative of the transmitted current, it is possible to accurately define the energy of the fine structure.

Sometimes, apparatus designed to measure inelastic or differential cross-sections can be adapted to measure the total cross section. An example of this was reported by J. A. Simpson of the Electron Physics Section, N.B.S. Washington (Simpson, 1963). A schematic plan of this apparatus is shown in figure 12. The monochromator and analyser are identical, and consist of concentric spherical deflectors providing a point-to-point

focus at 180° deflection (Purcell, 1938). In the mode of operation of interest to us, the monochromator and analyser voltages are held fixed and the scattering chamber voltage is varied. In this mode, any electrons losing enough energy to fall outside of the band of electrons passed by the analyser are not transmitted; and, as the beam is highly collimated, the transmitted current is reduced by an amount proportional to the total scattering. This kind of apparatus is very suitable for fine structure studies, having an energy spread of about 35 meV. With this apparatus Simpson studied the fine structure in helium and neon. (Kuyatt, Simpson and Mielczarek, 1964). Several other investigators have used similar techniques to study fine structure in the total cross section. (Golden and Nakano, 1966; Ehrhardt, Langhans and Linder, 1968; Boness and Schulz, 1970; Imhof and Read, 1969; and, Hasted, Boness and Larkin, 1968).

One problem that exists with this type of apparatus is the electron optical background. We have mentioned this effect before, but a more detailed description is now required. When the energy of an electron beam is varied, the electron current transmitted by the monochromator and the scattering region, can vary. When this happens it is necessary to record a background spectrum of the transmitted beam without gas in the scattering chamber, which is subtracted from the spectrum recorded with gas present. This is only an acceptable technique if it can be shown that firstly, the nature and pressure of the gas do not influence the behaviour of the

FIGURE 13.



HASTED'S APPARATUS.

(Nomenclature described in text).

monochromator, cathode or electron lenses; and secondly, no other changes occur in the performance of the spectrometer between the running of a spectrum and the running of a background spectrum. This effect is not so important in fine structure studies, where the energy range studied extends over only a few electron volts.

One way to overcome this problem, which is particularly evident at low energy, is that employed by Hasted and Larkin. (Hasted and Larkin, 1972). The design of their spectrometer is shown in figure 13. The actual spectrometer is described in detail in an earlier paper (Hasted and Awan, 1969). Electrons from the hot filament, F, pass through a pre-monochromator, M1, then through a 127° monochromator, M2, and an electron lens, L1, into the scattering chamber, S.C. The analyser, A, is set to pass only electrons which have not lost energy in the scattering cell. The electrons passing through the analyser are collected at the channel electron multiplier, Ch. The current from the electron multiplier is amplified by a floating picoammeter, PA, which gives an analogue voltage output, proportional to the electron current. The originality of this apparatus lies in the control circuitry, the actual apparatus described being similar to those cited earlier in this section.

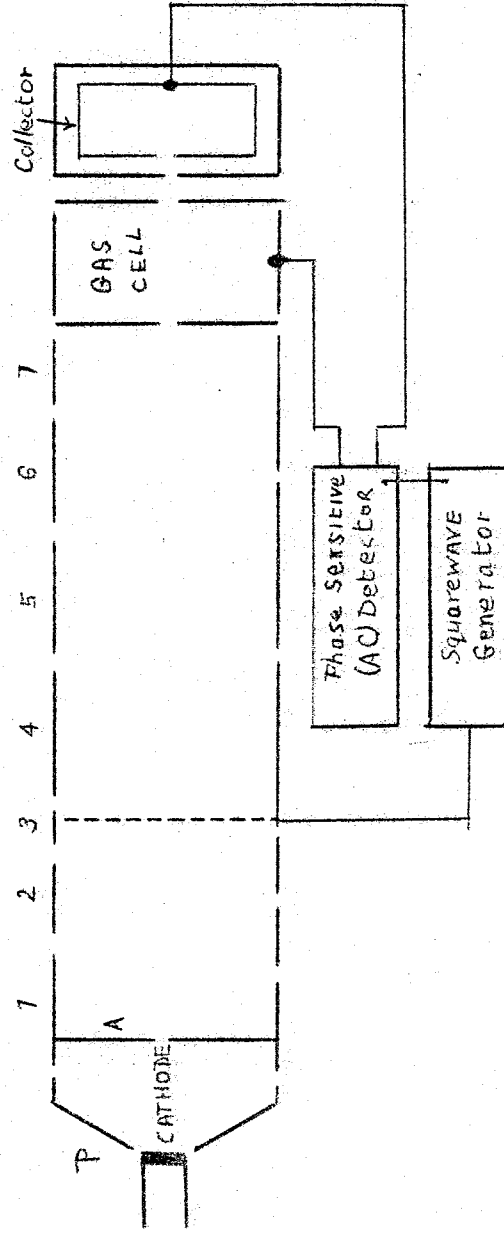
The principle is that a background function is recorded on the computer, $\mu 16$. This background is adjusted so that the transmitted beam current is, to a first approximation, not a function of the electron energy and the necessary lens voltages are stored in the computer

memory. This adjusting can be performed by the computer. To do this the analogue signal voltage is fed to an analogue-digital converter, A/D, which produces a coded digital signal suitable for input to the computer. The computer then outputs a signal, which is converted to analogue voltages by a digital-analogue converter, D/A. These voltages are used to control the lens L1, and the incident beam energy to give this approximately uniform background current. Having recorded this background, gas is introduced to the system and the computer scans the spectrometer voltages in the manner recorded for the background. This time, the analogue signal voltage is converted to a voltage suitable for an X-Y pen recorder by the two voltage/frequency converters, V/F. The signal is recorded on the Y-axis and the voltage difference between the filament and the scattering cell on the X-axis. This gives a direct plot of transmitted current versus electron voltage. This is the most complex transmission experiment in the literature so far.

We conclude our discussion of transmission experiments with some details of a new apparatus designed by Golden and Zecca (1971). Only one investigation (Golden and Zecca, 1970), of the fine structure in scattering by helium of electrons with energies between 19 eV and 20 eV, has been performed with this apparatus but because of its characteristics it seems likely to be worth reporting for its potential application to transmission studies. A diagram of the apparatus is shown in figure 14. The electron source is an oxide coated cathode. This is inserted in a Pierce 67.5°

FIGURE 14.

Golden and Zecca's Apparatus.



Electrode 3 is the retarding electrode.

Electrodes 5, 6, 7 are the beam shaping lenses.

electrode, P, which causes the electrons to leave the hole in the anode plate, A, as a parallel beam. The image of this anode hole, A, is focussed by two lenses onto the symmetry plane of electrode 3. This electrode is used as a retarding electrode to perform a retarding potential difference monochromation of the incident parallel beam. The principles of this were discussed earlier, but in this case there is no magnetic field. The extraction optics is designed to give a beam of small cross-section and angular divergence for a wide range of energies. After passing through the scattering chamber, the transmitted electrons are collected in a Faraday cup. This is a commercial apparatus (Advanced Research Instrument Systems, Inc., Austin, Texas) and full details of its operation are not available. However, the performance seems very suitable for transmission studies. The operating range is 0-60 eV, the lower limit being 0.05 eV; and the best energy resolution is 0.008 eV. This apparatus combines the energy range required to measure the broad features of the total cross-section and the energy resolution for fine structure studies.

We have considered all the major electron transmission experiments reported in the literature. There are, however, other techniques which are not based on the transmission of an electron beam by a static gas target, which can be used to measure total cross-sections. These are the crossed beam techniques and the optical line shift method.

The crossed beam technique employs an atomic beam rather than a static gas target. The atomic or

molecular beam and the energy resolved electron beam are designed to intersect at right angles. We can subdivide crossed beam techniques into three types according to which of the post collision species we observe. The observation of the scattered electrons is of wide application as many types of cross-section can be measured. Total cross-sections can be measured with this technique. (Brackmann, 1958). To do this, the scattered electrons are collected over an angular range around 90° and, with a knowledge of the angular distribution of the scattered electrons, an estimate of the total cross-section can be made. The second method depends on the observation of the atomic beam attenuation. This is also called the atomic beam recoil method. (Eisner, 1969; Bederson, 1962). The number of collisions is determined by measuring the reduction in intensity of the atomic beam as a result of recoil following electron collisions. The third method observes the unscattered beam and so, in some ways, is closely related to transmission experiments. (Neynaber, 1961). In practice, these experiments are often very complex and difficult to perform. The advantage over transmission techniques is that the geometry of the intersecting beams can be accurately probed and therefore the resolution can be calculated. In crossed beam techniques, the atom beam is mechanically modulated (usually with a rotating disc) and the in-phase electron signal is detected. Only a small fraction of the beam is scattered, as the gas density in a beam is much less than that of a static gas target, so there is usually a substantial noise signal

even with synchronous detection. Crossed beam techniques are the only direct method for measuring the total cross-sections of unstable species, such as hydrogen, nitrogen, and oxygen atoms. Measurements have also been made for the alkali atoms, helium and argon. The only measurement of a molecule is that of Bederson for the nitrogen molecule. (Bederson, 1964). Absolute cross-sections can be measured by this technique but these are problems associated with the solution of "overlap" integrals concerned with the interaction volume of the two beams.

Another technique for measuring the total cross-section, which has not been applied quantitatively yet, is the optical line shift or Fermi method. (Fermi, 1934). One mechanism responsible for the broadening and displacement of spectral lines can be attributed directly to low energy elastic electron scattering by ground state atoms. Fermi found that when a highly excited atom, which has a weakly bound orbiting electron, collides with a ground state atom then the interaction can be considered as an elastic collision between a quasi-free electron and a ground state atom. If the electron is to remain in a stationary state it must adjust its orbit slightly. This results in a small energy change of the excited state which can be observed optically. In practice the excited states have usually been produced in alkali vapours and the perturbing system is a high concentration of a rare gas. This technique should have application to the study of unstable species, particularly below thermal energies.

At approximately the same time as Ramsauer was developing the concepts and techniques of electron

transmission spectrometry, J.S. Townsend in the Cavendish Laboratory at Cambridge was investigating the related problem of the behaviour of electrons in a gas under the influence of applied electric and magnetic fields. (Townsend and Bailey, 1921; 1922; 1923). This work grew out of the famous studies of J.J. Thomson on the free electron, and was concerned with the passage of electrons through gases under steady-state conditions. By steady-state conditions we mean that the electrons make large numbers of collisions with the gas particles. An experiment performed under these conditions, where the electron density is low enough for space charge effects to be neglected, is called a "swarm" experiment. Given a theory relating the cross-sections for the fundamental processes to the macroscopically observable electron transport properties of a gas, one can calculate back from the laboratory observables, such as transport coefficients, to the required cross-sections with the connecting link being provided by the Boltzmann equation with appropriate collision terms. The cross-section, in this type of experiment, is the momentum-transfer cross-section. Swarm experiments are performed with electrons of energies from a few electron volts to thermal energies, with a lower limit of about 0.001 eV. There are three types of swarm experiment. These are d.c. swarms, microwave or a.c. swarms and time-of-flight methods. These are comprehensively reviewed by Massey and Burhop (1969).

There are several recent review articles dealing with d.c. swarm techniques. (Phelps, 1968; Crompton and

Huxley, 1962; Crompton, 1969). The properties of the swarm observed are the electron drift velocity along a uniform magnetic field E , W_{\parallel} , the ratio D_{\perp}/μ , where D is the diffusion coefficient perpendicular to the electric field, E , and μ is the mobility (the ratio of the drift velocity to E), and the ratio W_{\perp}/W_{\parallel} , where W_{\perp} is the electron drift velocity at right angles to crossed, uniform electric and magnetic fields. Each of the observables is related to the momentum transfer cross-section, Q_m , by a collision integral that contains both Q_m and $f(V)$, the electron-velocity distribution function. The distribution function is obtained from a solution of the Boltzmann equation, which itself depends upon Q_m . When more than one type of interaction is involved, for example with inelastic processes, the unfolding procedure is complicated and need not be unique. The modern analysis of swarm techniques requires computers and would not be feasible otherwise. Before these were available one had to assume that Q_m varied slowly over the range of velocities in the distribution function. For this reason we can regard early data from swarm experiments as being primarily of qualitative value.

The microwave technique was developed at M.I.T. Radiation Laboratory by Brown and Phelps. (Brown, Fundingsland and Phelps, 1951). An "afterglow" is the state of a partly ionised system after the ionising agent is removed. After a certain period of time, during which metastable and short lifetime states can decay, this afterglow plasma relaxes into a quiescent state in which

the electrons are in equilibrium with the gas particles. The charge density of the afterglow plasma then decays because of various ion and electron collision processes. If microwave radiation is passed through the afterglow at this stage, the electron density and conductivity can be measured as a function of time. Recent reviews of the cross-sections determined by this method are those of Brown (1959) and Golant (1961).

The third approach is that of time of flight swarms. This is a recent technique (Nakai, 1967) which has not, as yet, been employed quantitatively. However most of the experimental problems involved have been solved as the technique has been known in nuclear physics for some time. Simply, what happens is that an electron pulse of known energy is introduced into a scattering region. The arrival-time spectrum of the electrons is recorded with and without gas. The difference in the two spectra will be due to scattering out. An effective total cross-section can be derived from these observations. (Baldwin and Friedman, 1967).

Of all the techniques discussed in this section only the Ramsauer type of experiment and recently the crossed beam experiments have provided reliable total cross-section data. Similarly most momentum transfer cross-section data comes from d.c. swarms — the more recent of these experiments seems to be producing reliable results — with a little information coming from a.c. swarms.

TOTAL CROSS-SECTION CURVES (1930)

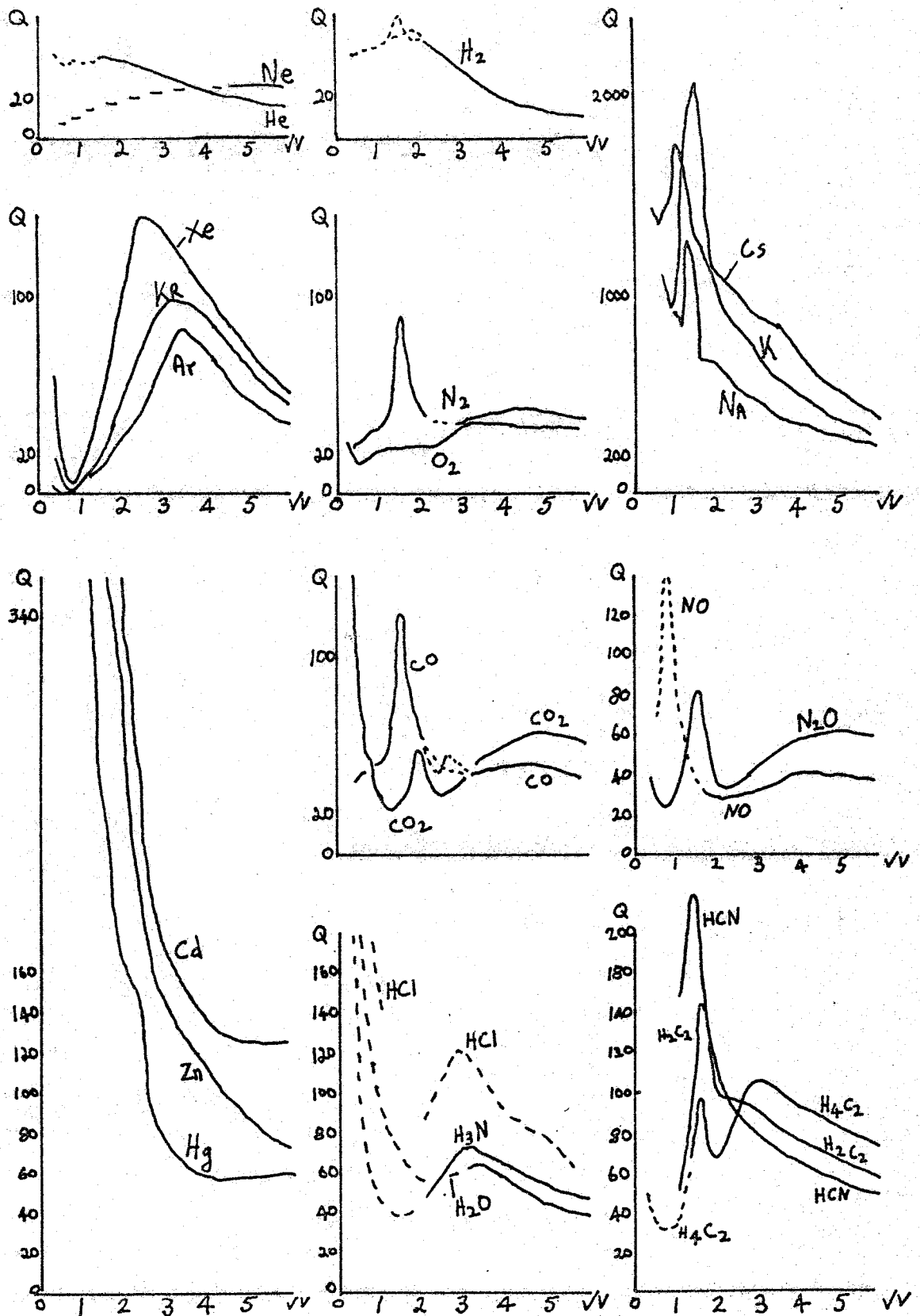


FIGURE 15.

TOTAL CROSS-SECTION CURVES. (1930)

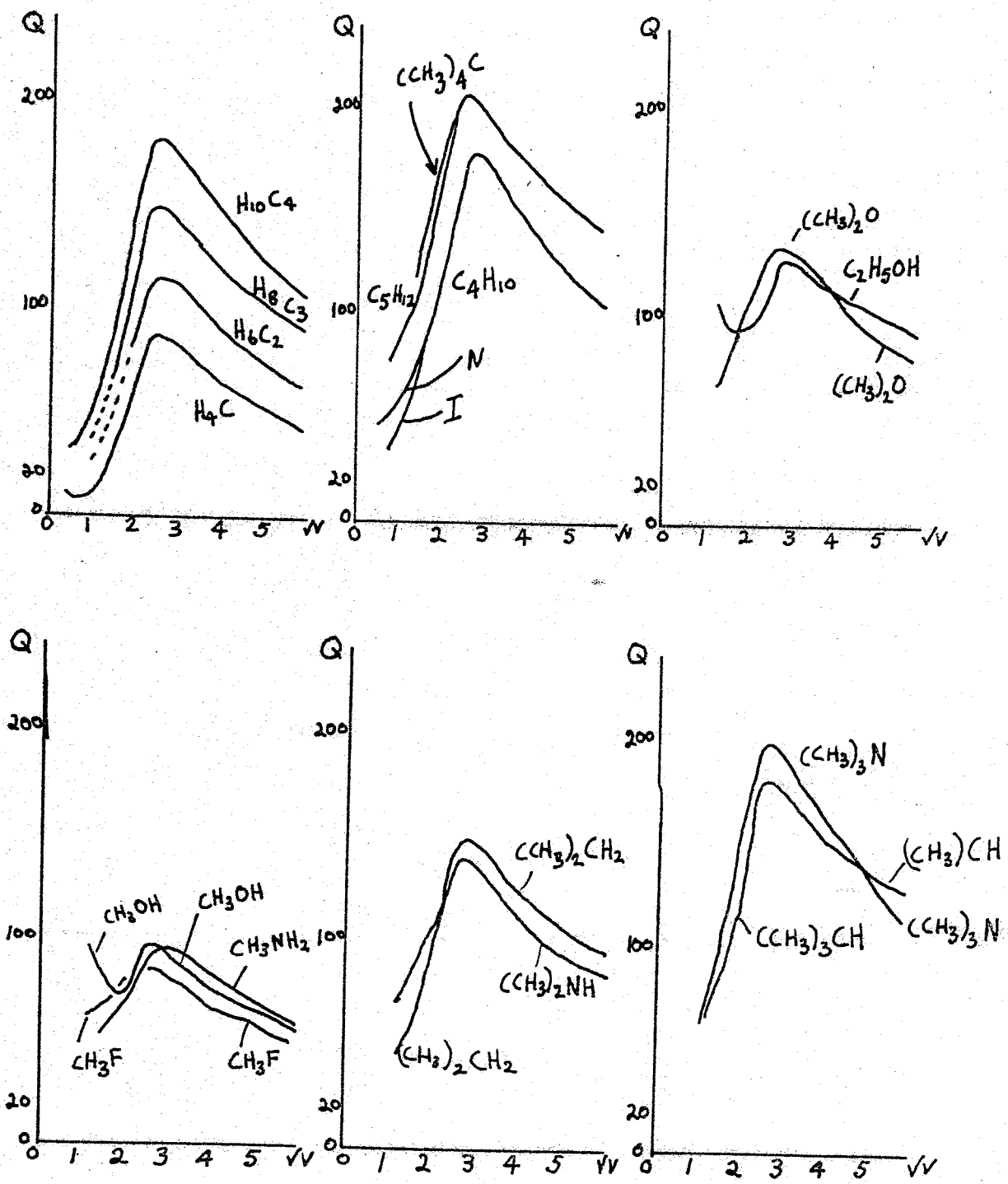


FIGURE 15.

I.3 The Observed Total Cross-Section Functions

In this section we review some of the published total electron/atom and electron/molecule collision cross-sections. We consider only atoms and molecules which are stable in their electronic ground state, in the gas phase, at laboratory temperatures and pressures; and electron beams of mean energy less than one hundred electron volts. An observed total collision cross-section is a complex function of the incident electron energy. To help in the interpretation of this function we distinguish between the comparatively gradual variations in cross-section observed for changes in electron energy of a few electron volts, which we call broad features, and the sharp variations in cross-section that occur within less than one electron volt, due to many-body resonance effects, called fine structure. The broad features of all the atoms and molecules discussed are shown in figure 15.

Helium.

The first studies on helium were all in 1921 at Heidelberg. The first was that of Mayer using a Lenard-type transmission tube (Mayer, 1921) but, as discussed in the previous section, there was some doubt about these results. Two points on the cross-section curve close to 1 eV were obtained by Ramsauer (1921a) using his early

apparatus and later that year with the improved version he recorded the total cross-section function from 1 eV to 40 eV. This had a maximum at about 3.5 eV and the cross-section decreased slowly as the electron energy decreased. (Ramsauer, 1921b). Townsend and Bailey (1923), using an electron swarm apparatus, observed the same broad low energy maximum but positioned its energy slightly lower. The general features of the curve were confirmed by the later observations of Brode (1925), Brüche (1927a), Ramsauer and Kollath (1929) and Normand (1930). The Ramsauer and Kollath study was carried out at low energies (below 1 eV) and suggested structure between 0.4 and 0.9 eV. Golden and Bandel (1965a) paid special attention to this region when they performed the first transmission study on helium for thirty years. However with their Ramsauer type apparatus they could not continuously record the variation of the total cross-section with electron energy in this region. To overcome this Golden and Nakano (1966) employed a transmission apparatus with a 127° energy selector to study energies below 3 eV. They found no evidence of structure in this region and this is still the accepted picture. O'Malley (1963) has suggested that the structure seen in the earlier experiments was due to the presence of N_2 and O_2 as impurities.

In 1963 Schulz reported the first observation of a fine structure feature due to a resonance effect at 19.3 eV by observing the electrons scattered by helium at 72° . The same year Simpson observed the same feature in transmission. (Simpson, 1963). This was later identified

as the $^2S_{1/2}$ state of He^- . ($1S, 2S^2$). Detailed studies were then made by Simpson and Mielczarek (1964) using a hemispherical monochromator and Schulz (1964) using a transmission tube with retarding electrodes to monochromate the electron beam. A very detailed transmission study was made by Kuyatt, Simpson and Mielczarek (1965) who found two resonances at 57.1 eV and 58.2 eV and several other features between 19.3 eV and 24.6 eV, which is the onset of He^+ . They observed no features at all below $\text{He}^- (^2S_{1/2})$ at 19.3 eV. The major excitations in this region were the onsets for He ($2^3S, 2^2P, 2^2D, 3^2S, 3^2P$ and an $n=4$ state and an $n=5$ state). However in 1970, Golden and Zecca, using the zero field retarding potential difference spectrometer reported twenty four different structures between 19 and 25 eV. In order to clarify the position, as Golden and Zecca and Kuyatt et al had comparable electron resolutions of about 50 meV, Sanche and Schulz (1972a) made a detailed study of this region using their axial magnetic field transmission tube discussed in the last section. They were not able to find any new structures which had not been reported by Kuyatt, Simpson and Mielczarek (1965). No explanation for the extra features observed by Golden and Zecca has yet been proposed. The two higher energy resonances have been studied by Burrow and Schulz (1969) and Golden and Zecca (1970) as well as Kuyatt et al who first reported their existence. Here the agreement is better and all three groups agree with the assignment by Fano and Cooper (1965) that the feature at 57.1 eV is due to $\text{He}^- (^2P, 2S^2 2p)$ and the 58.2 eV resonance is due to $\text{He}^- (^2D, 2S, 2p^2)$.

Neon.

This was first studied by Ramsauer (1921b) who recorded a cross-section that increased very gradually from 1 eV to 40 eV. Rusch (1925), employing the radial monochromator and collimator discussed earlier, showed that below 1 eV the cross-section tended towards zero as the energy fell. This low energy behaviour was confirmed by Ramsauer and Kollath (1929). Brüche (1927d) agreed with Ramsauer on the higher energy cross-section function, but Normand (1930) reported a minimum at 4 eV and another at 15 eV. A very careful study of the total cross-section from 0.37 to 20 eV was performed by Salop and Nakano (1970) using the Golden version of the Ramsauer apparatus. Their results agreed well with those of Brüche above 2 eV and Ramsauer and Kollath below 2 eV. They observed a smooth curve over the whole region so it seems Normand's results are in error. A double resonance at 16.0 eV and 16.14 eV was observed first by Simpson (1963) and later in more detail by Kuyatt, Simpson and Mielczarek (1965). Schulz (1964) observed the resonance but did not resolve it into two features. Sanche and Schulz (1972a) found twelve features between 16 and 20 eV. They agreed with Kuyatt's designation of the resonances as $\text{Ne}^- (3p^5, 4s^2)$ $^2P_{3/2}$ and $^2P_{1/2}$ states. More structure is evident in the region 42-50 eV and seems to involve excitation of a 2S electron.

Argon, Krypton and Xenon.

Argon was first investigated in 1921 by Mayer and then Ramsauer (1921a-1921b). Ramsauer found that below 1 eV argon appeared to be almost transparent to electrons. Townsend and Bailey (1922) showed that the cross-section in fact went through a minimum. Ramsauer (1923) performed the experiment again more carefully to try to position the minimum on the energy scale. He also found that krypton and xenon possessed this transparency. Townsend and Bailey (1923) checked their results and several other workers joined in the investigation. (Brode, 1925; Rusch, 1925; Rusch, 1926; Brüch, 1927d; Beuthe, 1927; Ramsauer and Kollath, 1929; and Normand, 1930). It was Ramsauer and Kollath who produced the agreed value of 0.4 eV for the minimum. The effect was named after Ramsauer and Townsend. Golden and Bandel (1966) carefully investigated the region of the minimum. They measured the cross section to be 0.125 \AA^2 at 0.285 eV. Kuyatt, Simpson and Mielczarek (1965) found two resonances about 0.5 eV below the first excited state of argon (11.7 eV and 11.9 eV) due to the two $3p^5 4s 4p$ states of Ar^- . Resonances associated with higher excited states of argon in the region 13-14 eV have been found by Sanche and Schulz (1972a). This work also showed structure between 24 and 32 eV due to excitation of states such as $\text{Ar}(3s 3p^6 4p)$ and $3s 3p^6 3d$ and $\text{Ar}^-(3s 3p^6 4s^2)$. Krypton was found by Kuyatt et al (1965) and Sanche and Schulz (1972a) to have structure in the region 9.5 eV to 12 eV. The two intense peaks being due to the $^2P_{3/2}$ and $^2P_{1/2}$ states of $\text{Kr}^-(4p^5 5s^2)$. More structure likely involving the $\text{Kr}^-(4s 4p^6 5s^2)$ state is

evident between 22 eV and 27 eV. Xenon shows similar structure in the regions 8-12 eV and 18-20 eV.

Molecular Hydrogen.

The first reliable study was that of Akesson (1916). This was followed by the investigations of H.F. Mayer using an apparatus of the Lenard type. (Mayer, 1921; Lenard, 1903). This data was shown to be unreliable by Ramsauer (1921a) with his first apparatus. In the same year, Townsend with his swarm technique showed that there was maximum scattering at an energy of about 1.1 eV. The cross-section falling rapidly either side of this feature. (Townsend, 1921; Townsend and Bailey, 1923). Brode, with his modified Ramsauer type of apparatus, confirmed that the cross-section rose as it approached 1 eV. but could not produce a beam with energy lower than this to confirm the maximum. (Brode, 1925a). However, Rusch, with the circular sector apparatus, confirmed this maximum in 1925 (Rusch, 1925). Brüche also observed the maximum with a Lenard type of apparatus (Brüche, 1926) but a little later, using a Ramsauer type of apparatus, he found that the position of the maximum had shifted to about 3 eV. (Brüche, 1927b). The next investigations of hydrogen were not until 1930 when Ramsauer and Kollath presented results recorded at energies below 1 eV, which seemed to confirm the observations of Townsend and Rusch. None of the other experiments had been performed at energies below 1 eV. (Ramsauer and Kollath, 1930). C. E. Normand (1930) found that just below 1 eV the cross-section rose rapidly to infinity. At 3 eV he observed a sharp peak, which agreed with Brüche's

observation, and between 4 and 6 eV he observed a region of oscillations in the cross-section. These oscillations occur in several of Normand's spectra for different gases, but no other investigator has observed them. The infinite cross-section which he observes in hydrogen and all other gases which he investigated at this energy, is caused by no electrons entering the collector. Whether this is due to all the electrons being scattered out of the incident beam or to some complex electron optical background cannot be decided from his results alone. On consideration of all the available data on all the gases studied by Normand it seems that below 6 eV his apparatus background function dominates the observed cross section. His results must therefore be regarded with some suspicion. To summarise this early work on the broad features in the total cross-section, the cross-section falls smoothly on either side of a maximum somewhere between 2 and 4 eV. The absolute value of the cross-section maximum varies by a factor of two for different investigators. All the data of this period is reported with a non-linear energy axis in units of electron velocity. This leads to difficulties in accurately defining the energy of a feature without having access to the original data.

No more was done until 1965 when Golden investigated H_2 and D_2 with an improved Ramsauer apparatus. (Golden and Bandel, 1965). Simpson, Kuyatt and Mielczarek (1964), in an experiment involving energy analysis of the unscattered beam, had already observed fine structure between 11.0 and 13.0 eV which consisted of a series of sharp

scattering maxima (about eight were observed) decreasing in amplitude as the energy increased. Golden and Nakano (1966) searched for structure between 0.1 and 11.0 eV, using a 127° monochromator, but they found nothing. Golden, Bandel and Salerno (1966), using the improved Ramsauer type of apparatus, performed a detailed study of the broad features of the total cross-section function. This work has become the accepted broad feature spectrum for molecular hydrogen. They agreed on the position of the maximum with Brüche (1927b) who had placed it at 3 eV. The cross-section then falls smoothly from 3 eV to 0.1 eV and falls more gradually from 3 eV to 15 eV. The data of Normand (1930), Brode (1925a) and Brüche (1927b) remains the only available data at incident energies greater than 15 eV. The disagreement between these results is very marked. The fine structure in the region between 13.6 and 16.0 eV had been investigated by Ehrhardt, Weingartshofer and Hermann (1970), with a differential scattering apparatus, and they had designated this resonance series as being vibrationally excited levels produced by the decay of the $^2\Sigma_g^-$ state of H_2^- . This was later observed in the transmission mode by Golden (1971) using the zero magnetic field R.P.D. transmission spectrometer which was discussed in the previous section. Golden did not have the energy resolution in this experiment to investigate further the 11 - 13 eV resonance series, which has been shown by Simpson, Kuyatt and Mielczarek (1966), in a differential study, to be two overlapping resonance series. Sanche and

Schulz (1972b) performed a very detailed analysis of the 11 - 16 eV region in H_2 and D_2 . They list seven resonance series or bands, although only six of these are observable in transmission.

Molecular Nitrogen.

This was first studied by Akesson (1916) and then by Mayer (1921). Neither of these studies produced reliable quantitative results. Two points on the cross-section curve were found by Ramsauer (1921a) with his first apparatus. These were found to lie on the curve produced by Townsend (1921) in a swarm experiment. This curve had a broad maximum between 1 and 4 eV. Brode (1925a) observed the cross-section down to 2 eV. He noted a small gradual maximum around 18 - 20 eV and a sharp rise in the cross section, starting about 5 eV, and increasing sharply as it approached 2 eV. Brüche (1926), using his Lenard type apparatus, placed the maximum at about 2.3 eV, with a basewidth of approximately 2 eV. Ramsauer and Kollath (1930) checked the cross-section below 1 eV and found, in agreement with Townsend, that the cross-section slowly decreases as the electron energy approaches zero. Normand (1930) confirmed these observations, but the oscillations between 4 and 9 eV and the infinite cross-section at low energy, mentioned in our discussion of hydrogen, once again make us suspicious of his results. Fisk (1937), with an apparatus of the Brode design, agreed with Brüche but showed the sharp rise at low energy which Normand showed. This seems to be a common problem with the Brode type of apparatus as Normand, Brode and Fisk all observe this

behaviour when they work at energies less than 1 eV. The Ramsauer design does not show this. There are no later measurements of the total cross-section covering this range. Schulz (1964) set the maximum at 2.25 eV and showed it was composed of several very large resonances with widths about 0.25 eV. Heidemann, Kuyatt and Chamberlain (1966), using Simpson's double 180° spectrometer in a transmission mode, observed this elastic resonance and another at about 11.5 eV with more structure just above it. The low energy resonance is accepted as being due to the decay of N_2^- in the $^2\pi_g$ state, leading to vibrational excitation. Golden and Nakano (1966) also observed this structure with their 127° monochromated transmission experiment, and Boness and Hasted (1966) observed the 2.25 eV resonance and suggested that low energy fine structure occurred below 1.8 eV. It is not, as yet, known whether this structure is elastic, inelastic or direct vibrational excitation of the electron ground state. It is interesting to note that Ehrhardt and Willman (1967) do not find this low energy structure in their differential scattering studies. The 11.5 and 11.9 eV structures are suggested by Massey (1969) to be caused by excitation of the E state and a resonance associated with another excited neutral molecular state. Sanche and Schulz (1972B) in a detailed study show that structure is very evident between 7 eV and 15 eV. They identify four bands which overlap to some extent. Complete identification of all the resonance processes occurring was not possible.

Molecular Oxygen.

Brüche (1927c) was the first to measure the total cross-section of oxygen, from 2 eV to nearly 100 eV. He found that the cross-section slowly increases from 3 eV to about 7 eV, then the slope increases sharply until 10 eV. Above this energy the cross-section remains approximately constant. Ramsauer and Kollath (1930), in a low energy study below 1 eV, observed a minimum at about 0.3 eV, which agrees with what was observed in an electron swarm experiment by Brose (1925). This general shape was recently confirmed by Salop and Nakano (1970) who also recorded practically the same magnitudes of cross-section. Sunshine et al. (1967) had earlier measured the total cross-section using an atomic beam recoil technique, but although they confirm the general shape of the curve the absolute values of their cross-sections are, on average, about 25% higher than those of Brüche and Salop. Boness and Hasted (1966) Boness et al (1968), Hasted and Awan (1969) and Hasted and Larkin (1972) have found structure below 1 eV, which they suggest is caused by resonant scattering from the ground $^2 \pi_g$ state. Schulz and Sanche (1971) using the magnetic field transmission tube with trochoidal monochromator found two sharp features at 8.02 and 8.25 e V. They suggest that these resonance states indicate that at least one parent electronic state of O_2 exists in the region 8.3 - 9.0 eV. A detailed study of the 8 - 13 eV region has been made by Sanche and Schulz (1972b) showing two resonance bands. Unfortunately they did not investigate the low energy structure reported by Hasted.

Carbon Monoxide.

The first transmission study of CO was that of Brode (1925). He found that the total cross-section fell rapidly from 2 eV to a minimum about 9 eV, rising to a broad maximum at 18 eV. Skinker and White (1923) had already shown, in an electron swarm experiment, that the cross-section increased rapidly from thermal energies to 1 eV with a distinct bump around 0.5 eV. Brüche (1927c) found a sharp, very intense maximum at between 2.1 and 2.3 eV, very similar to the maximum which he had found in nitrogen. Normand (1930) observed a very similar spectrum with the usual background features, which we have already commented on. Ramsauer and Kollath (1930) confirmed the bump below 1 eV but did not measure any higher. The carbon monoxide spectrum is thus remarkably like that of molecular nitrogen. The 2.5 eV resonance is more intense in CO. Boness and Hasted (1966), Boness et al (1968) and Hasted and Awan (1969) have observed fine structure in this resonance but it has not been identified in transmission yet. Schulz and Sanche (1971) observed fine structure due to inelastic excitation of the $a^3\pi$, $b^3\Sigma^+$, $B^1\Sigma^+$, $C^1\Sigma^+$ states and a new resonance at 10.04 eV. They have since shown that the 10.04 eV resonance is associated with the $b^3\Sigma^+$ and $B^1\Sigma^+$ states of CO. (Sanche and Schulz, 1972b).

The Oxides of Nitrogen.

Three oxides of nitrogen-nitric oxide, NO, nitrous oxide, N₂O, and nitrogen dioxide, NO₂. Skinker and White (1923), using a Townsend swarm apparatus, investigated both nitric oxide and nitrous oxide at

energies from 2 eV to thermal energies. They found a sharp maximum at about 0.8 eV in nitric oxide, and a distinct minimum for nitrous oxide at about the same energy. Brüche (1927c) extended this investigation from 2 eV to 40 eV. He found a broad maximum for N_2O , at just over 2 eV, and a very broad maximum starting at 4 eV, increasing until 25 eV and then gradually falling. Nitric oxide has a similar maximum centred around 16 eV. The N_2O data was confirmed by Brode (1933) and the low energy minimum checked by Ramsauer and Kollath (1930). Extensive studies on the fine structure of these molecules have recently been carried out by Larkin and Hasted (1972) on N_2O , NO_2 and NO , and by Sanche and Schulz (1972b) on NO . These studies show that several of the broad features consist of overlapping series of resonance peaks.

Other Inorganic Gases.

The only other inorganic gas which has been investigated for fine structure is carbon dioxide. Larkin and Hasted (1970) confirmed the nature of the low energy elastic cross-section, which is essentially the same as the total cross-section, that had been observed earlier by Skinker (1922), Brüche (1927c), Ramsauer and Kollath (1930) and Brode (1933). The broad features of several other gases have also been investigated; Hydrogen chloride by Brüche (1927a), ammonia and water by Brüche (1927b, 1929a), hydrogen cyanide by Schmeider (1930) and chlorine by Fisk (1937).

Organic Gases.

No transmission studies of the fine structure in organic gases have yet been made. Methane, CH_4 , was

investigated by Brode (1925), then by Brüche (1927c) and Ramsauer and Kollath (1930). The alkane series, up to butane, was reported by Brüche (1930a) then by Brode (1933). Brüche (1930b) made a very interesting study of the isomers of butane. Schmeider (1930) studied pentane and its isomers; the hydroxyl series C_3H_7OH , C_2H_5OH , CH_3OH and H_2O ; the isomers of C_2H_6O ; the isoelectronic series CH_3F , CH_3OH , CH_3NH_2 ; and the isoelectronic pairs $(CH_3)_3NH$, $(CH_3)_3CH$ and $(CH_3)_3N$, $(CH_3)_3CH$. Holst and Holtsmark (1931) studied ethylene, acetylene and benzene; and the chlorinated methane series CCl_4 , $CHCl_3$, CH_2Cl_2 and CH_3Cl .

I.4 Theoretical models and the interpretation of the total cross-section function.

In the previous sections, we have defined the total cross-section, discussed how it can be measured and reviewed those cross-sections which have been measured. In this section we consider how to interpret the total cross-section function in terms of theoretical models. The broad features of the function are the occurrence of maxima and minima, in particular that low energy minimum exhibited by certain atoms and molecules and known as the Ramsauer-Townsend effect; the similarity in the cross-section functions of chemically similar atoms and molecules and the heavier rare gases; and the large cross-sections for the alkali metals. We must also explain the occurrence of fine structure due to resonance processes.

So far, no one theoretical model satisfactorily explains all of these phenomena. However several models are available which account for particular cross-section phenomena more or less satisfactorily. To systematise our discussion we divide the models into three classes: classical mechanical models, wave mechanical models and chemical models. Our definition of the word "model" is any theoretical description of the electron-atom or electron-molecule system which correctly predicts an observed feature in the cross-section curve.

Classical Models.

In the simplest classical mechanical model, we represent both the electron and the target atom or molecule by smooth, impenetrable elastic spheres of appropriate relative mass. If the distance between the particles is r , and the sum of the radii of the two particles is D , then we can express the interaction potential $V(r)$ as,

$$V(r) = \begin{cases} \infty & (r < D) \\ 0 & (r > D) \end{cases} \quad (\text{I.4.1})$$

This is called the classical mean free path model or "billiard ball" model. The detailed mathematical analysis of this system was considered in the introductory section. It was shown there that all directions of motion after collision were equally probable ie. the scattering was isotropic. Also, according to this model, the total cross-section is not a function of the incident electron energy, which contradicts the observed facts.

To improve upon this model we must introduce a more realistic interaction potential. It is known that a charged particle close to an atom or molecule causes it to become polarised (ie. the centres of positive and negative charge do not coincide). Let us suppose, as a first approximation, that when this occurs the charges are distributed with spherical symmetry about their respective centres. Thus the target particle will acquire an induced dipole moment due to the proximity of the incident electron. In reality, the charge distribution formed can cause

induced quadrupole moments and octupole moments as well. Now, by analogy with a parallel plate condenser, the polarisation P , induced in a gas of dielectric constant K , by an electric field of strength E is:

$$P = (K-1).E/4\pi \quad (\text{I.4.2})$$

and if N is the number density of the gas particles, the induced dipole moment per atom or molecule is μ where:

$$\mu = P/N = (K-1).E/4\pi N \quad (\text{I.4.3})$$

and let us assume that we can consider the electric field of the electron as coulombic, except at small distances, so that if r is the separation of the electron and the target dipole then,

$$E = e/r^2$$

and,

$$\mu = (K-1).e/4\pi Nr^2 \quad (\text{I.4.4})$$

Now the force of attraction between a dipole and a point charge is given by:

$$F = 2\mu.e.\cos\beta/r^3$$

where β is the angle between the axis of the dipole and the direction of the incident electron. Since the dipole, in this case, is induced by the incident electron the angle β will always be zero. Thus,

$$F = (K-1).e^2/2\pi Nr^5 \quad (\text{I.4.5})$$

and the interaction potential for this model is:

$$\begin{aligned} V(r) &= - \int_r^{\infty} ((K-1).e^2)/(2\pi Nr^5) dr \\ &= -(K-1).e^2/8\pi Nr^4 \quad (\text{I.4.6}) \end{aligned}$$

This is only an approximate expression as it assumes that the field of the electron is constant over the whole target molecule. The complete analysis of this model for a molecule with a spherically symmetric electron distribution shows that (I.4.6) represents only the first term of a series solution, the next term being a constant times r^{-6} and corresponding to the induced quadrupole of the molecule. (Margenau, 1941).

These considerations suggest that a more suitable interaction potential would be of the form:

$$V(r) = -c/r^n \quad (\text{I.4.7})$$

where c is a positive constant and n is the multipole index. The mathematical difficulty of the analysis of this model depends upon the value chosen for n .

If $n = 1$, we have Coulomb or Rutherford scattering. If θ_1 is the scattering angle, as defined in figure 2, then it can be shown that the classical differential total cross-section for Coulomb scattering, $\sigma_T(\theta_1)$, is given by:

$$\sigma_T(\theta_1) = C/v_0^4 \sin^4(\theta_1/2) \quad (\text{I.4.8})$$

This is an improvement on our previous model as the cross-section is now a function of the incident electron energy or velocity, v_0 . However, because of the $\sin^4(\theta_1/2)$ term in the denominator, when we integrate the differential cross section to obtain the total cross section thus,

$$Q_T = \int_0^\pi \int_0^{2\pi} \sigma_T(\theta_1) \cdot d(\theta_1) \cdot d\phi \quad (\text{I.4.9})$$

the first integral diverges to give an infinite value for

Q_T , and for the momentum transfer cross-section also. No matter how large an impact parameter we have, some deflection will occur and so the sum of all contributions to the integral must be infinite. This problem can be overcome by using "shielded" Coulomb potentials in which the range of the interaction is limited (ie. there is a maximum value for r in equation (I.4.7)). The shielded Coulomb potential is discussed by McDaniel (1964) and the "exponentially screened" Coulomb potential was considered by Everhart (1960). Neither of these approximations improve the classical Coulomb model for low energy electron-atom or electron-molecule collisions.

It can be shown that if the interaction potential between the colliding particles is of the form of equation (I.4.7) then the variation of the differential scattering cross section with velocity is given classically by;

$$\sigma(\theta) \propto v_0^{-4/n} \quad (\text{I.4.10})$$

where v_0 is the incident particle velocity, θ is the polar scattering angle and n is the multipole index. (Kennard, 1938).

If $n = 4$ in (I.4.7) we have a point charge-induced dipole polarisation potential. From equation (I.4.10) we see that this shows that the differential scattering cross section varies inversely with the velocity. The collision frequency, which is proportional to $\sigma(\theta) \cdot v_0$, is thus independent of v_0 and for this reason the model is sometimes called the constant mean free time model. These classical models are summarised in Table I.

Table I

Model	Interaction potential	Multi-Polar Index	Differential cross section dependence
Constant mean free path model	$V(r) = \begin{cases} \infty & (r \leq a) \\ 0 & (r > a) \end{cases}$	$n = \infty$	$\sigma \propto f(v_0)$
Coulomb Potential model	$V(r) = -C/r$	$n = 1$	$\sigma \propto 1/v_0^4$
Constant mean free time model. (point charge-induced dipole)	$V(r) = -C/r^4$	$n = 4$	$\sigma \propto 1/v_0$
point charge-induced quadrupole	$V(r) = -C/r^6$	$n = 6$	$\sigma \propto (1/v_0)^{2/3}$

Table II

Interaction	Velocity dependence of cross section	Multipole Index
dynamic scattering	$Q_T \alpha v^2$	--
charge-charge	$Q_T \alpha (1/v)^4$	$n=0$
charge-dipole	$Q_T \alpha (1/v)^2$	$n=1$
charge-quadrupole	$Q_T \alpha (1/v)^{4/3}$	$n=2$
Charge-octupole	$Q_T \alpha (1/v)$	$n=3$

In a model involving scattering by a centre of force with infinite range, we cannot define the total cross-section properly and so cannot calculate the velocity dependence. However we can calculate a velocity dependence for the momentum transfer cross-section because the small angle contribution to the differential cross section is suppressed by the weighting factor $(1-\cos\theta)$ in the integral for Q_m . However these models do not account for any features in the cross-section curve.

It would appear, therefore, that the low energy scattering of electrons by atoms or molecules is "non classical", for we have failed to produce a model that will explain the features of the total cross-section dependence upon electron velocity. Modern monographs on atomic collision physics, such as Massey (1969), Massey and Burhop (1969), Mott and Massey (1965), Massey (1956), Schiff (1955), Burhop (1961) and Hasted (1972) all employ Heisenberg's uncertainty principle to show why classical physics should, in general, fail to give a satisfactory qualitative or quantitative description of collision processes. This principle applies to any pair of canonically conjugate variables in the scattering system. These are dynamical variables, such as spatial position and linear momentum or total energy and time, which satisfy a conjugate pair of Hamilton's "canonical equations of motion". The principle states that the order of magnitude of the product of the uncertainties in the knowledge of the two variables must be at least as great as $h/2\pi$, where h is Planck's constant. For example,

$$\Delta X \cdot \Delta P_x \approx h/2\pi \quad (\text{I.4.11})$$

If ΔX , the uncertainty in the position of the colliding electron, is to be no greater than the dimensions of the target molecule, say (10^{-8} cm), then from the above inequality, the resultant uncertainty in momentum, ΔP_x , corresponds to an uncertainty in velocity ($\Delta V_z \sim 10^8$ cm sec^{-1}) which is roughly the velocity of a 3 eV electron. This discussion does not prove that classical mechanics is not applicable to low energy problems. But combined with the fact that classical considerations could not explain the Ramsauer-Townsend effect or indeed any other total cross-section effect, whereas wave mechanics successfully accounts for some of these phenomena, in the general case if not the specific, we can see how this system became regarded as "non-classical". In fact, the success of wave mechanics in interpreting these phenomena, notably the Ramsauer-Townsend effect, was regarded as the key experimental evidence supporting the advent of the wave theory.

Recently M. Gryzinski of the Institute for Nuclear Research in Poland has proposed a diametrically different classical approach to the problem of low energy atomic scattering. Gryzinski assumes interaction to occur through the time dependant periodically varying potential field of the atom or molecule produced by the point charge fields of the constituent electron as they classically rotate about the nucleus. This system of charges, under the action of Coulomb's law and Newtonian dynamics, exists in a state of dynamic equilibrium. The nature of the scattering undergone by a particular incident electron being

determined by the actual value of the atomic or molecular multipole moment at the point of closest approach. The potential, Φ , is a function of the impact parameter, r , the polar and azimuthal scattering angles, θ and ϕ , and the time, t . It can be expressed as a Fourier series expansion of this form:

$$\Phi(r, \theta, \phi, t) = \sum_k \sum_n A_{nk}(\theta, \phi) \cdot \exp(-i \cdot w_k \cdot t) / r^n \quad (\text{I.4.12})$$

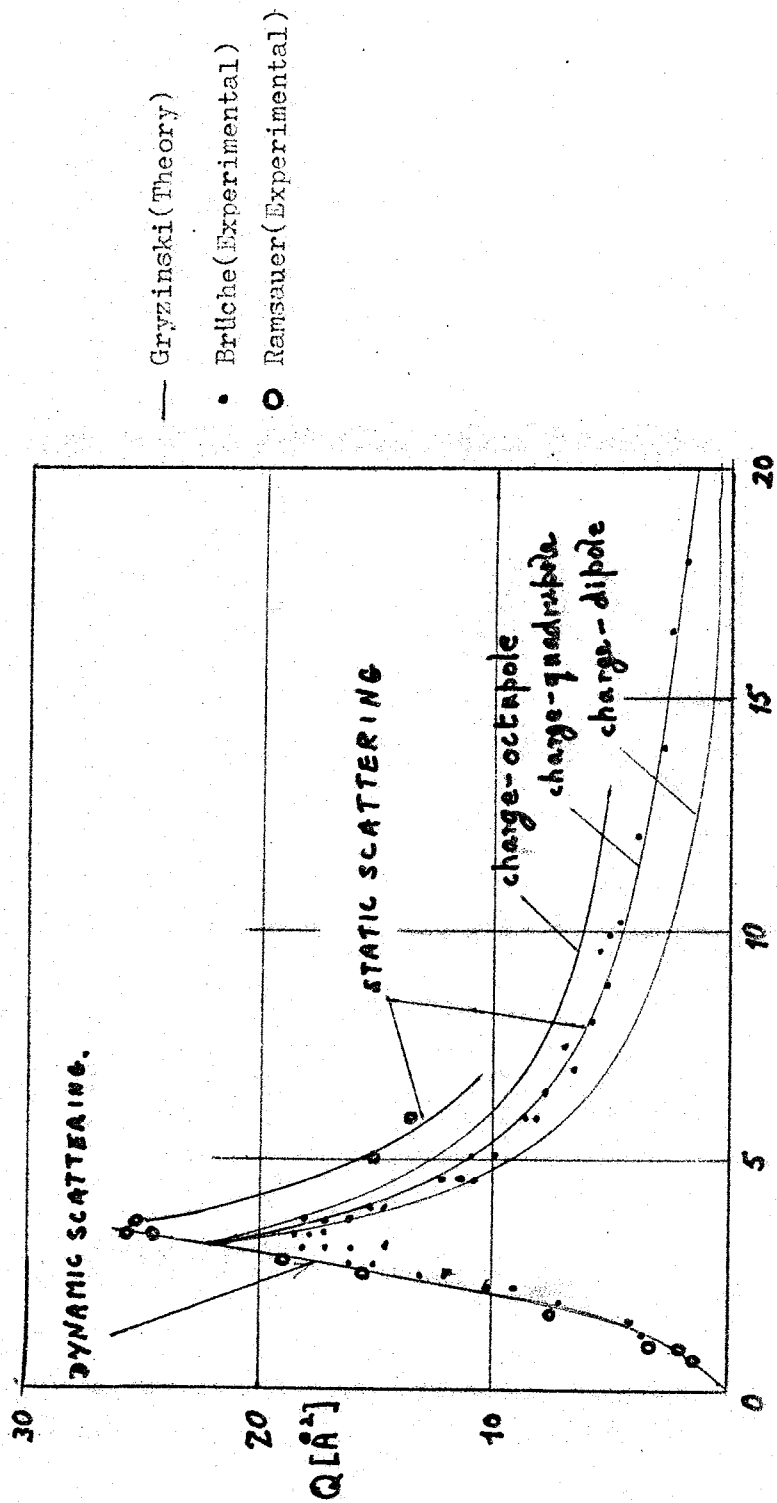
where A_{nk} represents the component corresponding to the frequency w_k in the Fourier expansion of a multipole moment of the n th order. (Gryzinski, 1959; 1965a; 1965b; 1965d; 1965e; 1971b).

To overcome the problem of defining the total cross-section, Gryzinski proposes that a minimum value of scattering angle exists and can be determined. This minimum angle is determined by the nature of the apparatus. He considers in particular the size and shape of the beam-forming slits and the detector slits, but gives no practical details of how to calculate this angle accurately. In the experiments he considered, (those of Brüche, Normand, Brode and Ramsauer which were discussed in section I.2), the value of the angle is of the order of several degrees. (Gryzinski 1970b). Using classical small angle scattering theory (Gryzinski, 1970a) he relates the scattering angle, θ , the collision parameter, D , and the electron velocity, v , thus:

$$\tan \theta \propto A_{nk} \cdot \exp(-w_k \cdot D/v) / (D^{n+1} \cdot v^2) \quad (\text{I.4.14})$$

The limiting value of this expression depends upon the frequency, w_k , of the target system. The expressions for the total cross-section then take the form:

FIGURE 16. Total Cross-Section of Argon. (Gryzinski).



— Gryzinski (Theory)

• Brüche (Experimental)

○ Ramsauer (Experimental)

$$Q_T \propto (1/v)^{4/n+1} \quad \text{for } v > v_1 \quad (\text{I.4.15})$$

and,

$$Q_T \propto v^2 \quad \text{for } v < v_1 \quad (\text{I.4.16})$$

where v_1 is a boundary velocity dependant on the frequency w_k .

Using these ideas, Gryzinski "interprets" the published total cross section data. He divides the observed curve into ranges defined by the velocity of the incident electron. In his most recent article (1971b) he divides the curve into three regions: a region of squared Coulomb scattering (from about 0.1 to 1.0 eV); region of exponential scattering (from about 1.0 to 100 eV); and a region of quasi-Coulomb scattering. In his earlier work, more regions were involved and, certainly for molecules, it seems unlikely that the number of different kinds of interaction can be reduced. The interactions possible, as derived from expressions (I.4.15) and (I.4.16) are listed in Table 2.

This approach does work with the observed curves. For numerical agreement it is necessary to correct the experimental values for the angular resolution of the particular apparatus used. The Ramsauer-Townsend minimum in argon is verified if we assume dynamic scattering to occur from 0.5 eV to 10 eV and a quadrupole moment interaction above that energy. Figure 16 shows the agreement between experiment and theory. Xenon and krypton calculations are similar to argon whereas helium and neon show the quadrupole dominance over the whole energy range. Thus for the rare gases, the dynamic

quadrupole is the basic scattering interaction and the agreement is good above 1 eV.

For molecules, recognition of the dominant dynamic multipole can provide information about the electronic structure of the molecule. For example, Gryzinski found that electron scattering from the hydrogen molecule was best explained by assuming a dominant dynamic quadrupole moment. The absence of any dipole moment suggests that the electrons have motions symmetric with respect to the molecular centre. The absence of a permanent quadrupole suggests that the electron motion is axially symmetric with respect to the internuclear axis. Molecular nitrogen is explained with a dynamic dipole region, and a dynamic octupole region at higher energy. This dynamic charge-dipole interaction is found to be characteristic of a π bond in a molecule. So ethylene and acetylene both have dynamic dipole regions, whereas ethane which has only σ molecular bonds has not. The saturated hydrocarbon series, of methane, ethane, propane and butane, shows a very characteristic charge-octupole interaction. The dynamic multipole model, then, is useful for the molecular physicist interpreting scattering data; in particular when looking at possible correlations between chemically similar molecules and their cross sections. However, whether this purely classical model is a physically realistic alternative to the quantum theory models is still a matter of some debate. (Gryzinski, 1971a).

In summary, the only classical model of any help in interpreting the observed cross sections is the dynamic multipole model. No classical model can explain resonance fine structure, however, as this obviously depends on quantised energy levels.

Wave Mechanical Models.

According to the classical models an electron, of mass m and velocity v , which is directed towards a centre of force will be deflected unless the force due to the centre vanishes everywhere along the trajectory. If the electron is not deflected it will pass the centre at a distance r , called the impact parameter. In treating this problem quantum mechanically we can assign a probability $\alpha(r)$, that a particle with an impact parameter between r and $r+dr$ will suffer an "observable" deflection. (Mott and Massey, 1965; Massey and Burhop, 1969).

$$\begin{aligned} Q_T &= \int_0^{\infty} \int_0^{2\pi} \alpha(r) \cdot r \cdot dr \cdot d\phi \\ &= 2\pi \int_0^{\infty} \alpha(r) \cdot r \cdot dr \end{aligned} \quad (\text{I.4.17})$$

As in most quantum mechanical formulations it is convenient to rewrite this in terms of the angular momentum, J , of the electron about the centre of force, so:

$$Q_T = (2\pi/m^2 v^2) \int_0^{\infty} J \cdot \beta(J) \cdot dJ \quad (\text{I.4.18})$$

where $J = m \cdot v \cdot r$ and $\beta(J)$ is the probability that an electron with angular momentum between J and $J+dJ$ suffers an "observable" deflection. Now the angular momentum about a centre of force is quantised, so we can write:

$$J = \{\ell(\ell+1)\}^{\frac{1}{2}} \cdot \hbar \quad (\text{I.4.19})$$

where ℓ is the angular momentum quantum number of the electron. In accordance with the usual nomenclature, if $\ell=0$ we have an S wave electron, $\ell=1$ a p wave electron and so on.

The integral for the total cross-section will now become an infinite series, thus:

$$\begin{aligned} Q_T &= (\pi \hbar^2 / m^2 v^2) \sum_{\ell=0}^{\infty} (2\ell+1) \gamma(\ell) \\ &= (\pi/k^2) \sum_{\ell=0}^{\infty} (2\ell+1) \gamma(\ell) \end{aligned} \quad (\text{I.4.20})$$

where $k = 2\pi/\lambda$ is the wave number of the incident electron, and $\gamma(\ell) = \beta(J)$.

We now interpret the probability $\gamma(\ell)$. The incoming electron may be considered as a plane de Broglie wave of wavelength $\lambda = h/mv$. After passing the centre of force the electrons will have a spherical wavefront. (Faxen and Holtmark, 1927). An analysis of this model in detail for head on collisions of zero angular momentum or S wave electrons with a centre of force, shows that the probability $\gamma(0)$, that these electrons undergo an "observable" deflection is a function of the phase shift, η_0 , in the electron wave before and after collision. Now it is impossible to count the electron waves, so a phase change that is an integral multiple of 2π will not be observable. So $\gamma(0)$ will be a periodic function of η_0 , never be negative and will vanish when the phase change vanishes. A function satisfying these three conditions is $\gamma(0) = A \sin^2 \eta_0$. By analogy we let $\gamma(\ell) = A \sin^2 \eta_\ell$, where η_ℓ is the phase shift produced in ℓ -wave electrons. A full quantum mechanical proof of this problem, involving a solution of the Schrödinger equation for the electron/target system to give the asymptotic wave functions before and after collision, is given by Mott and Massey (1965) and leads to the same final expression, viz:

$$Q_T = (A\pi/k^2) \sum_{\ell=0}^{\infty} (2\ell+1) \sin^2 \eta_\ell \quad (\text{I.4.21})$$

To evaluate A, we compare our partial wave model cross-section with the classical constant mean free path model cross-section. These cross-sections we would expect to be identical when we consider the case of electron scattering by a billiard ball of radius a. The classical and quantum definitions of angular momentum, J, are:

$$J = \{\ell(\ell+1)\}^{\frac{1}{2}} \cdot \hbar$$

$$= m \cdot v \cdot r$$

The radius of the billiard ball, a, defines a limiting impact parameter and hence angular momentum, J_{LIM} , where:

$$J_{LIM} = m \cdot v \cdot a$$

For large values of ℓ , $J \simeq \ell \cdot \hbar$ and so,

$$\ell \simeq m \cdot v \cdot r / \hbar$$

and,

$$\ell_0 = m \cdot v \cdot a / \hbar = k \cdot a$$

where ℓ_0 is the quantum number corresponding to J_{LIM} .

Now if $\ell > \ell_0$, we expect the phase η_ℓ to be approximately zero as this corresponds to an impact parameter greater than the radius of the ball. Thus, $\sin^2 \eta_\ell$ will be zero and the value of Q calculated from (I.4.21) will be zero.

If $\ell < \ell_0$, we can rewrite (I.4.21) in the form;

$$Q \simeq A\pi/k^2 \int_0^{\ell_0} (2\ell+1) \cdot \sin^2 \eta_\ell \cdot d\ell \quad (I.4.22)$$

We expect η_ℓ to be large for scattering from a billiard ball, and can replace $\sin^2 \eta_\ell$ by its average value of $\frac{1}{2}$,

$$Q \simeq A\pi/k^2 \left[\ell^2/2 + \ell \right] \frac{\ell_0}{0}$$

and as $\ell_0 = k_a a$,

$$Q \simeq A\pi \cdot k \cdot a / k^2 (k \cdot a / 2 + 1) \quad (\text{I.4.23})$$

So, in the limit of high values of ℓ , $ka/2 \gg 1$ and we can write:

$$Q_T = A \cdot \pi \cdot a^2 / 2 \quad (\text{I.4.24})$$

If we make $A=2$, (I.4.24) corresponds to the classical cross section of $\pi \cdot a^2$ for high incident energy electrons. The more detailed treatment of this problem involves solving the Schrödinger equation for the system and gives a value for the constant A of 4. The difference in value being due to shadow diffraction of the electrons at small scattering angles. (Mott and Massey, 1965). Thus, the partial wave expansion of the total cross-section is now,

$$Q_T = (4\pi/k^2) \sum_{\ell=0}^{\infty} (2\ell+1) \sin^2 \eta_{\ell} \cdot d\ell \quad (\text{I.4.25})$$

and the momentum transfer cross-section in terms of partial waves is,

$$Q_m = (4\pi/k^2) \sum_{\ell=0}^{\infty} (\ell+1) \sin^2(\eta_{\ell} - \eta_{\ell+1}) \quad (\text{I.4.26})$$

Classically, the deviation produced by the scattering potential will be small if the kinetic energy of the electron is very much greater than the interaction potential. Wave mechanically, the impact parameter corresponding to the angular momentum, J , is $r = J/m \cdot v$. Thus, by analogy, we expect that $\sin^2 \eta_{\ell}$ will be small for values of ℓ such that the interaction potential, $V(J/mv)$ instead of $V(r)$, is very much less than the kinetic energy

of the incident electron. We now consider how this small phase shift condition arises. Let the interaction potential be of the form;

$$V(r) = C/r^n \quad (\text{I.4.27})$$

Then the condition for a small phase shift η_ℓ is that

$$C/r^n \ll T \quad (\text{I.4.28})$$

where T is the kinetic energy of the electron.

This requires that

$$r \gg (C/T)^{1/n} \quad (\text{I.4.29})$$

and

$$\begin{aligned} r &= J/mv \\ &= \{\ell(\ell+1)\}^{1/2} \hbar / mv \\ &\simeq \ell \hbar / (2mT)^{1/2} \end{aligned}$$

So we can rewrite condition (I.4.29) wave mechanically as,

$$\ell \gg C^{1/n} T^{1/2-1/n} (2m/\hbar^2)^{1/2} \quad (\text{I.4.30})$$

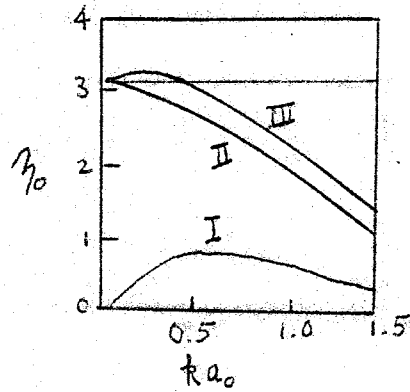
Thus for interactions with $n > 2$ all phases, except perhaps the zero order one, tend to zero as the kinetic energy tends to zero. It follows that the greater the value of T , the incident electron kinetic energy, the larger the number of significant phases in the series expansion of (I.4.25). For very low kinetic energies only the zero order phase is significant and the scattering cross section reduces to:

$$Q_T = (4\pi/k^2) \sin^2 \eta_0 \quad (\text{I.4.31})$$

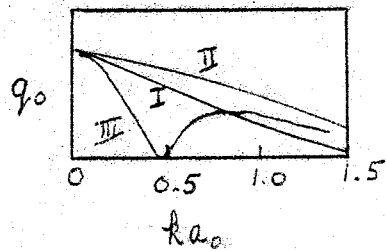
This result is valid for exponential scattering potentials also. Equation (I.4.31) expresses the first useful result for this model. It provides an explanation for the Ramsauer-Townsend minimum. We will consider this in detail later.

FIGURE 17.

Variation of zero order phase, η_0 , with electron energy. Curves I,II,III refer to the cases discussed in the text.



Variation of the zero order partial total cross-section with electron energy.



Any particular angular momentum will make only a small scattering contribution if $\sin \eta_\ell$ is small. This will be so, not just for $\eta_\ell \simeq 0$ but also $\eta_\ell \simeq n\pi$ where n is an integer. By definition, we choose the low velocity limit of a phase to be $n\pi$ rather than zero, and n is the number of zero values introduced into the plane wave function by the action of the scattering field on zero velocity electrons. Thus η_ℓ is a steadily decreasing function of ℓ for fixed electron velocity in a given scattering field. If, with this convention, the phase $\eta_\ell \rightarrow n\pi$ as the velocity tends to zero, then n bound energy levels exist, each of angular momentum $\{\ell(\ell+1)\}^{\frac{1}{2}} \cdot \hbar$.

We can express (I.4.25) in an alternative form.

$$Q_T = \sum q_\ell \quad (\text{I.4.32})$$

where $q_\ell = (4\pi/k^2)(2\ell+1)\sin^2 \eta_\ell$ is the ℓ th order partial cross-section. We showed that, for very slow electrons, the only significant partial cross-section is the zero order one. Thus:

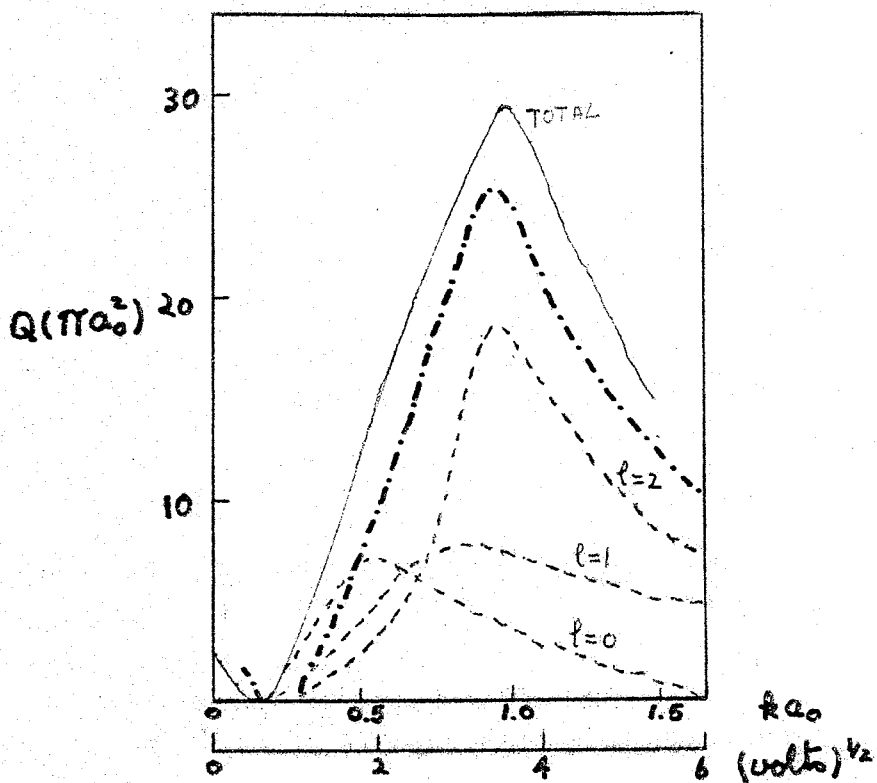
$$Q_T = q_0 = (4\pi/k^2) \sin^2 \eta_0 \quad (\text{I.4.33})$$

As the velocity tends to zero, the wave number $k = mv/\hbar$ also tends to zero and η_0 tends to $n\pi$, where n is determined by the strength of the scattering field as discussed above. We will consider three cases to show how the Ramsauer-Townsend minimum occurs.

Case I. Here we have a weak field in which $n = 0$.

Figure 17 shows the variation of η_0 with k and q_0 with k . Clearly no Ramsauer-Townsend effect occurs in this case.

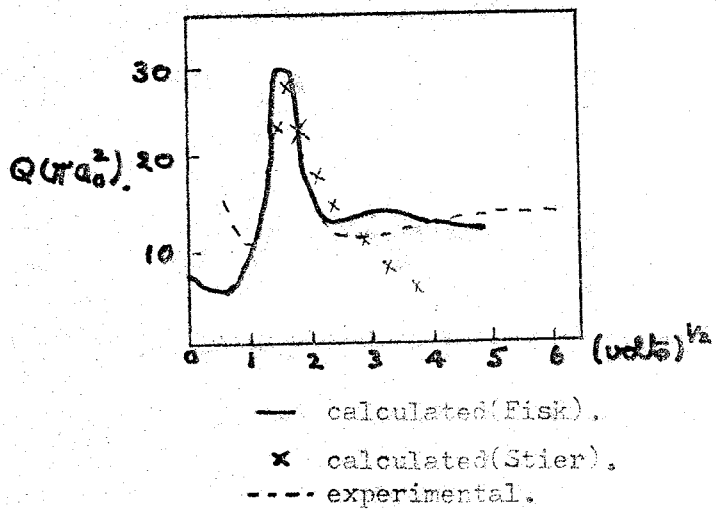
FIGURE 18.



TOTAL CROSS-SECTION OF ARGON.

- · - · - Total cross-section (Experimental).
- Total Cross-Section (Theoretical).
- - - Partial Cross-Sections.

TOTAL CROSS-SECTION OF MOLECULAR NITROGEN.



- calculated (Fisk).
- x calculated (Stier).
- - - experimental.

Case II . Here $n = 1$ and we have a stronger field. This is similar to Case I and again no Ramsauer-Townsend effect occurs.

Case III. Here $n = 1$, again, the field is stronger still, and q_0 returns to the value π at a finite electron energy and the variation of q_0 with k is typical of the Ramsauer-Townsend effect. Similar effects can arise for stronger fields with $n > 1$.

Whether we have a Case II condition with no minimum or a Case III condition with a minimum depends upon the scattering potential, at a particular energy, being of just the right strength to introduce a whole number of additional waves. One further condition for a true Ramsauer-Townsend minimum is that at the zero of q_0 the contributions to Q_T from higher order partial cross-sections must be negligible. This discussion is based on Mott and Massey (1965) and Holtsmark (1929). From this latter work we show how an observed total cross-section can be built up from theoretically calculated partial cross-sections. This is shown for the case of argon in figure 18. The heavier rare gases, krypton and xenon, also show a Ramsauer-Townsend minimum. This is due to the quasi-periodic behaviour of the zero order partial cross-section, q_0 , as the atomic number of the scattering atom changes. Thus in going from argon to krypton and krypton to xenon the scattering field increases in strength just the correct amount for a complete additional wavelength to be added

within the range of the field. The partial cross-section, q_0 does not alter but the zero order phase is increased by π . (Holtsmark, 1930).

The lighter rare gases, neon and helium, do not show a Ramsauer-Townsend effect. This is explained, in terms of the partial wave model, by Massey (1969). In the change of scattering field as we go from argon to neon the phase η_0 does not pass through a complete period. Massey also points out that the molecule methane (CH_4) gives a mean scattering field which produces a phase η_0 differing from argon by approximately π . It would seem that methane is the fourth member of the anomalous transmission series, preceding argon. We note that both methane and neon have atomic number ten and thus similar scattering fields. It would seem that neon corresponds to Case II, above, and methane to Case III. Thus, in summary, the partial wave model correctly predicts the Ramsauer-Townsend effect for the heavier rare gases. The zero order phase, η_0 , tending to $3\pi, 4\pi, 5\pi$ at low electron energies for argon, krypton and xenon respectively. It also correctly predicts that although the phases, η_0 , of helium and neon tend to π and 2π at low electron energies these will be no cross-section minimum as the variation of q_0 with k is not of the correct form. The common cross-section maximum for argon, krypton and xenon at about 13 eV is explained by η_2 tending to $\frac{1}{2}\pi, 3/2\pi, 5/2\pi$ respectively. There is no such effect for the lighter rare gases.

The large cross-sections of the alkali metals can also be explained by partial wave theory. The atomic field

of the alkali metals extends over greater distances than the field of the rare gas atoms and so the first order phase shifts are more important. The sharp maximum occurs when n_1 tends to an odd multiple of $\pi/2$. (Mott and Massey, 1965).

The similarity in the total cross-section function of the chemically similar atoms is perhaps one of the most significant results of this model as it permits an experimenter to predict qualitatively the cross-section function for a previously unstudied system. The chemically similar triads are argon, krypton and xenon; sodium, potassium and caesium; and zinc, cadmium and mercury. To show the generality of this model, Allis and Morse (1931) proposed a schematic atomic field of the form:

$$V(r) = \begin{cases} -Ze^2(1/r - 1/r_0) & (r < r_0) \\ 0 & (r > r_0) \end{cases} \quad (\text{I.4.34})$$

and calculated the phases for different values of the constants Z and r_0 . This is, in essence, a "shielded" coulomb interaction. They defined a quantity β as:

$$\beta = (Zr_0/2a_0)^{\frac{1}{2}} \quad (\text{I.4.35})$$

and showed that the partial cross-sections were quasi-periodic in β with a period of unity. Morse (1932) carried out more advanced calculations with an exponentially screened interaction.

This model can be used qualitatively with some success in considering the cross-section functions of molecules. We will consider this in more detail when we consider chemical models.

To obtain a satisfactory theory for low energy electron/molecule collisions we must extend the partial wave model. Atomic fields, to a first approximation, can be considered as possessing spherical symmetry. For molecules this is seldom possible, and even when it is, the ignorance of molecular structure leads to problems. The use of spheroidal coordinates permits solutions of the Schrödinger equation in terms of partial wave expansions which, for certain axially symmetric fields, can be applied to diatomic molecules.

We present, in outline, the theory of Stier (1932) and Fisk (1936) so that we can consider the applicability of this model.

The total angular momentum, J , about the centre of scattering is no longer a constant of motion. Instead, the component of angular momentum in the direction of the diatomic internuclear axis is constant and quantised in the usual form $m \hbar$ where $m = 0, 1, 2, \dots$. The incident wave can now be resolved into partial waves for which $m = 0, 1, 2, \dots$ and the total angular momentum in the united atom limit is $\{(\ell+m)(\ell+m+1)\}^{\frac{1}{2}} \hbar$. For each of these partial waves a phase shift, $\eta_{\ell m}$, is produced by the scattering field. Thus:

$$Q_T = \sum_{m\ell} q_{m\ell} \quad (\text{I.4.36})$$

where

$$q_{m\ell} = \begin{cases} (2\pi/k^2) \sin^2 \eta_{m\ell} & (m=0) \\ (4\pi/k^2) \sin^2 \eta_{m\ell} & (m \neq 0) \end{cases}$$

As k tends to zero (ie. electron velocity tends to zero) all the partial cross-sections tend to zero, except q_{00} which tends to a finite value. Fisk (1936) extended the

method of Allis and Morse (1931) for chemically similar atoms to molecules. He defined β in terms of Z and p_0 , analogous to the β of Allis and Morse in terms of Z and r_0 . As in the atomic case the partial cross sections are periodic with respect to β . The method was applied to the diatomic molecules hydrogen, nitrogen, oxygen and chlorine. The agreement for N_2 and O_2 is good but H_2 and Cl_2 show irregularities. The results for nitrogen along with the experimental values of Brüche and the calculation of Stier (1932) are shown in figure 18.

An approximate self consistent field for methane has been obtained by averaging the proton distribution over all orientations so as to obtain a spherically symmetric field due to all the nuclei. (Buckingham, Massey and Tibbs, 1941). They calculated the phases for scattering of electrons by this spherically symmetrical field, as previously explained, and found that close similarity to argon would be expected below 20 eV.

More recently Garrett (1972) has reviewed theoretical approaches to very low energy electron scattering by strongly polar molecules. He calculates values of the momentum transfer cross-section for molecules with permanent dipoles. This work and the work of Takayanagi and Itikawa (1968) may well be extended to give meaningful total cross-sections at higher energies for these polar molecules which are not, at the moment, amenable to a partial wave analysis. The work of these two groups is basically an extension of the work of Altshuler (1957) who applied the Born approximation to the scattering of

electrons by a stationary point dipole, with some success at thermal electron energies. The Born approximations are described in detail by Mott and Massey (1965).

Molecular hydrogen is the only molecule simple enough for "ab initio" calculations of scattering based on the theoretical structure of the molecule. Nagahara (1954) calculated the scattering by expanding the solution of Schrödinger's equation for the system in terms of spheroidal harmonics. Massey and Ridley (1956) included electron exchange in a variational solution of the Schrödinger equation. More recently Hara (1967) included dipole distortion of the molecule during impact. Only Hara's results have the same shape as the experimental results, but even here the quantitative argument is not very good.

To conclude this section on wave mechanical interpretations of the broad features of the total cross-section, we consider the agreement between advanced partial wave theory and modern experiment.

O'Malley (1963) applied effective range theory to calculating the total cross-section for low energy electron/helium and electron/argon scattering. He considered the case where the scattering interaction potential $V(r)$ falls off faster than any power of r , at large r . Then for all values of ℓ ,

$$k^{2\ell+1} \cot \eta_\ell = -1/a_\ell + \frac{1}{2} k^2 r_\ell + \text{higher order terms} \quad (\text{I.4.37})$$

where a_ℓ and r_ℓ are constants known as the scattering length and effective range respectively. It follows that

$$\lim_{k \rightarrow 0} Q = q_0 = 4\pi a_0^2. \quad (\text{I.4.38})$$

where a_0 is the scattering length for zero angular momentum. (O'Malley, Spruch and Rosenberg, 1960;1961; 1962). O'Malley writes the partial wave expansion of the total cross-section as:

$$Q_T = 3.517 \sum_{\ell=0}^{\infty} (2\ell+1) \sin^2 \eta_{\ell} / k^2 \quad (\text{I.4.39})$$

where $k^2 = (2m/\hbar^2) \cdot T$ and $T(\text{eV}) = 13.6 (ka_0^2)$, and calculates the phases in terms of effective range expansions of the form:

$$\tan \eta_0/k = -A - 0.284\alpha \sqrt{E} - 0.04902A\alpha E \ln E + BE$$

and,

$$\tan \eta_{\ell}/k = 0.8518\alpha \sqrt{E} / (2L+3)(2L+1)(2L-1)$$

where A is the scattering length, α is the atomic electric polarisability and B is another constant. O'Malley uses values of these constants derived from the experimental data of Golden (1966) to calculate values of the momentum cross section which he then compared with the experimental electron swarm data of Frost and Phelps (1964). The agreement is good. This technique may well prove very useful in the future for relating momentum transfer cross-sections and total cross-sections in the very low energy region.

Resonance Fine Structure.

An electron/atom or electron/molecule resonance may be defined as a temporary negative ion state capable of decaying by electron emission. The lifetime of such a state is usually between 10^{-5} seconds and 10^{-16} seconds. If the lifetime, τ , of the resonance is long compared

with the time the projectile takes to traverse the target then structure will be observed in the total cross-section due to the severe distortion of the incident electron wavefunction. Resonances are classified according to the mechanism by which the electron is trapped. The most fundamental division involves Type I resonances (or closed channel or core excited or Feshbach or compound state) and Type II resonances (open channel or one-body or shape). (Massey and Burhop, 1969; Bardsley and Mandl, 1968).

Type I resonances occur at energies below that of an excited atomic or molecular energy level, where one or more bound or compound states can occur. These bound states decay into lower energy states of the molecule and a free electron. The bound state lifetimes are between 10^{-12} seconds and 10^{-14} seconds.

Type II resonances occur at energies slightly higher than that of the atomic state. The interaction between an electron and a target molecule is sometimes repulsive at large separations passing through a maximum in intermediate separations and becoming attractive at closer distances. This maximum or barrier can trap an electron which then has to tunnel through the barrier to decay to the original state plus an electron. Excited states, as well as the ground state, can produce shape resonances.

A resonance can occur with energy corresponding exactly to the state of the atom or molecule. This unusual type of resonance, a mixture of type I and type II, is called a "virtual state" resonance. (Hasted, 1972).

The quantum mechanical treatment of resonances is complex and requires a good knowledge of the molecular wave functions of the states of the parent molecule and the transient compound state. A resonant state, ψ_n , has the same time dependence as a bound state, viz:

$$\psi_n \propto \exp(-i.W_n.t/\hbar) \quad (\text{I.4.40})$$

where W_n is, for a resonant state, a complex energy,

$$W_n = E_n - \frac{1}{2}.i.\Gamma_n$$

This shows an exponential decay,

$$|\psi_n|^2 \propto \exp(-\Gamma_n t/\hbar) \quad (\text{I.4.41})$$

where Γ_n is the width of the resonant state, and $\tau = \hbar/\Gamma_n$ is the lifetime of the state. Herzberg (1967) showed that near a resonance the cross-section $Q_\alpha(E)$ for any final decay channel, α , consists of three terms;

$$Q^\alpha(E) = Q_{nr}^\alpha(E) + Q_r^\alpha(E) + Q_{int}^\alpha(E) \quad (\text{I.4.42})$$

where E is the energy, Q_{nr} is the non-resonant cross-section ($\propto |\psi_{nr}|^2$), Q_r is the resonance cross-section ($\propto |\psi_r|^2$) and Q_{int} is an interference term proportional to the real part of the complex conjugate $|\psi_{nr}^*\psi_r|$. The maximum in cross-section observed in a transmission experiment comes from Q_r , while Q_{nr} contributes a smooth background. Under single collision conditions, the transmitted current is $I_0(1-\pi.Q_T)$. where I_0 is the incident electron current, π is the target parameter which we defined earlier, and Q_T is the total electron collision

cross-section. At higher pressures, the current is $I_0 \exp(-\pi Q_T)$. The fine structure in the transmitted current is thus enhanced at higher pressures where $\pi Q_T \gg 1$. A discussion of the interpretation of resonances in experimental transmission functions is given by Hasted (1972).

In molecules, a type I resonance may involve an electron being temporarily bound to either a valence or Rydberg excited state. A Rydberg state is a hydrogen-like orbital of high principal quantum number. Calculations, by Weiss and Krauss (1970), on the nature of the binding force on the additional electron in a type I resonance showed that only Rydberg excited states have a positive electron affinity for a fixed internuclear separation in the Franck-Condon region. Therefore, we can expect to find sharp resonances slightly below the excitation thresholds only for Rydberg excited states (ie. not for valence excited states). The temporary negative-ion consists of two Rydberg electrons trapped in the field of a positive-ion core. This positive-ion is called the grandparent state by Sanche and Schulz (1972b). The parent state is a single Rydberg electron bound to the grandparent ionic core.

Type I resonances have lifetimes which are long compared to the vibrational period of a molecule and so give rise to bands, each of which consists of a progression of vibrational levels. In experimental observations these progressions may overlap, which makes identification difficult. Sometimes the progression is cut off sharply

Periodic Group.

	IV	V	VI	VII	O	I
0	C	N	O	F	Ne	Na
1		CH	NH	OH	FH	
2			CH ₂	NH ₂	OH ₂	(FH ₂)?
3				CH ₃	NH ₃	OH ₃
4					CH ₄	NH ₄

No. of H atoms.

FIGURE 19.

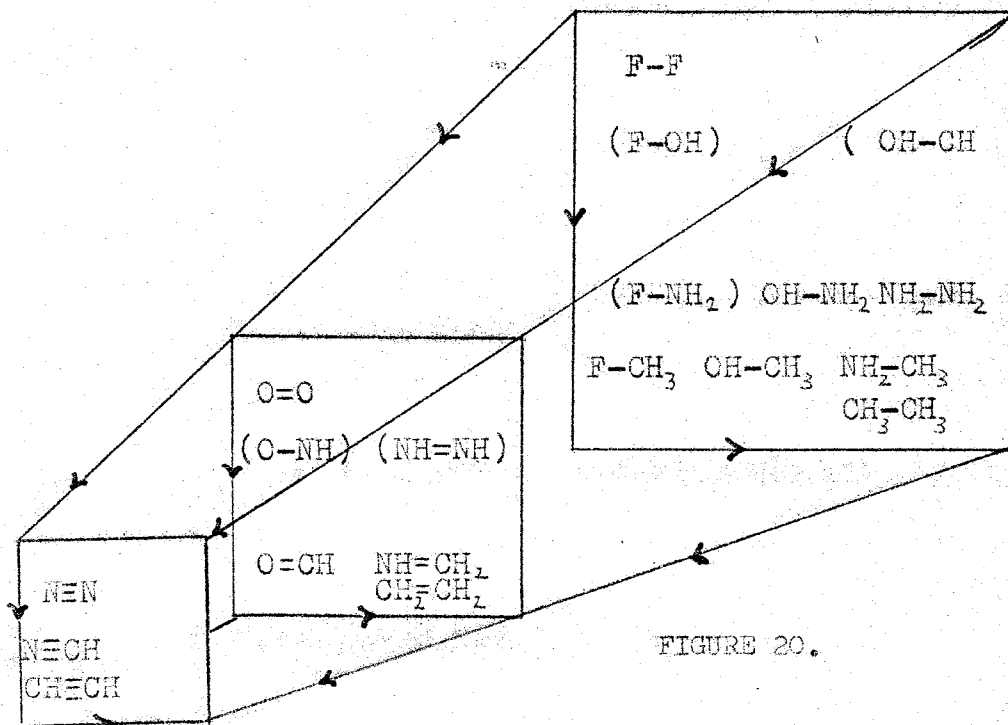


FIGURE 20.

at a certain vibrational level due to an alternative channel of decay existing at that energy. Finally, certain negative ion states are not seen at all in transmission experiments because their natural width is too large or because the Franck-Condon probabilities for excitation from the ground state are too small.

Chemical Models.

In this section we consider whether knowledge of the chemical structure of molecules can be used to correlate similarities in their total cross-section functions. This is not a topic which has been considered in any detail in the literature. The only work devoted to this topic is that of Schmieder-Oppau (1930).

We look first at relationships governed by Grimm's hydride shifting rules. The hydride shifting rule is shown in figure 19. The rule is based on the idea that if a hydrogen atom combines with another atom, e.g. a carbon atom, the hydrogen nucleus will be deep inside the electron shell of the new compound and its field strength will be shielded towards the outside almost completely. The new compound, the radical CH, with its five outer valence shell electrons should behave very similarly to any other atom with five outer shell electrons, such as the nitrogen atom. In the same way one expects that CH₂ would behave similarly to an oxygen atom, CH₃ to a fluorine atom and CH₄ to a neon atom. The hydride shifting rule shows a systematic change in atomic or pseudo-atomic radius and certain other characteristics as one proceeds

from CH_3 to neon. The cross-sections of the pseudo rare gases, a term introduced by Brüche, in the zero group of the periodic table in figure 19 have already been investigated in detail. Figure 15 of section I.3 shows very reasonable agreement for this correlation. The atoms and pseudo-atoms in groups IV-VII do not exist as stable entities on their own and can be considered only in molecular compounds.

Schmieder-Oppau (1930) presented a three dimensional table, shown in figure 20, which shows all possible stable molecular combinations of two atoms or pseudo-atoms from groups IV-VII. Again from figure 15, we can compare some of these groupings. For example, CH_3F , CH_3OH , CH_3NH_2 and CH_3CH_3 all show similar cross-section variation above about 9 eV. The absolute magnitudes of the cross sections are in the same ratio as the dimensions derived from the hydride shifting rule. At low incident energies we would not expect agreement as the electron is moving slowly enough to experience small variations in field. Another grouping which agrees well is that of nitrogen, hydrogen cyanide and acetylene. Again, above 9 eV the agreement is good but below this energy the individual peculiarities of the molecules are dominant. The common maximum at about 2 eV would seem to agree with the hydride rule, but the absolute magnitude of the HCN curve should be between that of N_2 and C_2H_2 . The very intense interaction shown, which does not agree with the hydride rule, is probably due to the dipole moment of HCN. Schmieder-Oppau tried to correlate the variation of dipole

moments with similarities in the cross-sections, but this was unsuccessful. Consideration of the wave mechanical models suggests that polarisabilities and induced multipoles are as important as permanent dipoles. The application of the rules to the pseudo-group O, NH, CH₂ is shown by the curves for (CH₃)₂O, ((CH₃)₂NH and (CH₃)₂CH₂. Here the agreement above about 6 eV is remarkable and the correct ratio of intensities is shown. As these are larger molecules the change in size in fitting in the radicals is smaller compared with the molecular size than in the previous example and therefore the change in cross-section with relationship is smaller. The last hydride relationship we consider is that between (CH₃)₃N and (CH₃)₃CH. The correlation here is similar to the other groups considered. We note that at higher energies (say above 25 eV) the molecular weight is important. The cross-section being higher for the lowest molecular weight compound in a group.

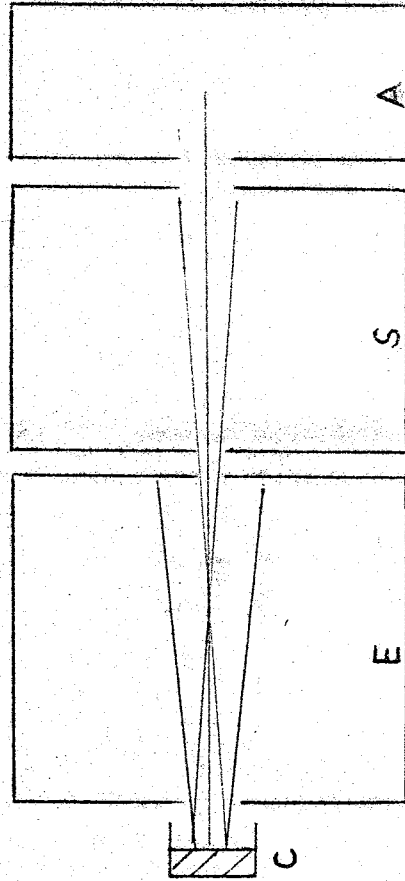
We next consider the influence of molecular shape. By considering chemical isomers, molecules containing the same atoms but differing in shape, it seems that molecular shape has little or no effect upon the total cross-section. It is only at low electron energies that any difference at all is seen. Figure 15 shows the following isomer cross-sections: C₅H₁₂ (n-pentane and tetramethylmethane), C₄H₁₀ (butane and isobutane) and C₂H₆O (dimethyl ether and ethanol). The C₂H₆O pair of isomers show distinct differences below 4 eV and these are likely due to dipole moment and polarisability effects.

A final possible correlation has been suggested. At low energies a radical, common to a group of molecules, can produce similarities in the cross-section curves. There is little evidence to support or qualify this. However, from figure 15, we see that compounds containing the hydroxyl radical (an electronegative grouping) such as propanol (C_3H_7OH), ethanol (C_2H_5OH), methanol (CH_3OH) and water all show a distinct minimum at about 4.5 eV. Further investigation of this might prove rewarding.

Chemical models do not compete with classical mechanical models or wave mechanical models. In fact they complement these detailed models and might prove useful in choosing empirical interaction potentials and estimating the cross-section curves of as yet unstudied compounds.

CHAPTER II. THE DESIGN OF AN ELECTRON TRANSMISSION
SPECTROMETER.

FIGURE 21. Schematic of Electron Transmission Spectrometer.



C - ELECTRON SOURCE.

E - ELECTRON OPTICAL REGION.

S - SCATTERING REGION.

A - COLLECTOR.

II.1 Electron Transmission Spectrometry

A basic electron transmission spectrometer consists of a source of electrons C, an electron optical region E, a scattering region S, and an electron collector A. The arrangement of these elements is shown schematically in figure 21. The purpose of the electron optical region is to focus the electrons from the source into a well-defined beam of the required energy, intensity, diameter and energy resolution.

Let $I_{(s)}$ and $I_{(a)}$ be the electron currents to the scattering region and the anode or collector, respectively. The sum of these two quantities is constant, if we neglect secondary electrons produced by ionisation of the gas in the scattering region or by secondary emission from metal surfaces. This constant current, I , is the current entering the scattering cell.

$$I = I_{(s)} + I_{(a)} \quad (\text{II.1.1})$$

We define $T(\epsilon)$ as a beam shape factor which describes the two-dimensional beam shape. $T(\epsilon)$ is normalised to unity by integrating over a reference plane, normal to the beam direction, which for convenience we take as the exit aperture of the scattering region. Thus $T(\epsilon)dS$ is the fraction of the full current passing through a differential element of area dS , normal to the electron beam axis, and,

$$\int_{\text{exit aperture}} T(\epsilon) \cdot dS = 1 \quad (\text{II.1.2})$$

The beam form factor does not depend on any effects attributable to the presence of scattering gas in the apparatus. It does depend upon

the nature of the electron optical region, space-charge effects, cathode effects, metal surface effects and collector efficiency. Thus

$$dI_{0(a)} = dI_0 \int_{\text{entrance aperture}} T(\epsilon) \cdot dS \quad (\text{II.1.3})$$

where the differential currents refer to currents in the energy range $\epsilon \rightarrow \epsilon + d\epsilon$, and the zero subscripts refer to currents measured with no scattering gas present ie. background currents.

When scattering gas is present the differential transmitted current, $dI_{(a)}$, is attenuated both by the scattering out of $dI_{0(a)}$ and the scattering in of $dI_{0(s)}$. To allow for this we define the event factor $G(\theta, \vartheta; \mu)$ as the fractional number of electrons scattered from a point in the interaction region, denoted by the generalised coordinate μ , into the solid angle $d\Omega (= \sin\theta \cdot d\theta \cdot d\vartheta)$ which are registered as scattering events at the collector. The total transmitted differential current is then,

$$dI_{(a)} = dI_0 \cdot \exp \left[-n \cdot \int T(\epsilon) \cdot G(\theta, \vartheta; \mu) \cdot \sigma_T(\theta, \vartheta) \cdot d\tau \cdot d\Omega \right] \quad (\text{II.1.4})$$

where n is the target gas number density and the integration is performed over the entire scattering region where there are beam electrons and any region outside this where the presence of gas can cause attenuation of the beam. If we now allow for the electron energy distribution of the beam, $f(\epsilon)$, then,

$$dI_{0(a)} = I_{0(a)} \cdot f(\epsilon) \cdot d\epsilon \quad (\text{II.1.5})$$

and the total transmitted current is obtained by integration with respect to energy, thus:

$$I_{(a)} = I_0 \int f(\epsilon) \cdot \left\{ \exp \left[-n \int T(\epsilon) \cdot G(\theta, \vartheta; \mu) \cdot \sigma_T(\theta, \vartheta) \cdot d\tau \cdot d\Omega \right] \right\} d\epsilon \quad (\text{II.1.6})$$

This is the basic equation for an electron transmission spectrometer relating the observable $I_{(a)}$, to the desired parameter Q_T where

$$Q_T = \int \sigma_T(\theta, \vartheta) \cdot d\Omega \quad (\text{II.1.7})$$

Under the ideal conditions of a beam of infinitesimal diameter in an apparatus with infinitesimal collimating slits then, $G=1$ for scattering out of $I_{0(a)}$, $G=0$ for scattering in of $I_{0(s)}$, $T=1$ for $I_{0(a)}$, $T=0$ for $I_{0(s)}$ and if this beam is monochromatic then $f(\epsilon) = 1$. In this case (II.1.6) reduces to the more familiar equation,

$$I_{(a)} = I_{0(a)} \cdot \exp(-n \cdot Q_T \cdot x). \quad (\text{II.1.8})$$

This discussion is based on the analysis of scattering experiments by Bederson and Kieffer (1971). For completeness we add here a point which they omit. In most electron spectrometers the current, I_0 , entering the scattering region is a function of the electron energy. This is due to the shape of the post-monochromator beam being altered when the voltage of the electrode defining the electron energy in the final stage of the electron optical region is varied. This can be allowed for either by including I_0 within the energy integral in (II.1.6) or, preferably, by defining I_0 as the current leaving the electron monochromator before the energy defining optical stage. The latter correction involves redefining the integration limits in (II.1.3). I_0 can also be a function of the gas pressure. This can be caused by gas effects on the emitting power of the cathode, background gas effects in the monochromator and associated optics, surface effects due to adsorbed gas and so on. One further source of error, which cannot be corrected for, is that $\sigma_T(\theta, \phi)$ which should be zero when $\theta = 0$, so that only the unscattered electrons are included, includes electrons scattered inelastically at $\theta=0$. This is not a very significant source of error. The "effective" total cross-section measured in any non-ideal transmission experiment is thus,

$$Q_T = (1/x) \int T(\epsilon) \cdot G(\theta, \phi; \mu) \cdot \sigma_T(\theta, \phi) d\tau \cdot d\Omega \quad (\text{II.1.9})$$

If we assume that the total transmitted current in the absence of gas $I_{0(a)}$, is proportional to the total available current

in the absence of gas I_0 , then we can write (II.1.8) in the form:

$$I_{(a)} = k.I_0.\exp(-n.x.Q_T). \quad (\text{II.1.10})$$

where k is a constant. Therefore, taking natural logarithms of (II.1.10),

$$\ln(I_0/I_{(a)}) = n.x.Q_T + k \quad (\text{II.1.11})$$

and from this result we see that a graph of $\ln(I_0/I_{(a)})$ versus $n.x$ should be linear with a slope of Q_T . This is a necessary, but not sufficient, condition for a meaningful transmission experiment.

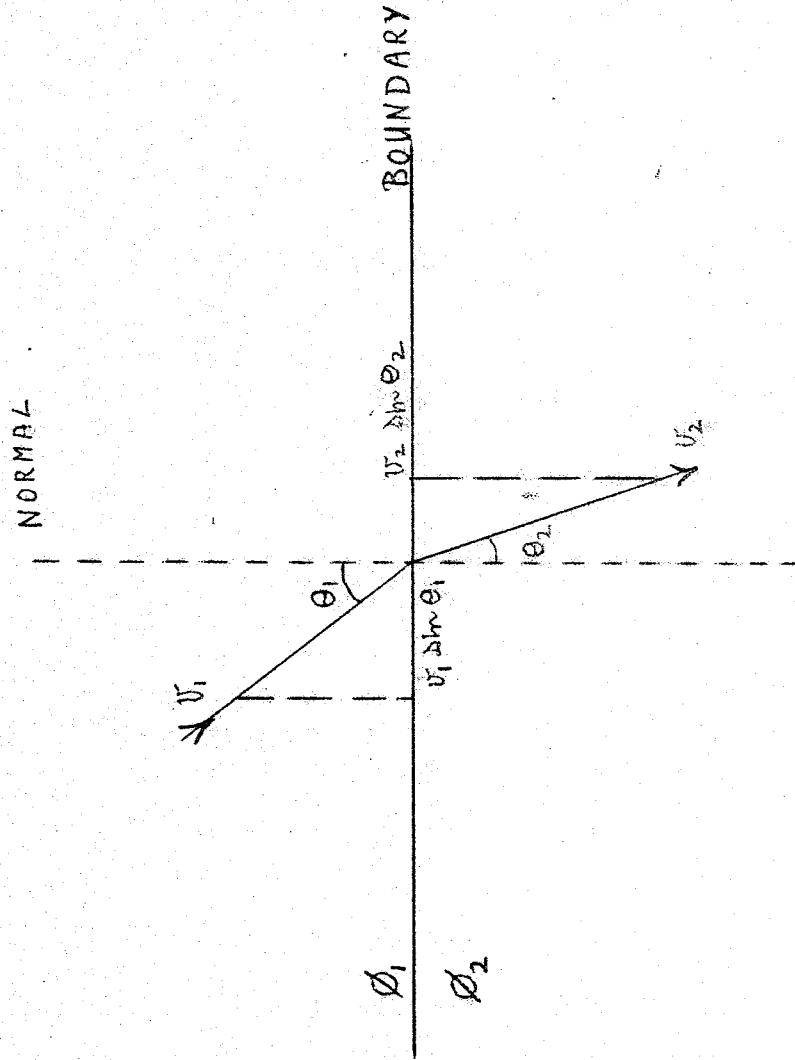
A quantitative treatment of the correction factors discussed in this treatment is not possible. However we can try to minimise their effect on the transmitted current when designing a transmission spectrometer and one approach to this is discussed in the next section.

After consideration of the factors discussed in the first chapter, it was decided to design and construct an electron transmission spectrometer capable of measuring the total electron collision cross-section of atomic and molecular gases and observing any fine structure in the transmitted current. To do this, we require an electron beam with certain properties. The intensity of the beam must be as great as possible, commensurate with any other properties we may require of the beam. The lower limit of current will be decided by the electron detector and the upper limit by space charge limits in the electron optical region. The energy of the beam will require to be variable over a wide range say, from 1 eV to 100 eV. As the energy is varied we will try to ensure that the current does not vary. The energy resolution required to observe fine structure can be decided by referring to literature of published resonance features. From this it appears that a suitable full width at half maximum (F.W.H.M.) of the electron energy distribution curve is better than 0.05 eV. We

also require that the beam diameter is as small as possible so that the entrance and exit apertures can be made small to reduce escape of gas from the scattering region and the scattering in and out discussed above.

Electron beam design or "electron optics" is in the process of transition from empirical rules based upon experience to mathematical design based upon theoretical models. From the relatively few published details on this topic we will present a simple design procedure which we have found to be practicable. We start by considering the basic phenomena of electron optics which are relevant to this problem, then consider the design of electron lenses to produce beams with desired properties.

FIGURE 22. Refraction of an electron ray at boundary between two regions of different potential.



II.2 Electron Optics Design.

Principles of Electron Optics.

The term "electron optics" is used when dealing with the behaviour of electrons that are under the influence of electric and magnetic fields. This arises because many of the laws that govern the behaviour of light rays are applicable to electrons. It is important to note that electron optics is based on a wave-particle analogy not a wave-particle duality.

We consider firstly, the properties of electrons in uniform electrostatic fields. Imagine an electron which moves in a region of uniform potential ϕ_1 . Its trajectory will be a straight line. If it now passes across a plane boundary to a region of potential ϕ_2 , the component of its velocity normal to the plane will alter, but that parallel to the plane will not be affected. This situation is shown in figure 22. Expressing electron speeds in terms of potential,

$$(2e.\phi_1/m)^{\frac{1}{2}} \cdot \sin\theta_1 = (2e.\phi_2/m)^{\frac{1}{2}} \cdot \sin\theta_2 \quad (\text{II.2.1})$$

and,

$$\sin\theta_1/\sin\theta_2 = (\phi_2/\phi_1)^{\frac{1}{2}} \quad (\text{II.2.2})$$

This is the electron optical form of Snell's law of refraction. The square root of the potential (or voltage with respect to cathode in a practical beam) can be regarded as the index of refraction. All the established rules applying to refractive indices in optical systems can be applied in electron optical systems, but electrons travel faster the greater the voltage, whereas light waves travel slower the higher the refractive index. One consequence of this difference is that although all light rays travelling from one point to another take the same time, electrons in the same situation do not.

A lens is a device which can form the image of an object. Electron beams in axially symmetric electric fields have this property and so constitute an electron lens. We can think of any lens, optical or electron, as a combination of three different regions of space: the object space, the lens space and the image space. In light optics the object and image spaces nearly always have the same refractive index. This is not often so in electron optics where the analagous property is electrostatic potential. If we assume that the inclination of the trajectory of an electron beam with respect to the axis of an electron optical system will always be small enough to allow us to replace the sine of this angle by its tangent or its arc, the analysis is greatly simplified. This is the Gaussian or "first order" approximation, sometimes called the paraxial ray approximation as the electron rays are close to the axis, and involves letting $\sin \theta$ be approximated by θ , where θ is the first term in the Taylor series expansion of $\sin \theta$, which converges rapidly.

Particles starting from points on a plane in object space (all having the same energy) are focussed into conjugate points on a plane in image space (the Gaussian image plane) by the action of the lens space, if and only if the particle trajectories are paraxial. This leads to a stigmatic (correct point to conjugate point) magnified or diminished image. We can consider the action of a lens conveniently by looking at the electron trajectories in object and image space only, regarding the lens space as a "black box". The particular nature of the lens system need not concern us at this stage.

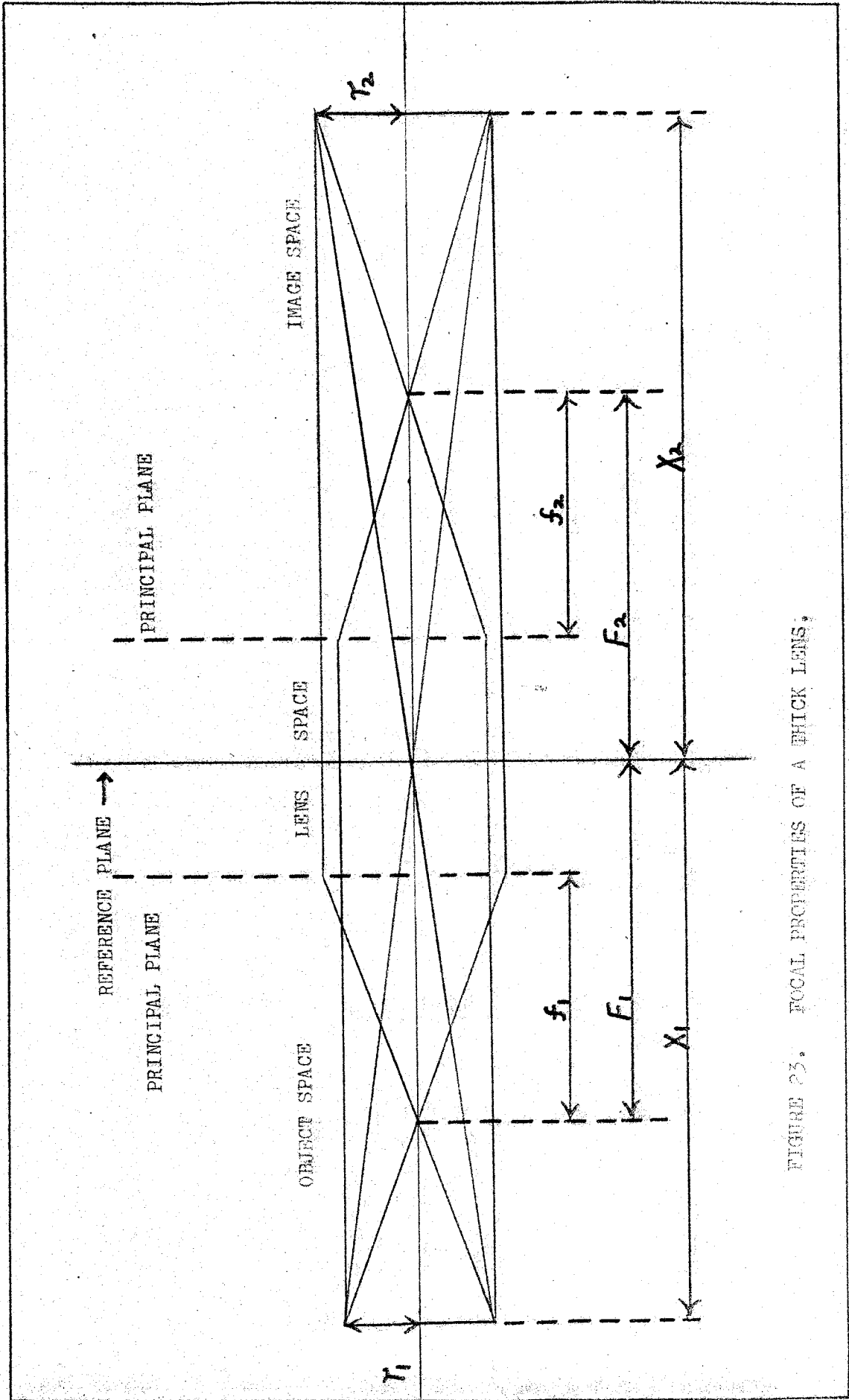


FIGURE 23. FOCAL PROPERTIES OF A THICK LENS.

The theory of Gaussian imaging (Klemperer and Barnett, 1971) shows that to uniquely define the properties of a lens or lens combination we need to know three special points on the axis in object space and their conjugate points in image space. These are the two focal points, two principal points and two nodal points. As a set, they form the cardinal points of the lens. In fact, only two pairs are independent and it is not usual to quote the nodal points of a lens as they can be calculated from the other cardinal points.

Figure 23 refers to any lens or combination of lenses. The focal points (where the focal plane intersects with the axis) are the image points of a beam of parallel rays (ie. objects at infinity). The principal points are the axial positions at which the planes of unit lateral magnification intersect with the axis and the nodal points are the axial positions of the planes of unit angular magnification. The distance between the geometrical lens centre and the focal point is called the mid-focal length, F . The distance between the principal point and the focal point is called the focal length, f .

The terminology referring to "thick" and "thin" lenses is different in light and electron optics. In light optics a lens whose physical dimensions are small (ie. thin) compared with the optical dimensions, such as focal length, is called a thin lens and the principal and nodal points are all coincident with the lens centre. Otherwise a lens is thick. In this sense, all electron lenses are thick lenses ie. they have distinct principal planes. Instead we

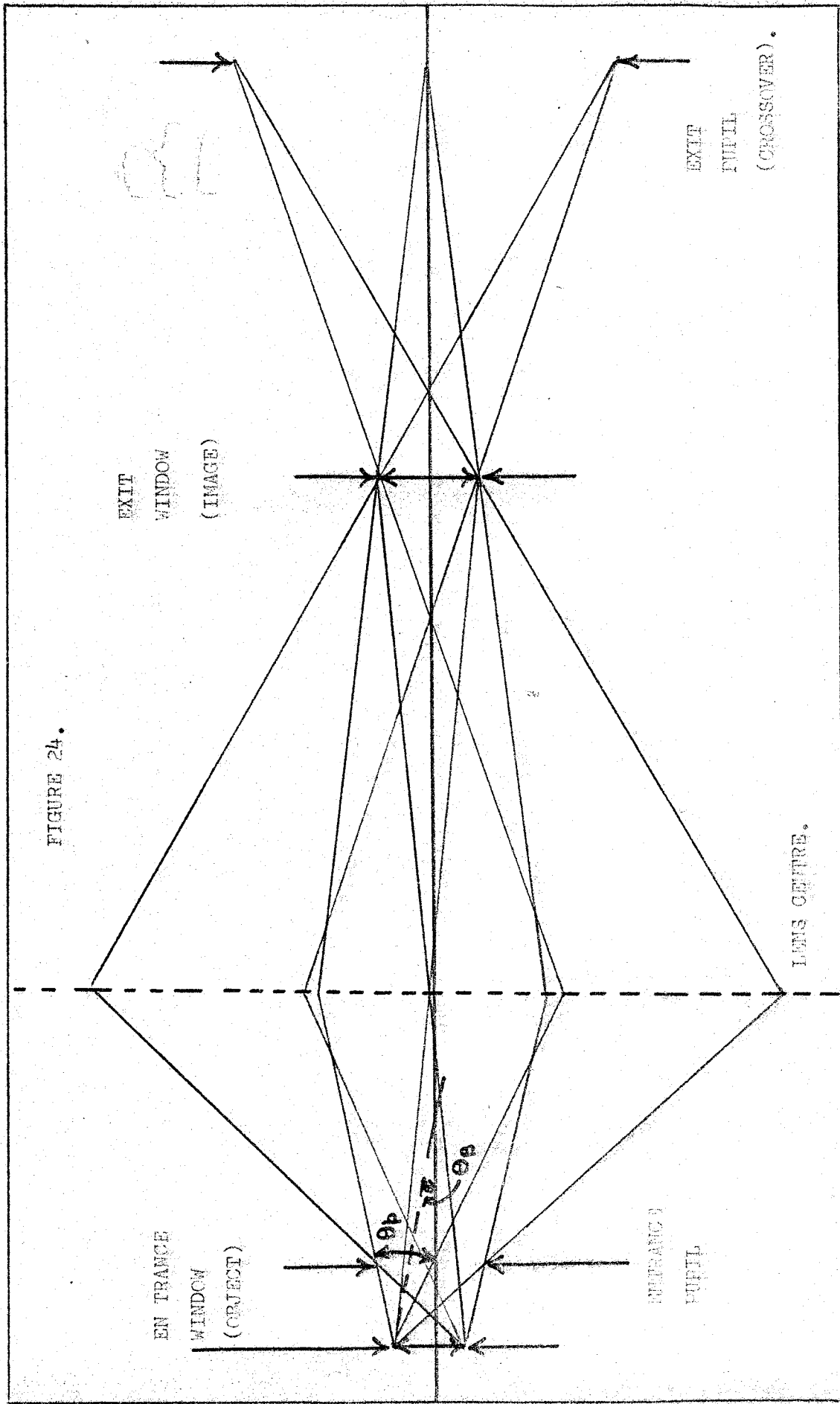


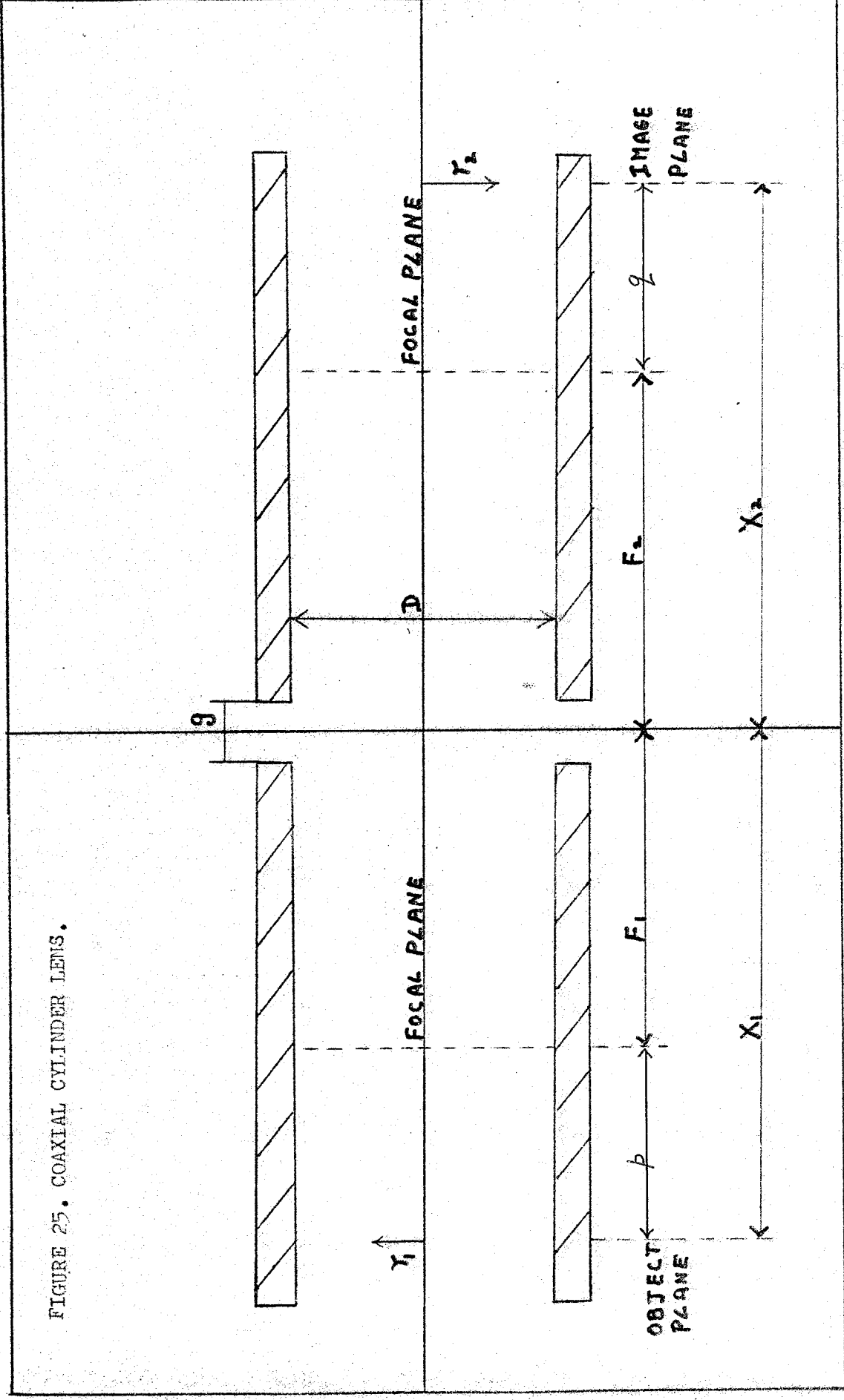
FIGURE 24.

introduce the terminology of a "weak" lens if the radial height of a ray does not change appreciably within the lens space, and "strong" lens if it does. Characteristically, strong lenses have short focal lengths, object and image distances etc. Weak lenses do not.

In this work all cardinal parameters are regarded as being positive numbers. The parameters referring to object space have the subscript 1, and those in image space the subscript 2. This simple convention is the same as that employed by Kuyatt and Simpson and by Read and his collaborators. Spangenberg uses the same nomenclature but introduces a cartesian sign convention whereby all parameters in image space are positive and those in object space negative. Heddle and El-Kareh use the same sign convention but a different nomenclature. The object and image focal lengths are (f_0, f_I); the mid-focal lengths are ($-Z_{m_0}, Z_{m_I}$) and the distances of the principal planes from the lens centre are ($-Z_{p_0}, Z_{p_I}$). The all positive sign convention has advantages in the preparation of lens data for computer handling.

Electron rays can leave a point on the object at any angle in the forward direction. However, the lens system limits the angular range of the rays which leave a point on the object plane and arrive at the conjugate point on the image plane. This bundle of rays is called a pencil. The maximum angle of the pencil is characterised by the pencil half-angle, θ_p , which is shown in figure 24. The pencil half-angle is not necessarily the same at the image as at the object. The central ray of the pencil makes

FIGURE 25. COAXIAL CYLINDER LENS.



an angle with the lens axis called the beam angle. The magnitude of this angle will depend upon the distance of the origin of the pencil from the axis. The maximum value of the beam angle is for the central ray of the pencil of rays connecting the extreme radial conjugate points on the object and image planes and is called the beam half-angle, θ_B . Another angular parameter, the angular divergence, is sometimes required. The angular divergence, θ , of any ray in the beam is the angle between that ray and the axis and the term "angular divergence of the beam" refers to the value for the extreme ray.

There are several types of electrostatic electron lenses. These involve cylinders and/or apertures. A basic lens can be formed by two cylinders, two apertures or an aperture and a cylinder. The simplest lens of all is a Calbick lens or a single aperture separating two regions of different potential. In electron lenses the potential of object and image space is not usually the same. If the image space voltage is greater than the object space voltage we say that the lens is accelerating and if not, then it is decelerating.

Figure 25 shows the thick lens terminology for a coaxial cylinder lens. This consists of two long thin coaxial cylinders of the same diameter, D , separated by a distance, g . The two cylinders are at potentials ϕ_1 and ϕ_2 (where the zero of potential is that at which the electrons would have zero kinetic energy) and the electrons are assumed to be travelling from the region at ϕ_1 to the region held at ϕ_2 . The principal planes are

reversed on the low voltage side for all two element lenses. Spangenberg and Field (1943) suggest this is not so for two-aperture lenses with the aperture spacing equal to the aperture diameter. The theory of Zworykin et al. (1945) shows this is impossible.

We define the lateral magnification of the lens, M , as

$$M = r_2/r_1 = f_1/p = q/f_2 \quad (\text{II.2.3})$$

and from this we can derive the analogue of the Newtonian Lens equation:

$$f_1 \cdot f_2 = p \cdot q \quad (\text{II.2.4})$$

If θ_1 is the angular divergence ($q.v$) at the object and θ_2 is the angular divergence at the image, then

$$\tan \theta_2 / \tan \theta_1 = p/f_2 = f_1/q \quad (\text{II.2.5})$$

For paraxial rays,

$$f_1/f_2 = (\theta_1/\theta_2)^{\frac{1}{2}} \quad (\text{II.2.6})$$

and from the definition in (II.2.3),

$$(\theta_1)^{\frac{1}{2}} \cdot \tan \theta_1 = M(\theta_2)^{\frac{1}{2}} \cdot \tan \theta_2 \quad (\text{II.2.7})$$

This is a form of Helmholtz and Lagrange's law, which we will discuss later. If the tangent function were replaced by a sine function, this equation (II.2.7) would be the Abbe-Helmholtz sine law. For paraxial rays these differences are trivial. For small angles, therefore;

$$(\theta_1)^{\frac{1}{2}} \cdot \theta_1 = M \cdot (\theta_2)^{\frac{1}{2}} \cdot \theta_2 \quad (\text{II.2.8})$$

If we define the angular magnification, m , as

$$\begin{aligned} \text{then,} \quad m &= \theta_2/\theta_1 \\ m \cdot M &= (\theta_1/\theta_2)^{\frac{1}{2}} \end{aligned} \quad (\text{II.2.9})$$

The accurate differential form of Helmholtz and Lagrange's law can be shown to take the form (El-Kareh and El-Kareh, 1970; Paszkowski, 1968):

$$E_1 \cdot d\Omega_1 \cdot dA_1 = E_2 \cdot d\Omega_2 \cdot dA_2 \quad (\text{II.2.10})$$

where E is the energy of the electron beam, $d\Omega$ the differential solid angle and dA the differential area perpendicular to the direction of motion of the electron beam. The subscripts 1 and 2 refer to any positions on the beam path. In words, the law states that current in the beam is conserved provided there is no energy dispersing device between positions 1 and 2. It is of advantage to define a quantity to represent electron beam brightness, current intensity or Richstrahlwert, R , where:

$$R = dI/dA \cdot d\Omega \quad (\text{II.2.11})$$

and dI is the current through the area dA . Thus combining the principle of conservation of current with equation (II.2.10),

$$dI/E_1 \cdot d\Omega_1 \cdot dA_1 = dI/E_2 \cdot d\Omega_2 \cdot dA_2 \quad (\text{II.2.12})$$

or

$$R_1/E_1 = R_2/E_2 \quad (\text{II.2.13})$$

So the ratio of Richstrahlwert to energy is a conserved quantity.

We cannot pass unlimited current through a lens. This is due to space charge effects from the mutual repulsion of the electrons in a beam. It can be shown (Pierce, 1954) that I_{\max} , the maximum current that can be passed through a tube of length x and diameter $2r$ is given by:

$$\begin{aligned}
 I_{\max} &= 38.5 \times 10^{-6} \cdot V^{3/2} \cdot (2r/x)^2 \\
 &= 38.5 \times 10^{-6} \cdot V^{3/2} \cdot \tan^2 \theta \quad (\text{II.2.14})
 \end{aligned}$$

where V is the kinetic energy of the electron beam (in eV) and θ is the beam divergence half-angle. The current is measured in amperes.

The incoming rays to a lens system are often defined by apertures. In fact, two apertures are necessary to specify the limiting rays accepted by a lens. Figure 24 shows the definitions of windows and pupils in a lens. The entrance window in object space (the object) becomes the exit window in image space. The entrance pupil becomes the exit crossover. In terms of the characteristic beam angles already defined, the beam half-angle θ_b and the pencil half-angle θ_p are, by definition;

$$\begin{aligned}
 \theta_b &= r_w / Z_0 \\
 \theta_p &= r_p / Z_0
 \end{aligned} \quad (\text{II.2.15})$$

where the separation of the window and pupil is Z_0 , and their respective radii are r_w and r_p . The pencil half-angle at the object is equal to the beam half-angle at the crossover, and the beam half-angle at the object is the pencil half-angle at the crossover. These relationships are very useful in design.

In a combination of several two-cylinder lenses, if two real apertures are given as the entrance window and pupil in the first object space, then we can calculate the exit (image) window and pupil for the first lens. Then use

this exit window and pupil as the entrance window and pupil for the second lens, and so on. With this knowledge, the redundancy and lack of design control which results from using more than two limiting apertures for a given lens system can be avoided. (Kuyatt, unpublished).

Before considering the application of these principles to lens design, we digress to consider one final constraint in the design of electron beams. This is the limit on the phase space of a beam imposed by Liouville's Theorem.

Phase Space restrictions

There is no published treatment of the application of phase space restrictions to electron lens design. A general treatment of Liouville's theorem in electron optics has been presented by Klemperer (1953) and Pierce (1954). Detailed treatments are available for heavy particle beams in magnetic fields mostly in advanced nuclear technology textbooks such as Banford (1966). The treatment presented here is based on unpublished communications with C.E. Kuyatt of N.B.S. Washington and F.H. Read of Manchester University.

A particle is completely specified if we know where it is and where it is going. Therefore we require to know the three cartesian coordinates x, y, z of the particle moving in a three dimensional cartesian coordinate system or configuration space. We also need to know the three momentum coordinates $m\dot{x}, m\dot{y}, m\dot{z}$. All this information can be represented by the position of a point in a six-dimensional space with the coordinates $x, y, z, m\dot{x}, m\dot{y}, m\dot{z}$

known as phase space. This is not the only phase space. In this six-dimensional phase space the motion of each particle depends on its own phase space coordinates alone, not on those of every other particle in the beam as well. In a system which allows mutual electrostatic repulsions between particles, we require a phase space of dimensionality $6N$ where N is the number of particles in the beam. The entire beam, in this case, is represented by one point in $6N$ -dimensional phase space. If we allowed for spin dependent effects, we would require an even higher dimensionality of phase space. Pierce (1954) has pointed out that the uses of phase spaces of dimensionality greater than six are of doubtful utility in beam transport problems.

A particle in a beam is represented by a point in phase space which moves in a manner connected with the motion of the particle in real or configuration space. A beam of particles is represented by a group of points in phase space. One for each particle in the beam. Thus, for a beam of finite dimensions the representative points will lie within a six-dimensional hypervolume in phase space.

We consider an infinitesimal volume element in six-dimensional phase hyperspace $dx, dy, dz, dp_x, dp_y, dp_z$. Now the 'face' of a volume element in N -dimensional hyperspace will have a dimensionality of $N-1$ and $2N$ faces. We consider the flow of representative points across the 12 five dimensional 'faces' of the infinitesimal six dimensional volume element and it can be shown that the divergence of n , the number of points, is given by:

$$\text{div } n = 0.$$

In words, this is Liouville's Theorem:

"Under the action of forces which can be derived from a Hamiltonian, the motion of a group of particles is such that the local density of the representative points in the appropriate phase space remains everywhere constant."

So if we can construct a Hamiltonian, as we can for any conservative system, then we can apply this theorem. Macroscopic external E and B fields are conservative but interactions with radiation or targets are not conservative. If the fields are time varying it is still possible to construct a Hamiltonian. We also impose the conditions: a). that there is no interaction between particles in the beam (eg. space-charge) and b). that there are no interactions dependant on spin, as either of these would involve a higher dimensionality of phase space.

Liouville's Theorem states that the local density of the particles in the hypervolume is constant under the action of conservative forces. This means that the shape of the hypervolume can change but not its volume. In fact, beam transport optics consists of the manipulation of phase space hypervolumes into shapes which represent the desired particle beam. Liouville's Theorem imposes a restriction on what may be done without loss of current, namely the conservation of the hypervolume.

If the three components of motion in configuration space are mutually independent then in phase space the motion is confined to three planes (x, p_x) , (y, p_y) and (z, p_z) which can be treated separately and Liouville's

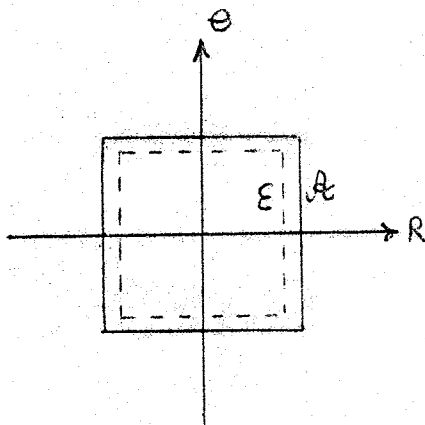
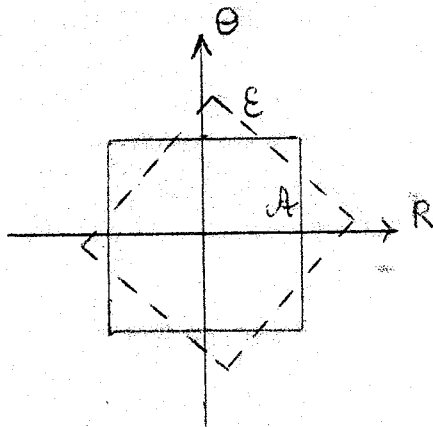
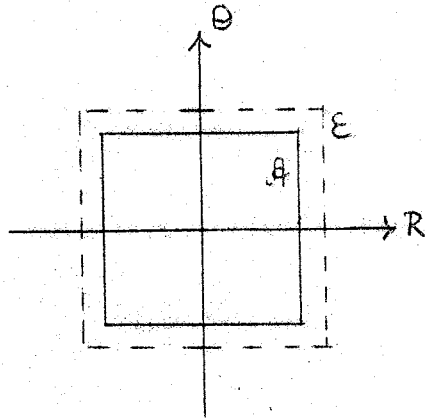
Theorem states that the areas of regions containing the representative points in each plane remain invariant though their shape may change. This is in fact the case for axially symmetric electric fields. Also, in regions where the axial momentum of the beam remains constant, such as object space or image space, but not in the lens itself, the electrostatic potential is constant and so the axial momentum is constant. If the z axis is the lens axis then in regions of constant potential, p_z is invariant, and the axial position coordinate z has no particular significance unless the beam possesses time structure.

Now the angular divergences x' ($=dx/dz$) and y' ($=dy/dz$) of a particle relative to the beam axis are equal to the ratio of transverse to axial momentum. Since axial momentum is constant we can replace p_x, p_y by dx/dz and dy/dz ; ie. by the angular divergences in the planes xz and yz . As we have rotational symmetry, these planes are equivalent. So, combining the above ideas we can use one transverse phase plane with coordinates x and x', y and y' or more usually R and θ . These two coordinates form a phase space parallelogram called an (R, θ) diagram. (Kuyatt, unpublished.)

If the phase space parallelogram represents some stage of an electron beam such as a real object or its crossover, a real image or its crossover, a virtual entrance or exit window or pupil in a system, we can define a new quantity: the emittance of a beam, ϵ ;

$$\epsilon = \frac{\text{area of phase space occupied by the beam}}{\pi}$$

FIGURE 26.



MATCHING OF R- θ ACCEPTANCE AND EMITTANCE PARALLELOGRAMS.

If the (R,θ) diagram represents some stage of an optical system (as opposed to the electron beam) such as a real aperture defining an object, image, pupil, etc., then we can define a quantity for the system analogous to the emittance of a beam. This is the acceptance of the system, A ;

A = phase space area containing all the points whose input displacement/divergence coordinates are such that the particles they represent will be transmitted by the device.

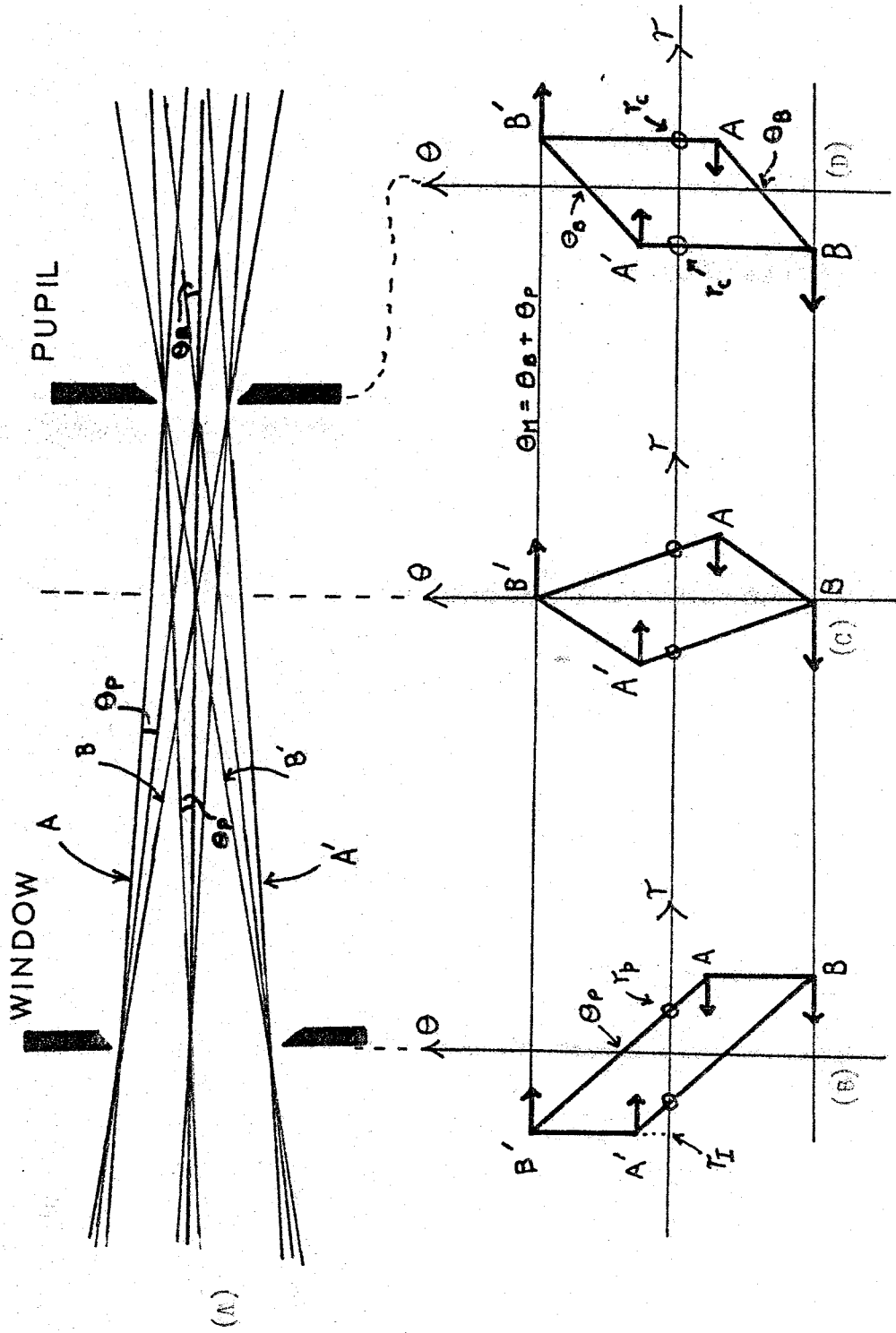
If A is less than ϵ then only that part of ϵ falling within A will be transmitted. The shape of ϵ and A is important, not just the area. The area we cannot control beyond making sure that ϵ is less than A but the shape we can control. This is called matching. (Banford, 1966).

Diagram 26a. shows a case where the beam is not matched to the optical system, diagram 26b shows a case where the emittance matches the acceptance of the system but the shape of the phase space hypervolume forbids total transmission and diagram 26c. shows a well matched system. The full lines represent the parallelogram for the acceptance of the system and the dotted lines represent the parallelogram for the emittance of the beam.

Our main use of (R,θ) diagrams is in studying relations between windows and pupils in object or image space. If these are real we have an emittance parallelogram and if virtual we have an acceptance parallelogram.

PHASE SPACE DIAGRAMS IN ELECTRON OPTICS.

FIGURE 27.



As an example we calculate the (R, θ) diagrams for a system comprising an image and crossover (ie. a virtual exit window and pupil). (Figure 27a).

The area of the parallelogram does not change as we pass along the system, showing Liouville's Theorem in practice, but the shape does. The edges of the parallelogram represent the extremes of the system but all rays in the system are represented within the parallelogram.

The extreme value of the radius is $\pm r_I$ and the extreme values of the divergence angle θ for the pencils at $\pm r_I$ are $\pm (\theta_B + \theta_P)$ and $\pm (\theta_B - \theta_P)$. Thus the four points of the parallelogram are:

$$\begin{aligned} & (+r_I, -\theta_B - \theta_P), (+r_I, -\theta_B + \theta_P), (-r_I, \theta_B + \theta_P) \text{ and} \\ & (-r_I, \theta_B - \theta_P). \end{aligned}$$

Note that the angle convention is that if the angle made with the axis is greater than 90° then that angle is negative. (In practice the lesser angle with the axis is always chosen but if it does not slope in the direction of the axis it is negative). The (R, θ) diagram for the image is shown in figure 27b.

This is sufficient information for plotting the parallelogram but it is interesting to plot the points where the parallelogram would cut the axis. The R-axis is cut at $\pm r_C$. This is because on the R-axis, $\theta=0$ and for a ray to be transmitted by the system the maximum radial height it can have when parallel ($\theta_B=0$) is r_C , the pupil radius. The θ -axis is cut where $r=0$, and here the maximum transmission angle is θ_P .

The diagram for position X_A is shown in figure 27c. Here the θ coordinates remain the same and as we move along the beam path the positive angle corners move to the right and the negative to the left. The extreme r values lie midway between r_C and r_I at, say, r_X . The parallelogram again cuts the axis at r_C , as this is the maximum radius at which transmission can still occur.

For the crossover the extremes are now $\pm r_C$ and the parallelogram cuts the R-axis at this point. (Figure 27d).

Electron Lens Design.

A convenient way to describe an electron beam is to specify it in terms of many infinitesimal pencils of electron rays. In purely electrostatic focussing systems an electron ray at any point along the beam is completely defined by its radial displacement r , and the angle of divergence θ . Paraxial electron rays have small spatial extent along the axis and negligible energy spread. For such rays the displacement and divergence of a point in object space and the conjugate point in image space can be related by linear simultaneous equations, thus:

$$\begin{aligned} r_2 &= a_{11} \cdot r_1 + a_{12} \cdot \theta_1 \\ \theta_2 &= a_{21} \cdot r_1 + a_{22} \cdot \theta_1 \end{aligned} \quad (\text{II.2.16})$$

where the subscripts 1 and 2 refer to object and image space, respectively. The coefficients a_{ij} are characteristic of the focussing device, which can be a single lens or a system of lenses.

Equations (II.2.16) can be more conveniently written in the matrix form;

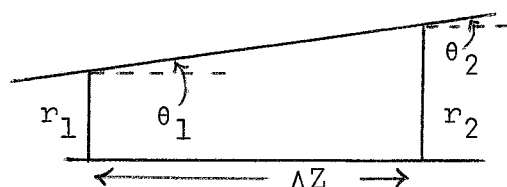
$$\begin{pmatrix} r_2 \\ \theta_2 \end{pmatrix} = \hat{A} \cdot \begin{pmatrix} r_1 \\ \theta_1 \end{pmatrix} \quad (\text{II.2.17})$$

where \hat{A} is the (2x2) matrix,

$$\hat{A} = \begin{pmatrix} a_{11} & a_{12} \\ a_{21} & a_{22} \end{pmatrix} \quad (\text{II.2.18})$$

We will call \hat{A} the lens transfer matrix. For a series of lenses the overall properties can be represented by a system transfer matrix which is the matrix product of the individual lens transfer matrices.

We consider initially the lens transfer matrix for a beam in object or image space. In this case, as we have a region of uniform potential, the lens action is merely that of linear displacement, not focussing. A linear displacement ΔZ in a uniform field can be represented as follows:



Now,

$$\left. \begin{aligned} r_2 - r_1 &= \Delta Z \cdot \tan \theta_1 \\ &\approx \Delta Z \cdot \theta_1 \end{aligned} \right\}$$

and

$$\theta_2 = \theta_1.$$

(II.2.19)

We can rewrite these equations in the form of equations (II.2.16), viz.,

$$r_2 = r_1 + \Delta Z \cdot \theta_1$$

$$\theta_2 = 0 + 1 \cdot \theta_1$$

which in matrix form gives the equation:

$$\begin{pmatrix} r_2 \\ \theta_2 \end{pmatrix} = \begin{pmatrix} 1 & \Delta Z \\ 0 & 1 \end{pmatrix} \cdot \begin{pmatrix} r_1 \\ \theta_1 \end{pmatrix} \quad (\text{II.2.20})$$

With the knowledge of the free space transfer matrix we can consider the focussing properties of a thick lens. As before, we split the lens into three sections. The object space, from the object plane to the first principal plane, which has a transfer matrix \mathcal{M}_I . The lens space, from the first to the second principal plane, which has a transfer matrix \mathcal{M}_{II} and the image space, from the second principal plane to the image plane, with transfer matrix \mathcal{M}_{III} . The terminology has already been described in figure 2.3. We have already derived the form of \mathcal{M}_I and \mathcal{M}_{III} .

$$\mathcal{M}_I = \begin{pmatrix} 1 & (X_1 - F_1) + f_1 \\ 0 & 1 \end{pmatrix} \quad (\text{II.2.21})$$

$$\text{and} \quad \mathcal{M}_{III} = \begin{pmatrix} 1 & (X_2 - F_2) + f_2 \\ 0 & 1 \end{pmatrix} \quad (\text{II.2.22})$$

\mathcal{M}_{II} must be such that the displacement r does not vary, whereas the divergence θ must change according to the ratio of the focal lengths and the incoming displacement.

$$\underline{m}_{II} = \begin{pmatrix} 1 & 0 \\ -1/f_2 & f_1/f_2 \end{pmatrix} \quad (\text{II.2.23})$$

It can be shown to be a consequence of Liouville's theorem that the matrix determinant $|A|$ of a transfer matrix A must be unity for conservative systems such as displacement in a uniform field. Thus $|m_I| = |m_{II}| = 1$. This will prove a useful check in our design procedure. The lens transfer matrix for a thick lens is obtained by matrix multiplication.

$$\underline{m} = \underline{m}_{III} \cdot \underline{m}_{II} \cdot \underline{m}_I \quad (\text{II.2.24})$$

The order of multiplication is important as the transfer matrix is an operator.

Thus combining equations (II.2.21) thru (II.2.24) we get the lens transfer matrix for a thick lens.

$$\underline{m} = \begin{pmatrix} \frac{-(X_2 - F_2)}{f_2} & \frac{-(X_1 - F_1)(X_2 - F_2)}{f_2} + f_1 \\ -1/f_2 & \frac{-(X_1 - F_1)}{f_2} \end{pmatrix} \quad (\text{II.2.25})$$

The meaning of this matrix can be expressed as:

$$\begin{pmatrix} \text{linear magnification} & \frac{\text{distance out}}{\text{input angle}} \\ \frac{\text{output angle}}{\text{input distance, parallel ray}} & \text{angular magnification} \end{pmatrix}$$

The details of this derivation are given by Halbach (1964) in a treatment of matrix methods in Gaussian light optics.

We can interpret the meaning of the transfer matrix by considering what happens when any of the matrix elements disappear.

If we set $a_{11} = 0$ in (II.2.18) then in (II.2.16) we see that if $\theta_1 = 0$ ie. a parallel beam, then $r_2 = 0$ independently of the value of r_1 . This is merely the definition of a focal point. Similarly, if $a_{22} = 0$, then for $r_1 = 0$ all $\theta_2 = 0$. This is the definition of the other focal point. If $a_{21} = 0$, then $\theta_2 = a_{22} \cdot \theta_1$ we have the condition for a telescope focussed at infinity. Finally, if $a_{12} = 0$ then $r_2 = a_{11} \cdot r_1$. This is the imaging condition.

The way in which we apply these relationships to design problems is as follows.

- 1). To calculate X_2 (the image distance) for a given object position at X_1 , the lens cardinal data being known. Here we set $a_{12} = 0$ and solve for X_2 . Note that X_1 does not need to be the object distance. It can be the axial position of anything in object space, such as an entrance pupil, a limiting aperture, etc. Obviously, if we should require to do so, we can specify an image distance and calculate the corresponding object distance. The linear and lateral magnifications of the lens are then found by evaluating the matrix elements a_{11} and a_{22} respectively.
- 2). To calculate the radius of a beam at various points in image space (X_2) for a given object distance (X_1). Again the lens cardinal data is known.

This problem is related to the discussion in section II.1. We showed there that if the electron beam entering a scattering region was strongly divergent then part of it, $I_{0(s)}$, would never reach the collector, even in the absence of gas. If we could calculate the beam radius at every point in the scattering region then we can design to overcome this problem. The technique in this case is to calculate a_{11} for various values of X_2 . Note in this case we are not solving (II.2.16) for an imaging condition.

3. To calculate the image position (X_2) where the beam will have a desired radius. Once again we assume that the object position (X_1) and the lens cardinal data are known. This is similar to case 2. We let a_{11} equal the quotient of the required image radius and the object radius, and solve the resultant equation for X_2 . This is useful for deciding where to place a limiting aperture in a design problem. For example, sometimes it is necessary to remove scattered electrons from a beam by inserting an aperture exactly the size of the beam in the beam path.
4. To calculate the divergency of a beam (θ_2) at a known position (X_2) in image space. This problem arises, for example, when designing the input stages to an electron monochromator. The details of this will be discussed at a later stage, it is sufficient here to state the

requirement that the electrons must enter the monochromator as nearly parallel as is possible (ie. $\theta_2 \rightarrow 0$). We insert the value of X_2 into the matrix elements (a_{21}, a_{22}), along with the fixed values of X_1 and the cardinal parameters, and evaluate the matrix elements. Substitution of these in the second equation of (II.2.16) gives the required value of θ .

There are many other applications but these examples were those that were found most useful in design problems. It is useful to note that the determinant of the lens transfer matrix (II.2.25) is always f_1/f_2 , the ratio of the focal lengths. This is a very useful check when performing lengthy calculations by hand or especially in the computer.

One of the most useful applications of the matrix method is in dealing with systems of lenses. If we have two lenses in the beam path we can, on paper, combine them into one composite lens by multiplying the individual transfer matrices together in the correct manner. However if the two lenses are so close together that no image is formed in that region which is the image space of the first and the object space of the second lens then we can still calculate the two transfer matrices, but in this case the object distance for the second lens will be zero. Thus we can calculate object and image space parameters for the three element or einzel lens by treating it as a combination of two simple two element lenses. An example of this is shown in the present design.

For completeness we give the transfer matrices for two other systems of electron optical interest. The first is the single aperture or Calbrick lens. This is the limiting case of the thick lens when $f_1 = f_2$. If ϵ_1 and ϵ_2 are the potentials at either side of the aperture and the aperture is at a voltage V_0 then the lens transfer matrix is,

$$\tilde{A} = \begin{pmatrix} 1 & 0 \\ -\frac{(\epsilon_2 - \epsilon_1)}{4V_0} & 1 \end{pmatrix} \quad (\text{II.2.26})$$

and the transfer matrix for a region where the beam is accelerated or decelerated is,

$$\tilde{A} = \begin{pmatrix} 1 & \frac{2V_0}{\epsilon} \left(\sqrt{\frac{V_1}{V_0}} - 1 \right) \\ 0 & \frac{V_0}{V_1} \end{pmatrix} \quad (\text{II.2.27})$$

Electrostatic lenses may be constructed with electrodes of many shapes, but for the control of electron beams of small angular divergence (say not greater than 0.1 radians) conventional aperture or cylinder lenses are adequate. The cylinder lens has certain minor advantages over the aperture lens. These are, firstly the ease of mechanical construction and of optical coaxial alignment; secondly, the ability to contain

stray electrons, because the gaps between the lens elements are smaller and easier to shield; and thirdly, less risk of perturbations when combining lenses because the elements are not short compared to their diameters.

The matrix technique can be applied to coaxial cylinder lenses if we know the focal parameters $-f_1$, f_2, F_1, F_2 . These parameters are functions of a) the gap between the two cylinders, b). the diameters of the two cylinders, which may or may not be the same, and c). the potentials of the two cylinders. These dependencies are normally expressed by listing values of each particular focal parameter for different values of the ratio of cylinder potentials, γ , (where γ is the ratio of image potential to object potential) for a fixed value of the ratio g/D , where g is the gap between the cylinders and D is the diameter of both cylinders.

Electron lens design involves selecting a value of the potential ratio γ , obtaining values for the focal parameters associated with this value of γ , employing these values of the focal parameters to evaluate the lens transfer matrix for a particular object distance (X_1) and finally using the matrix to calculate the required properties of the lens as discussed earlier. We then assess whether this value of γ gives a lens with the required properties and if it does not, select a new value of γ and repeat the procedure until the answer is suitable. If the value of γ does correspond to a suitable lens our problems may still not all be solved. For example, the value of γ may require that the electron energy in the final image space is unsuitable for the requirements of a

scattering experiment. Or, although the value of the final image parameter of interest is suitable, one of the other parameters may have an unsuitable value. Here we can try several possible alternatives. We can try a different lens diameter or lens gap, or alter the length of the object distance or the size of the object. If no suitable solution is found we can try and solve the problem in stages by using a combination of lenses.

This is obviously a "trial and error" procedure involving many repetitive calculations with several independently variable input parameters and with design constraints applied on one or more of the output variables. A system of this complexity which involves a large number of repetitive calculations is ideally suited for treatment by computer methods. To give an idea of the amount of human labour saved by employing a computer technique we will take as an example the design of a simple two-element aperture lens to provide an image of stated size with an upper limit on the magnitude of the extreme pencil angle. On paper the procedure was as follows.

- 1). The object distance was chosen arbitrarily and the object radius and angular divergence were fixed by earlier lenses in the system. The potential of the image was also fixed so the system variable became the object space potential.
- 2). A set of graphs relating γ and f_1, f_2, F_1, F_2 were consulted and the values of these parameters for an arbitrary value of γ were read off.

- 3). The lens transfer matrix was calculated (a time consuming process as units are involved) and the matrix elements solved to give the required parameters of M , the lateral magnification, m , the angular magnification, and the image position.
- 4). From M and m the image radius and image angular divergence were calculated.
- 5). These values were considered with regard to the limits set upon them in step 1).

This procedure takes about 15 minutes. If step 5) gives unsatisfactory results we now have to vary γ or X_1 . The possibilities are nearly unlimited. Sometimes M would be suitable but m unsuitable or vice versa. Selecting values of γ or X_1 at random it was very difficult to get a clear picture of the dependence of m and M on γ and X_1 . Before a suitable value of γ was found, over eight hours of calculation were involved and towards the end arithmetic mistakes became more and more frequent. Even then the answer was not perfect. The impression was that if we could vary X_1 slightly and adjust γ accordingly then the values of M and m might be even more suitable. However this could have doubled the calculation time so was not attempted. Some time later, when the computer design technique was in use, we repeated the above calculation. Although, there was now the capability to include many more input and output parameters we restricted the exercise to the variables stated in step 1). The

only work involved was typing an initial value of γ , an initial and final value of X_1 and the values of object radius and divergence on a computer data card. After 12 seconds of computation we had listings of values of γ (in steps of 0.1 from 2 to 20) with the corresponding values of X_2 , m , M , r_I , θ_I and θ_P for 20 values of X_1 . This involves 3,600 repetitions of steps 1-5. It was simple to pick out the correct conditions from such detailed lists. A similar study on paper would have taken 900 hrs, and this was one of the simplest lens design problems.

These comments might suggest that lens design without a computer is impossible, but this is not so. What is impossible is detailed design involving several parameters. If one merely requires to image an object at some point the problem is not involved. However the design of lenses to perform specific operations over a specified range of γ necessitates computer treatment.

Before a computer program or programs can be written to accomplish design requirements we require to store in the computer memory the relationship between γ and the focal parameters f_1, f_2, F_1, F_2 for the particular two-cylinder lens we are using. In the terminology of computer programming this is called the data base.

Before considering how to store the data base in the computer, we will consider the data sources. There are only two sources of experimental data on two cylinder coaxial lenses. (Spangenberg and Field, 1942;1943; Klemperer and Wright, 1939;Klemperer, 1953). Spangenberg

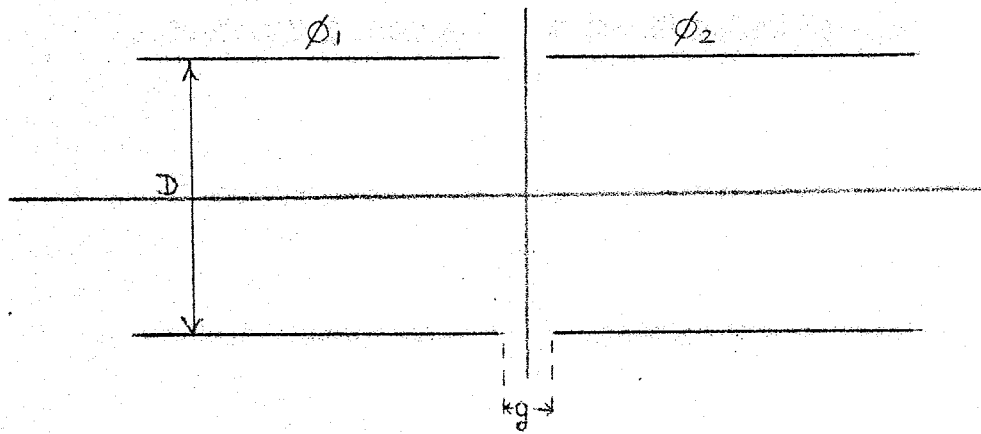
considered lenses with $g/D = 0.1, 0.5, 1.0$ and Klemperer only investigated the case of $g/D = 0$ ie. zero-gap lenses. Kuyatt (1967) in unpublished works claims that the accuracy of Spangenberg and Field's work is about 20%. In more recent theoretical work (Kuyatt, Natali, DiChio and Uva, 1972b) he revises this estimate to 10%. It is very difficult for a designer to assess the absolute accuracy of lens data. He cannot accurately measure the position of focal points etc. or even of derived parameters such as image position and magnification. The only design assessment we can make is that using a certain data set the lens behaves as predicted, whereas another data set does not work so well. However comparison of Spangenberg's data with recent theoretical data does seem to confirm this error estimate. The difficulties involved in making experimental measurements are fully reviewed by Klemperer and Barnett (1971). The first theoretical treatment was that of Epstein (1936) who used an electrolytic tank to determine the potential distribution of a two cylinder lens with $g=0$ for $\gamma = 4$. Firestein and Vine (1963) used a resistor network to find the potential distribution of the lenses with $g/D = 0$ to $g/D = 1.0$ for $\gamma = 3, 6, 11, 51$. Other theoretical work has been based upon solving the ray trajectory equation for a calculated potential (Bertram, 1940). The theoretical data sets which we considered for use were those of Ramberg (1942), Goddard (1946), Verster (1963), Grivet (1965), Bernard (1967), Paszkowski (1968), El-Kareh (1969,1970), Read (1969a,1971), Read, Adams and Soto-Montiel (1971) and Kuyatt et al. (1972a,1972b,1972c).

All of these present numerical focal values for selected values of γ between 1.5 and 50 . Verster and Grivet only considered $g/D=0$ lenses. El-Kareh and Read, Adams and Soto-Montiel (1971) studied $g/D=0,0.1,0.5$ and 1.0 . Kuyatt, so far, has only considered $g/D=0.1$. The most accurate are those of Kuyatt and Read, which are of the order of 0.1% or better. For practical purposes we can consider these two data sets as equivalent. One problem remained however. These calculations were only performed for about 20 values of γ between 1.5 and 50. A useful data base for computer calculations would require about 500 values of γ in this region. The problem cannot be solved by graphical interpolation as this would not preserve the accuracy of the data. The best way would be to present the data as a set of empirical equations representing the relationships between γ and the focal parameters. Grivet represented his data in this way and Wei (1969) employed these equations to provide a data base for some computer lens designs. Grivet's equations were not suitable for our purpose as, apart from the limited accuracy, the range of γ is only 1.5 to 10. We decided therefore to try and represent Read's data in the form of polynomial expansions. We call this study, the parametrisation of lens data. Our first attempt was a power series fit using a Chebychev polynomial of the form,

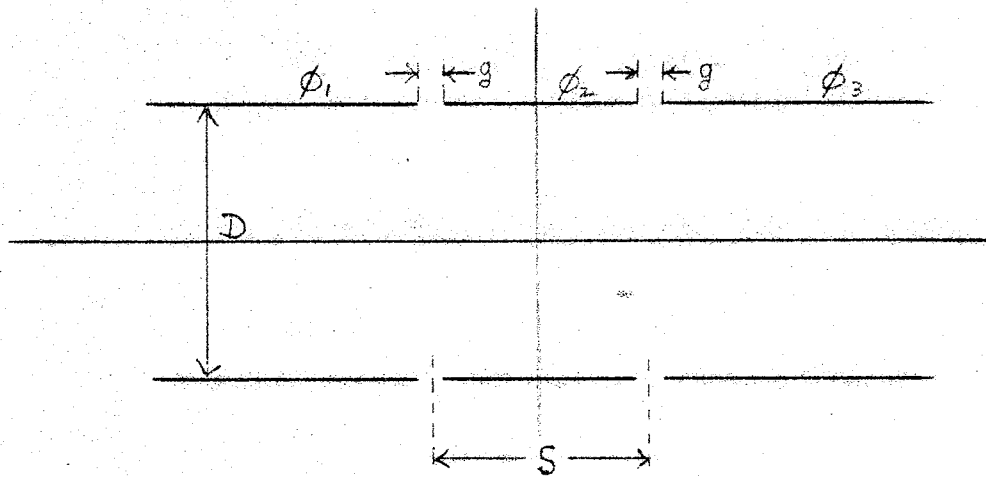
$$f = a_0 + a_1 \cdot \gamma + a_2 \cdot \gamma^2 + \dots + a_N \cdot \gamma^N \quad (\text{II.2.28})$$

The maximum value of N was 20. This necessitates at least $N+2$ known data points (ie. literature values). f is a

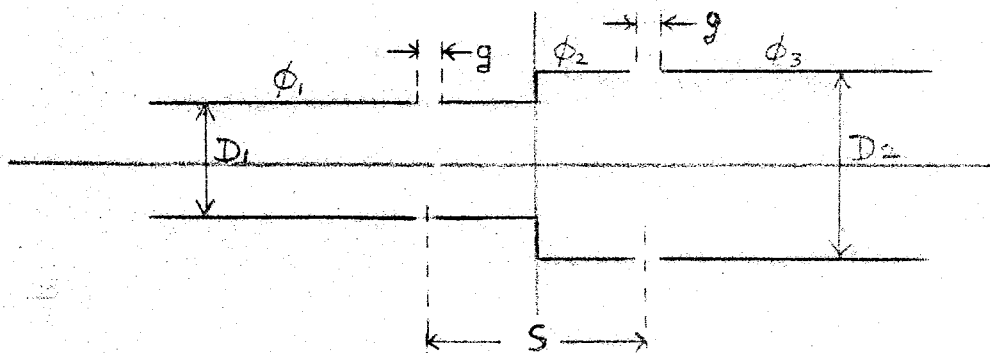
FIGURE 28.



TWO ELEMENT LENS



THREE ELEMENT LENS (equal diameters).



THREE ELEMENT LENS (unequal diameters).

generalised focal parameter. This was unsuccessful. We then attempted several alternative polynomials, the most successful of which was

$$f \cdot (\gamma - 1)^2 = \sum_{i=0}^N a_i \cdot (\gamma)^i \quad (\text{II.2.29})$$

This expansion can be tested by using certain of the data points to calculate the coefficients in (II.2.29). Then using the expansion we calculate the remaining data points and compare these with the literature values. A polynomial of degree 5 fitted the data of Read, Adam and Soto-Montiel with a maximum error of 0.3% in the range 2-20. A similar polynomial, also of degree 5, fitted the same data with a maximum error of 3% in the region $\gamma = 1.5$ to 50. This accuracy is more than sufficient for our purposes. Unknown to us Read was working on a similar parametrisation. His results are very similar to ours. The difference arises from the computational techniques used to evaluate the coefficients. Our calculations were based on the use of the subroutine CFIT, a standard Fortran I.C.L. 4100 software package. Table III lists our parametrisation coefficients for use in equation (II.2.29).

Previous work in computer lens design is very difficult to assess. The only published work is that of Heddle (1970) for three element lens properties. These were calculated from the two element theoretical lens properties of El-Kareh (1969,1970). No details of the computer programming technique or the data parametrisation are available. For discussion purposes, figure 28 shows the nomenclature that we employ for two element lenses,

Table III

Parametrisation coefficients for the two cylinder lenses with $g/D = 0.1$. This involves a polynomial of the fifth degree ($N=5$) in equation (II.2.29).

<u>Parameter</u>	<u>Coefficients</u>
f_1/D	$a_0 = 1.1895$
	$a_1 = 4.4226$
	$a_2 = 0.2063$
	$a_3 = -0.0012$
	$a_4 = 0.0$
	$a_5 = 0.0$
F_1/D	$a_0 = -0.8531$
	$a_1 = 5.2910$
	$a_2 = 0.7460$
	$a_3 = 0.0057$
	$a_4 = -0.0001$
	$a_5 = 0.0$
f_2/D	$a_0 = -1.7730$
	$a_1 = 5.6908$
	$a_2 = 1.4319$
	$a_3 = 0.0069$
	$a_4 = 0.0$
	$a_5 = 0.0$
F_2/D	$a_0 = -1.2605$
	$a_1 = 6.2670$
	$a_2 = 0.4415$
	$a_3 = -0.0115$
	$a_4 = 0.0001$
	$a_5 = 0.0$

three element equal diameter lenses and three element unequal diameter lenses. Heddle calculated from first principles, the overall focal properties $f_1^*, f_2^*, F_1^*, F_2^*$, for various values of $\gamma_1 (= \phi_2/\phi_1)$ and $\gamma_2 (= \phi_3/\phi_2)$. The only design variable he considered was the length of the centre element, S. This limits the designer to fixed values of γ and S. Also he still has to use the focal values to calculate the necessary object and image parameters to see if the lens is suitable. These 54 pages of tables are therefore of limited design use. Useful tables would give values of image space parameters for a variety of object space parameters for many different lenses. The lens variables would be S, the length of the centre element, g, the gap between elements, and D, the lens diameter. This would involve many thousands of pages of tables. We decided to approach this problem another way. A computer program capable of calculating these properties, and some others we will mention later, would be written and along with a data base of lens focal parameters for a reasonable selection of two element lenses would be stored in a computer. Then when a design problem was encountered the chosen input parameters would be fed in and the computer would generate tables of required output variables and, if necessary, any graphs required. Unpublished work along these lines had been performed by Kuyatt and Simpson (1967). As a data base they used Grivet's empirical equations for the range $\gamma=1.5$ to 10 and Spangenberg's experimental data for $\gamma=10$ to 20. They

used a set of subroutines written to perform the following calculations. FPROP regenerates lens focal parameters from the data base for a two element lens for a given value of γ . LENS calculates the lens transfer matrix for up to 20 lenses for 20 values of γ . The output is the final image position. IMAGE uses subroutine LENS to find the value of γ which will provide an image at a specified distance for a given object distance. They used another subroutine, called FIELD to help with the design of energy add lenses. These lenses are not involved in transmission spectrometers, however. In an unpublished report, Wei (1969) adds two further subroutines RTHETA and CURVIM. For a given distance in image space, RTHETA calculates the radial displacements and divergences of the limiting rays. CURVIM is merely a parameter plotting routine. We have no knowledge of how these subroutines operate in practice.

We have written two programs to perform a similar series of calculations. Program LENSONE is for a two-element lens and program LENSTWO is for a three-element lens.

The inputs to program LENSONE are X_1 , the object distance, and D , the lens diameter. The lens we used in all our designs was a two cylinder coaxial lens with $g/D = 0.1$. Optional inputs were the object radius r_1 , the object pencil half-angle θ_p and the object beam half angle. The program then cycles γ from 1.5 to 50 and prints out, for each value of γ , the image distance X_2 , the angular and lateral magnifications and if required, the

the pencil and beam half-angles at the image. The outputs are in inches, millimetres or in units of the lens diameter. Internal routines convert the angles from degrees to radians and radians to degrees. There are many ways we can use this program. We can vary X_1 and D easily and the angles and object size by inserting apertures of varying sizes in the beam path in object space.

Program LENSTWO is similar. Here the inputs are the same as for LENSONE, with two additions. These are S , the length of the centre element, and D_1 and D_2 the diameters of the two simple lenses comprising the three element lenses. This increases the number of design variables. The values of the lens transfer matrix elements are also output here. These can be fed into a minor program to perform calculations of the radial displacements and angles in a beam at selected points in image space.

Certain checks are built into the program to guard against arithmetic errors. The imaging condition is checked in two ways. Firstly we evaluate the image radius from the lateral magnification and then, we evaluate the same parameter by substitution of the matrix elements into the simultaneous mapping equations (II.2.16). Another check is to evaluate the determinant of the lens matrix and verify that this equals f_1^*/f_2^* as discussed earlier, and that $f_1^*/f_2^* = (\gamma)^{\frac{1}{2}}$ as shown in II.2.6. One other point is worth noting. The pencil and beam half-angles are calculated from the equations;

$$(\theta_p)_2 = a_{21} \cdot r_1 + a_{22} \cdot (\theta_p)_1$$

and

(II.2.30)

$$(\theta_b)_2 = a_{22} \cdot (\theta_b)_1$$

Several workers have published solutions of the ray trajectory equation for three element lenses. These are of limited design use as the parameter S is fixed. However, in certain cases they would provide a useful data base. The most accurate of these are Read (1969b,1970), Adams and Read (1972a,1972b) and Kuyatt, Natali and DiChio (1972c).

This discussion has been based on the assumption that our electron beam consists of paraxial rays only. For a real electron beam, the failure of the paraxial approximation, the finite energy spread, the large current density and finite beam size often cause lens errors or aberrations of the image. For a thick lens, the focal length reduces as the radial displacement of an electron beam increases (Spangenberg, 1948). This is known as positive spherical aberration and gives a spot focus instead of a point focus. One way to minimise this effect is to approximate the paraxial ray conditions. The fraction of the lens diameter used by the electron beam is referred to as the filling factor (Kuyatt, 1967; Read, 1971). The spreading of spots at filling factors of 1.00, 0.75, 0.50 and 0.25 are 18%, 12%, 7% and 4%, respectively. It has become regarded as good practice in lens design to keep the filling factor smaller than 0.5. Many of the

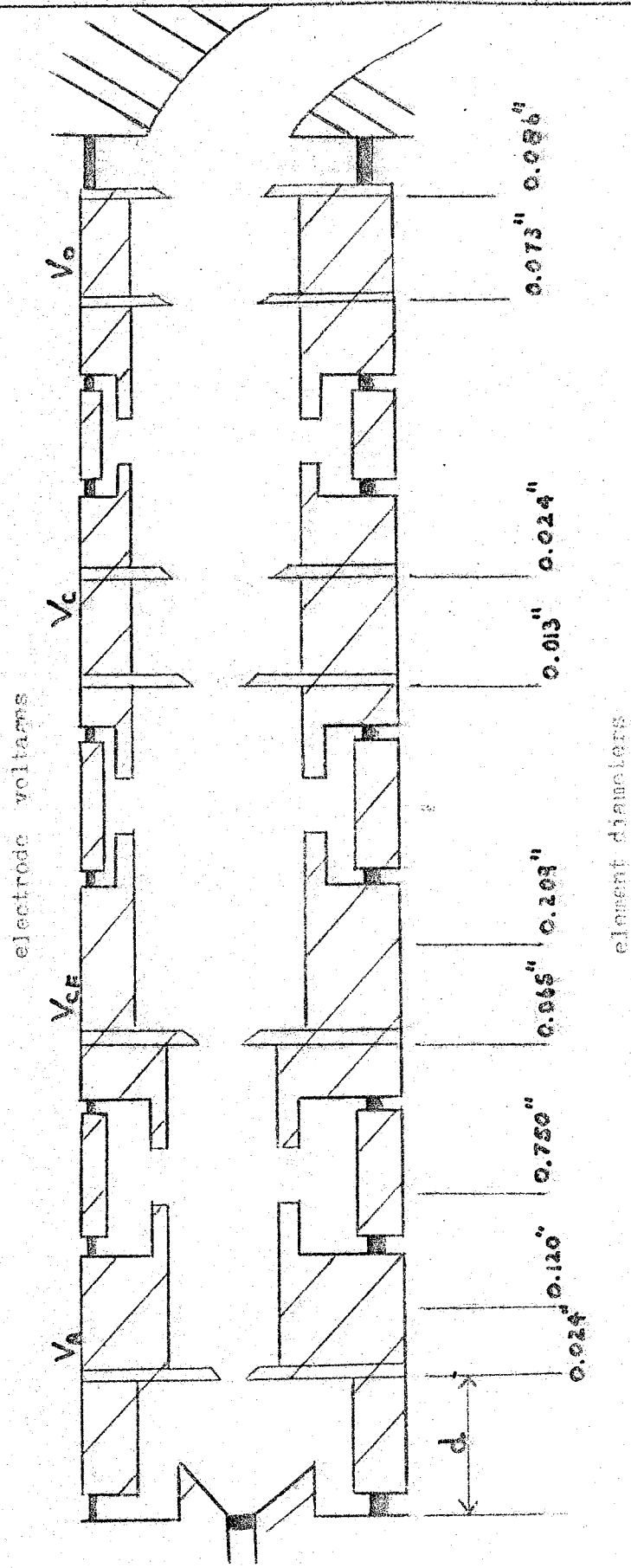
more recent calculations on lens focal parameters now include values for aberration coefficients. Apart from minimising the filling factors we have not taken account of lens aberrations as this data was not available at the time of our design.

II.3 The Spectrometer Design.

From our discussion in section II.1 we can now list the requirements for our spectrometer design.

- 1) Electron Gun. The purpose of the gun is to remove electrons from the thermionic cathode and shape them into an electron beam of the required size, angular divergence and energy for the monochromator. By necessity the electrons will have to be accelerated to a relatively high energy to produce a reasonable beam current, then decelerated before entering the monochromator at as low an energy as possible. The gun therefore consists of three separate stages:- An extraction stage for which we chose a Pierce parallel plate diode, a decelerating stage to reduce the beam energy and a matching stage between the diode and the decelerator to shape the beam as required. The decelerator operates with a fixed deceleration voltage ratio so the matching lens must allow us to vary the energy of the gun.
- 2) The electron monochromator. A hemispherical electron analyser was chosen as the monochromator because its two-dimensional focussing property was ideally suited to the axially symmetric lenses which we had decided to use.

FIGURE 29. SCHEMATIC OF ELECTRON GUN.



The success of workers like Simpson and Kuyatt (1967), Gibson and Dolder (1969), Comer and Read (1971) and Foo, Brion and Hasted (1971) with this monochromator encouraged us to make this decision.

- 3). The beam-forming lenses. These lenses had to provide a beam of the required energy whose current was, as far as possible, not a function of the beam energy.
- 4). The scattering cell. This has been discussed in section II.1.
- 5). The collector. As we wished to measure the electron current with an electrometer, rather than counting equipment, the collector was a Faraday cup.

The electron gun.

A schematic diagram of the three-stage gun and the nomenclature is shown in figure 29. The only design parameter for us to choose in the space charge limited diode is d , the cathode-anode spacing. The only criterion to guide us is that the smaller d is, the less the anode voltage is. Let us try $d = 0.220$ " and see how this affects the voltage and size of the beam at the end of the electron gun. From considerations of monochromator operating characteristics, we find that a limited selection of values of V_0 , the monochromating potential, with only one beam size, $r_0 = 0.010$ " would be satisfactory.

Now electrons leaving a thermionic cathode have a thermal energy distribution. An electron emitted

parallel to the cathode surface will have a trajectory of slope θ_A when it reaches the anode plane. This slope is,

$$\theta_A = (V_K/V_A)^{\frac{1}{2}} \quad (\text{II.3.1})$$

where V_K is the transverse kinetic energy of the electron and V_A is the anode voltage with respect to the cathode. The kinetic energy of an electron is approximately 0.1 electron volts for an oxide cathode. The space-charge limited current density, J , is given by the Child-Langmuir law,

$$J = \alpha \cdot V_A^{3/2} / d^2 \quad (\text{II.3.2})$$

where α is a constant, 2.335×10^{-6} .

Thus the Richstrahlwert at the anode will be, from equation (II.2.11)

$$R_A = 2.335 \times 10^{-6} \cdot V_A^{3/2} / (d^2 \cdot \pi \cdot \theta_A^2) \quad (\text{II.3.3})$$

and from equation (II.3.1),

$$R_A = 0.74 \times 10^{-6} \cdot V_A^{5/2} / (d^2 \cdot V_K) \quad (\text{II.3.4})$$

The Richstrahlwert at the end of the gun will be,

$$R_0 = dI_0 / dA \cdot d\Omega \quad (\text{II.3.5})$$

where these terms are as defined for (II.2.11).

Now Pierce (1954) showed that the maximum space-charge limited current passed by a tube at a voltage V_0 is,

$$I_0 = k \cdot V_0^{3/2} \quad (\text{II.3.6})$$

where k is the micropervance, which in terms of the angle of convergence of the beam at the end of the gun, θ_0 , is:

$$k = 38.5 \times 10^{-6} \cdot \alpha^2 \quad (\text{II.3.7})$$

from Kuyatt and Simpson (1967). Equation (II.3.5) now becomes,

$$\begin{aligned} R_0 &= (38.5 \times 10^{-6} \cdot \theta_0^2 \cdot V_0^{3/2}) / (\pi r_0^2 \cdot \pi \theta_0^2) \\ &= 3.904 \times 10^{-6} V_0^{3/2} / r_0^2 \quad (\text{II.3.8}) \end{aligned}$$

We showed in equations (II.2.11) through (II.2.13) that the ratio of beam Richstrahlwert to beam energy is conserved along the beam, if there are no energy dissipating devices in the path. Thus,

$$R_0/V_0 = R_A/V_A \quad (\text{II.3.9})$$

So if we combine equations (II.3.4) and (II.3.8) and rearrange we get V_A as a function of V_0 .

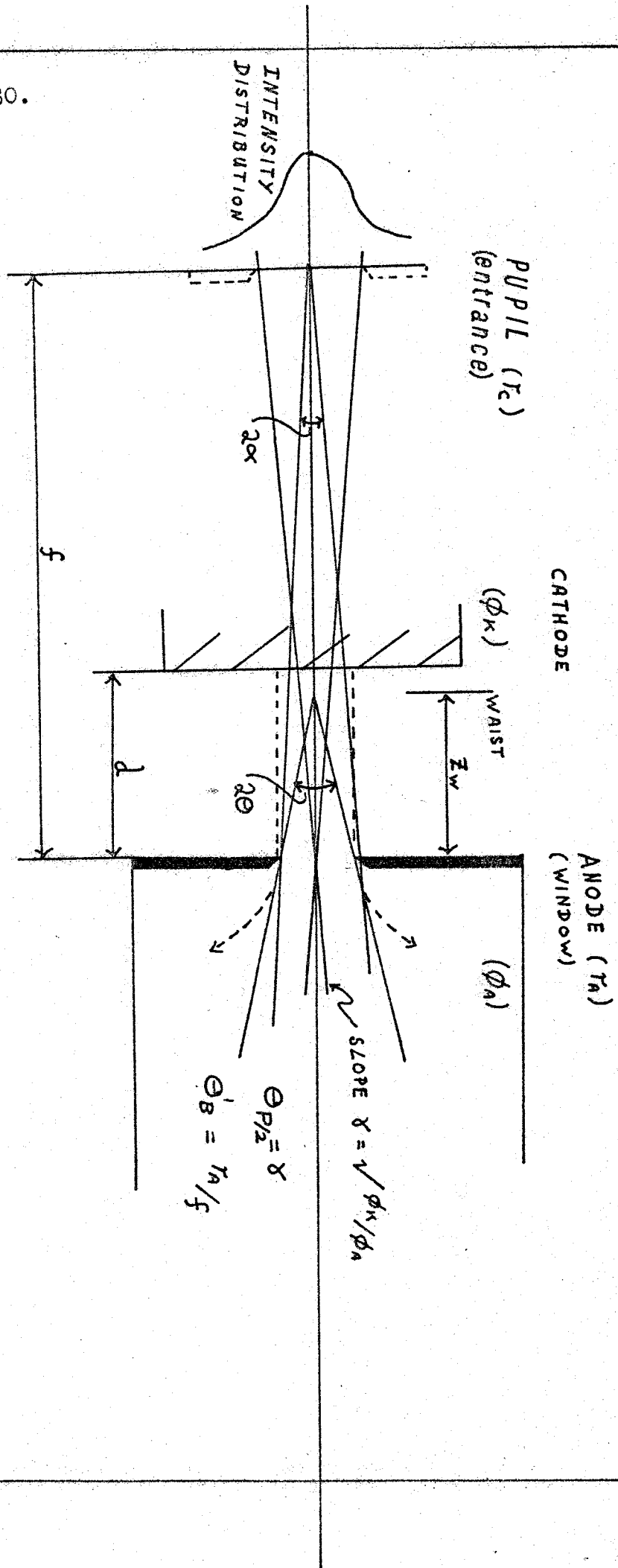
$$\begin{aligned} V_A^{3/2} &= (3.904 \times 10^{-6} \cdot d^2 \cdot V_K \cdot V_0^{1/2}) / (0.74 \times 10^{-6} \cdot r_0^2) \\ &= 5.275 (d^2 \cdot V_K / r_0^2) \cdot V_0^{1/2} \quad (\text{II.3.10}) \end{aligned}$$

In our suggested diode, $d = 0.220''$, $V_K = 0.1 \text{ eV}$ and $r_0 = 0.010''$, so a practical form of (II.3.10) for our purposes is,

$$V_A = 40.023 V_0^{1/3} \quad (\text{II.3.11})$$

Table IV shows of values of V_A for various values of V_0 . Note that so long as the matching lenses and the accelerator do not affect the conservation of Richstrahlwert then we do not need to know anything about them at this stage. This table also shows values for J_A , the anode current density, and $I_A = (\pi \cdot r_A^2) \cdot J_A$, the anode current. The choice of $r_A = 0.012$ is arbitrary. Kuyatt (1967) uses $r_A = 0.013''$ and although our other dimensions are not the same as his we decided to keep our anode hole close to his value, in case this was found by experience.

FIGURE 30.



Optical Theory of Space-Charge Limited Diode.

The final factor to be included in the design of the space-charge limited diode is the analogue lens action. The cathode plane acts as a Calbick lens, which we defined in section II.2, with the initial pupil on the right of the cathode at infinity and the final or exit window on the left of the cathode. The initial and final windows are at the same place. This is shown in figure 30. We choose the anode plane as the window for the system. The value of f , the focal length defined in the diagram, is a matter of debate at the present time. Klemperer and Barnett (1971) reduce the classical value of $f = 3d$, calculated from the Calbick lens formula (II.2.26), to a value of $f = 2.7d$ empirically. Coffey and Rowlands (1972) point out that the angular divergence of the beam, if this were the focal length, would give a different value of V_A from (II.3.1) to that expected by space-charge theory. In a calculation based on a simple space-charge model, which does not allow for the thermal emission velocities, they conclude that f is in error by a factor of about three. We felt this was too large a discrepancy and on checking the literature found that Harting and Burrows (1970) operated their space charge limited diode successfully on the assumption $f = 3d$. Without more experimental evidence we decided to work with the accepted value of $f = 3d$. In figure 30, $\theta_B = 0$ and $\theta_P = (V_K/V_A)^{1/2}$. Table IV shows values for θ_P and $r_C = 3d \cdot \theta_P$ as well. $\theta_B' = r_A/3d = 0.0182$ radians.

Table IV

V_O (v)	V_A (v)	J_A ($\mu\text{A}/\text{in}^2$)	I_A (μA)	θ_p (rad)	r_c (in)
1.0	40.023v	1.2214×10^4	5.521 μA	0.0499	0.033
1.5	45.78 v	1.4940×10^4	6.753	0.047	0.031
2.0	50.389v	1.7250×10^4	7.797	0.045	0.030
2.5	54.311	1.9306×10^4	8.726	0.043	0.028
3.0	57.713	2.1148×10^4	9.559	0.0416	0.027
3.5	60.755	2.2842×10^4	10.325	0.0406	0.027
4.0	63.517	2.4419×10^4	11.037	0.0397	0.026
6.0	72.722	2.9914×10^4	13.521	0.0372	0.025
8.0	80.046	3.4545×10^4	15.614	0.0354	0.023
10.0	86.210	3.8612×10^4	17.453	0.0339	0.022

$$r_A = 0.012''; d = 0.220''; r_O = 0.010''; \theta_B = 0; \theta_B' = 0.0182 \text{ rad.}$$

The deceleration stage.

From consideration of the requirements of the monochromator we can decide on optimum values for some parameters. The beam entering the monochromator from the exit window of the decelerator should have a radius $r_0 = 0.010''$. The beam half-angle at the window should be zero or approximately zero. The exit window pencil half-angle θ_p should be 0.070 radians. We arbitrarily choose the voltage ratio for deceleration to be 10:1 and the magnification to be 1.5. This choice defines other parameters in the system. For example, the entrance window radius = $(0.010/1.5) = 0.0065''$, and from the Helmholtz Lagrange law, the entrance window pencil half-angle, θ_p , is;

$$\begin{aligned} (\theta_p)_{\text{Entrance}} &\sim M(V_C/V_0)^{\frac{1}{2}} \cdot (\theta_p)_{\text{Exit}} \\ &\sim 0.0331 \text{ radians.} \end{aligned}$$

This value agrees well with those in Table IV. We have already decided to use a cylinder lens with $g/D = 0.1$. Use of program LENSONE gave the following output.

$$f_1 = 0.799D$$

$$f_2 = 2.582D$$

$$F_1 = 1.616D$$

$$F_2 = 1.179D$$

$$\text{overall length (object-image)} = 5.679D.$$

We can estimate the beam size at the lens centre, r , in the following projection from the low voltage side,

$$r = 2 \times \text{image radius} \times 2 \times (F_2 + Mf_2) \times D \times (\theta_p)_{\text{Exit}} \quad (\text{II.3.12})$$

where $(F_2 + Mf_2)$ is the image distance X_2 .

Substituting numerical values and dividing by D , we get an expression for the filling factor r/D .

$$r/D = 0.3941 + 0.020/D \quad (\text{II.3.13})$$

We chose $D = 0.209''$, which gives a filling factor of 0.49. This is an acceptable value in the light of our earlier discussion of filling factors. Thus the overall length of the lens is 1.187" and $X_1 = 0.599''$ and $X_2 = 0.588''$.

We next considered the position and size of a real entrance pupil. As we said in the previous section the beam passing through a lens can be controlled by either a real window and pupil on the entrance side or a real window and pupil on the exit or a combination of these, as long as there is only one real window and one real pupil in the system. Kuyatt and Simpson (1967) suggested that it was preferable to have a virtual image (ie. exit window) on the entrance plane of the monochromator. For the reasons they gave, we also decided to have the real pupil on the entrance side of the decelerator lens. For zero exit beam angle the pupil is placed at the entrance focal point ie. 0.246" on the left of the lens centre. The size we estimate by projecting the beam from the object to the lens centre. This gives $r_p = 0.012''$.

To try and inhibit electrons scattered within the gun entering the monochromator we placed another aperture on the low voltage side. We placed this one lens diameter from the lens centre and estimated the beam

size by projection to be 0.073" in diameter. As this aperture is wider than the beam it will not act as an angle limiter (ie. real exit pupil). Two real pupils in a beam will lead either to vignetting or to one of the apertures being redundant.

One final aperture has to be positioned. This is to correct for the "end effect" of the monochromator. The radial field of the hemispheres will be perturbed at either end if no steps are taken to correct for this. Herzog (1935) calculated how to correct for this. We employ his case A. This involves positioning an infinitely thin slit of aperture diameter $2b$, at a point a units from the end of the hemispheres. From mechanical considerations we decided a should be 0.065". This is sum of the length of our insulating spacer (0.040") and the thickness of our aperture material (0.025"). From the graph given by Herzog for d/k to be 0.32, where $2k$ is the hemisphere spacing, b/k must be 0.34. The aperture diameter is thus 0.086".

The matching condenser lens.

The image radius for this lens is 0.006" (ie. the object radius of the decelerator lens) and the object radius is 0.012" (the exit window of the diode). Thus the minimum magnification this lens can have is 0.54. The consequences of a magnification less than this can be seen by considering Liouville's Theorem and the $R-\theta$ diagram, as discussed in section II.2. The maximum magnification can be treated as for the decelerator, and we find M_{\max}
 $= 1.48$ for $V_0 = 4$ and $M_{\max} = 2.42$ for $V_0 = 1.5$ by substituting (θ_p) diode from table IV into,

$$M_{\max} = (V_A/10.V_0)^{\frac{1}{2}} \cdot \{(\theta_p)_{\text{diode}} / (\theta_p)_0\} \quad (\text{II.3.14})$$

where $(\theta_p)_0$ is the pencil angle at the monochromator entrance plane. Thus, again from the considerations of section II.2, the magnification of the lens must lie between 0.54 and 1.48.

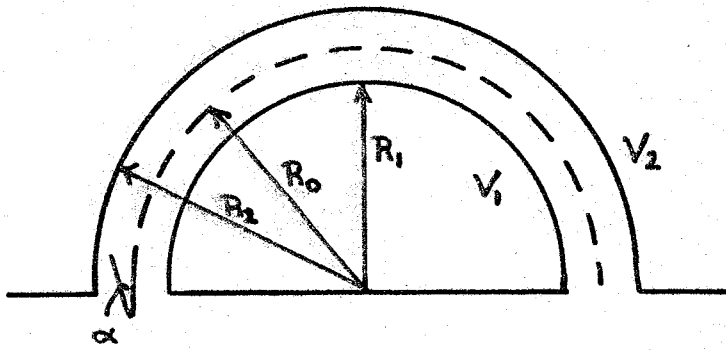
We know therefore that, if the paraxial approximation is valid, then

$$M_{\max} = -f_I/f_0 \cdot (\gamma)^{\frac{1}{2}} \quad (\text{II.3.15})$$

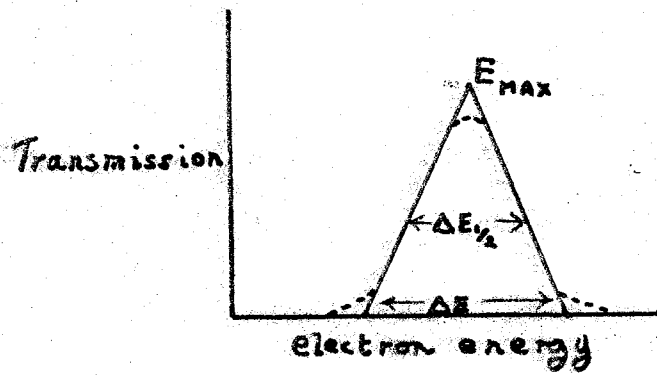
where f_I is the image focal length in units of the diameter of the second lens D_I and f_0 is the object focal length in units of D_0 . We used the computer to try various possible voltages. By trial and error we decided $M_{\max} = 1.10$, a safety choice, and $D_I/D_0 = 1.74$. The filling factor was calculated by projection as before, and $d/D \approx 0.5$ for $D_0 = 0.120''$ and $D_I = 0.209''$. Another factor influencing this rather arbitrary choice was that the lens should be as short as possible. Program LENSTWO was then used to calculate system lens transfer matrices for various voltage ratios, values of X_1 , etc. The principle is that $X_1 = 0$ for the second lens and X_2 of the first lens is S , the centre element length. Trial and error gives an object distance of $0.332''$, a centre element length of $0.300''$ and an image distance of $0.328''$. An estimation of the size of the beam at the compound lens centre suggested a diameter of $0.065''$ for the aperture positioned here.

The operation of the gun is therefore as follows. A value of V_0 is chosen from monochromator considerations. This defines V_A , whose value can be obtained from table IV.

FIGURE 31.



HEMISPHERE NOMENCLATURE.



TRANSMISSION FUNCTION OF MONOCHROMATOR.

The first stage of the decelerator is set at $10.V_0$ and V_{CF} (the condenser focus voltage) is optimised for maximum transmission by the spectrometer. There are two suitable values of V_{CF} for each set of gun voltages. These are the high and low voltage focus conditions, which are discussed in detail later.

The monochromator.

The focussing of charged particle beams was first worked out by Purcell (1938). He showed that for electrons of the same energy passing through a given point with a small angular divergence, a correctly tuned spherical condenser will give an approximate re-focussing of orbits after a revolution of π radians. Thus hemispheres are used. Several theoretical treatments of the design parameters are available (Simpson and Kuyatt, 1967; Kuyatt, 1968; Rudd, 1972). Trajmar, Rice and Kupperman (1968) worked out a derivation of the operating formula which we reproduce in outline, as it is unpublished. Figure 31 shows the nomenclature.

If $\bar{\Phi}(R, \theta, \phi)$ is the potential at R , where $R_1 \leq R \leq R_2$ and $0 \leq \theta \leq \pi$. To produce the required $1/R^2$ electrostatic field, $\bar{\Phi}$ must satisfy Laplace's equation:

$$\nabla^2 \bar{\Phi}(R, \theta, \phi) = 0 \quad (\text{II.3.16})$$

and solving for $\bar{\Phi}$,

$$\bar{\Phi}(R) = (R_1 R_2 \Delta \bar{\Phi} / R_2 - R_1) \cdot (1/R - 1/R_0) + \bar{\Phi}_0. \quad (\text{II.3.17})$$

where $\Delta \bar{\Phi} = \bar{\Phi}(R_1, \theta, \phi) - \bar{\Phi}(R_2, \theta, \phi)$ and $\bar{\Phi}_0 = \bar{\Phi}(R_0, \theta, \phi)$. Now, for $\alpha = 0$, in figure 31.

$$(-e \cdot \Delta \bar{\Phi}) / (-e \cdot \bar{\Phi}_0) = (R_2 / R_1 - R_1 / R_2) \quad (\text{II.3.18})$$

In terms of voltages,

$$(V_1 - V_2)/V_0 = (R_2/R_1 - R_1/R_2) \quad (\text{II.3.19})$$

Thus,

$$\begin{aligned} (V_0 - V_1) &= - \int \Phi(R) \cdot dR \\ &= (V_1 - V_2) \cdot (R_1 R_2 / R_2 - R_1) \cdot (1/R_0 - 1/R_1) \end{aligned} \quad (\text{II.3.20})$$

So, from (II.3.19) and (II.3.20)

$$\left. \begin{aligned} V_1 &= V_0 (R_2/R_1) \\ V_2 &= V_0 (R_1/R_2) \end{aligned} \right\} \quad (\text{II.3.21})$$

Thus $V_1 > V_2$, as we would expect and $(V_0 - V_2) \neq (V_1 - V_0)$ in general. In our design we chose $R_1 = 0.875''$, $R_0 = 1.000''$ and $R_2 = 1.125''$.

The general energy analyser equation is,

$$x_2/R_0 = -A \cdot x_1/R_0 + B \cdot \Delta E/E - C\alpha^2 - D\beta^2 \quad (\text{II.3.22})$$

where $\Delta E = E - E_0$, x_1 and x_2 are radial displacements from R_0 and α and β are divergences in the perpendicular input planes. For this particular analyser the constants A, B, C, D have the values $A = 1$, $B = 2$, $C = 2$ and $D = 0$. We can write (II.3.22) in the form,

$$x_2/R_0 = -x_1/R_0 + 2 \cdot \Delta E/E - 2\alpha^2 \quad (\text{II.3.23})$$

The first term in this equation shows that the input plane is imaged with unit magnification onto the output plane. The second term shows that there is linear energy dispersion and the absence of a term linear in α shows that there is first order angle focussing.

The energy resolution function is the transmission of electrons as a function of energy. With entrance and

and exit windows equal (real or virtual) and of width W then:

$$W/R_0 \approx -W/R_0 + 2 \cdot \Delta E/E \quad (\text{II.3.24})$$

and the energy resolution is,

$$\Delta E_{\frac{1}{2}}/E_0 \approx (W/2R_0) \cdot E_0 + \alpha^2/2 \quad (\text{II.3.25})$$

and,

$$\Delta E_{\text{base}} \approx (\alpha^2 + W/R_0) \cdot E_0 \quad (\text{II.3.26})$$

These quantities are defined in figure 31. In our system $r_1=r_2=W$; $R_0 = 1.000''$ and so,

$$\Delta E_{\frac{1}{2}}/E_0 \approx 1.25\% \quad (\text{II.3.27})$$

Thus for $E_0=1$ volt we expect a full width at half maximum energy of 0.012 volts; $E_0=2$ volts, $\Delta E_{\frac{1}{2}} = 0.025$; $E_0=4$ volts, $\Delta E_{\frac{1}{2}} = 0.050$ volts and so on.

We can allow for the effect of the cathode distribution on the transmitted current. If we assume a Maxwellian distribution at the cathode, viz;

$$dI = (4\pi \cdot m \cdot e/h^3) \cdot \exp(-e \cdot \emptyset/kT) \cdot \exp(-E/kT) \cdot E \cdot dE \quad (\text{II.3.28})$$

where m and e are the mass and charge of the electron, \emptyset is the work function of the cathode, h is Planck's constant, k is Boltzmann's constant and T is the absolute temperature of the cathode. Now it can be shown that, for this distribution,

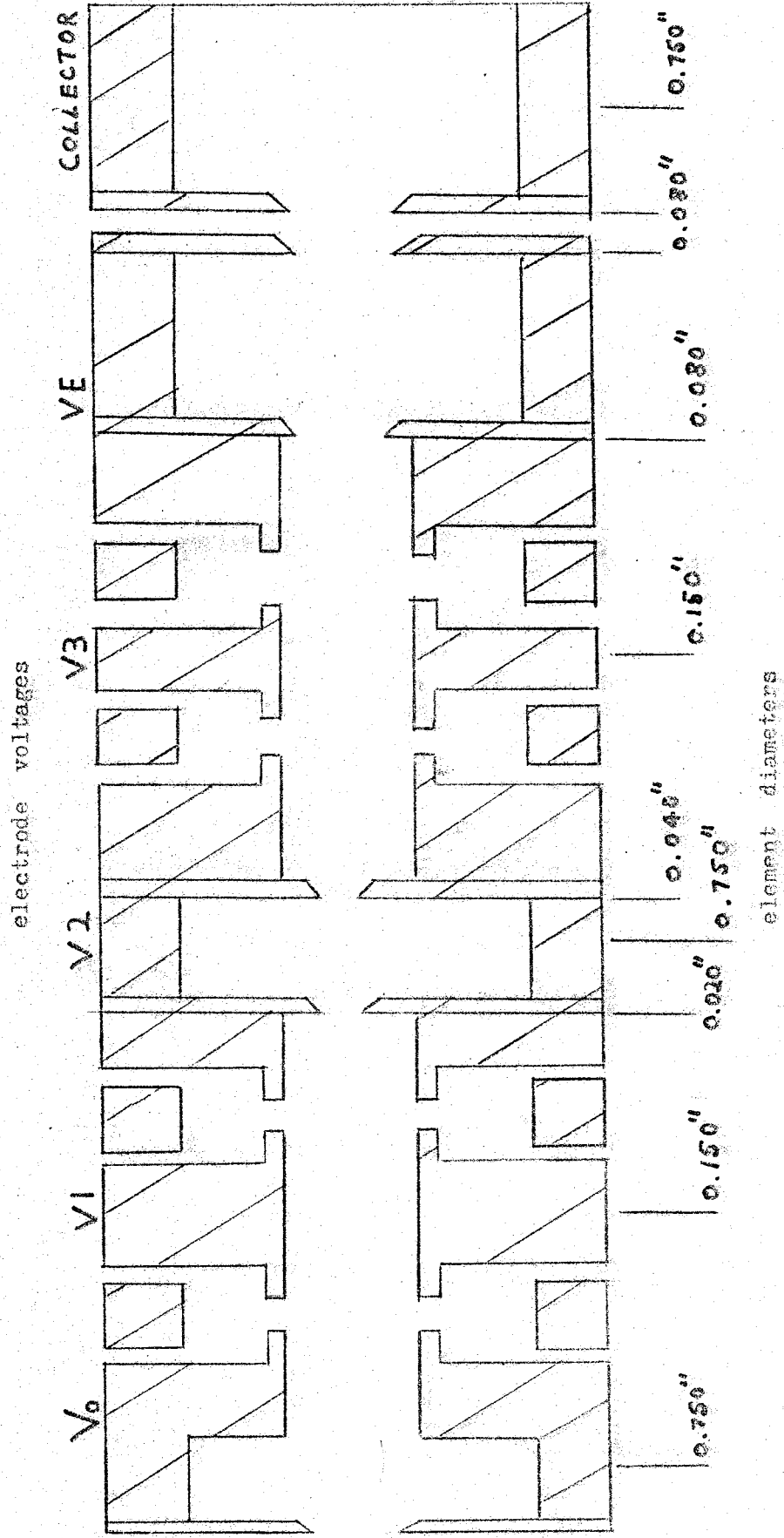
$$E_{\text{max}}^k = kT \text{ and } \Delta E_{\frac{1}{2}}^k = 2.45 kT$$

From space charge theory,

$$\begin{aligned} I_{\text{in}} &\approx 38.5 \times 10^{-6} V_0^{3/2} \cdot \alpha^2 & (\text{II.3.29}) \\ &\approx 0.19 \times 10^{-6} V_0^{3/2} \end{aligned}$$

where I_{in} is the current entering the monochromator and I_{out} the output current is,

FIGURE 32. SCHEMATIC OF BEAM-FORMING LENSES.



$$\begin{aligned}
 I_{\text{out}} &\approx (\Delta E_{\frac{1}{2}}^{\text{mono}} / \Delta E_{\frac{1}{2}}^{\text{K}}) \cdot I_{\text{in}} & \text{(II.3.30)} \\
 &\approx 1.1 \times 10^{-8} \cdot V_0^{5/2} .
 \end{aligned}$$

Beam forming lenses.

A schematic diagram of the beam-forming lenses is shown in figure 32. The first lens, which we call the fixed object lens, focusses the monochromator output image onto the aperture A8. This object position is fixed for various values of the voltage V_2 by varying the focus voltage, V_1 . Trial and error computer design was used here. We decided to use a diameter of 0.150" for the cylinder lenses to keep the focal lengths as physically short as possible. The centre element length was selected as 3.D to give a wide range of positions for an intermediate image to be formed. The object aperture, A8, is 0.020" in diameter. This choice was based on assessments of the filling factors. If the lens diameter is to be small then we must keep the beam small. The aperture A7 is chosen to correct the end effect in the way we discussed for the monochromator input.

The energy definition lens is designed to produce a beam of as nearly parallel electrons as possible for a range of voltages on V_E . In this way we hoped to ensure that the beam after leaving aperture A8 is not impeded by the gas cell or collector apertures. We start with a small object at A8 of 0.020" diameter, then form an object at infinity by placing a real pupil aperture at the focal point. This is aperture A9.

We could not optimise this design as there were two mechanical constraints on the system. Firstly, due to the size of the vacuum tank we were using, there was

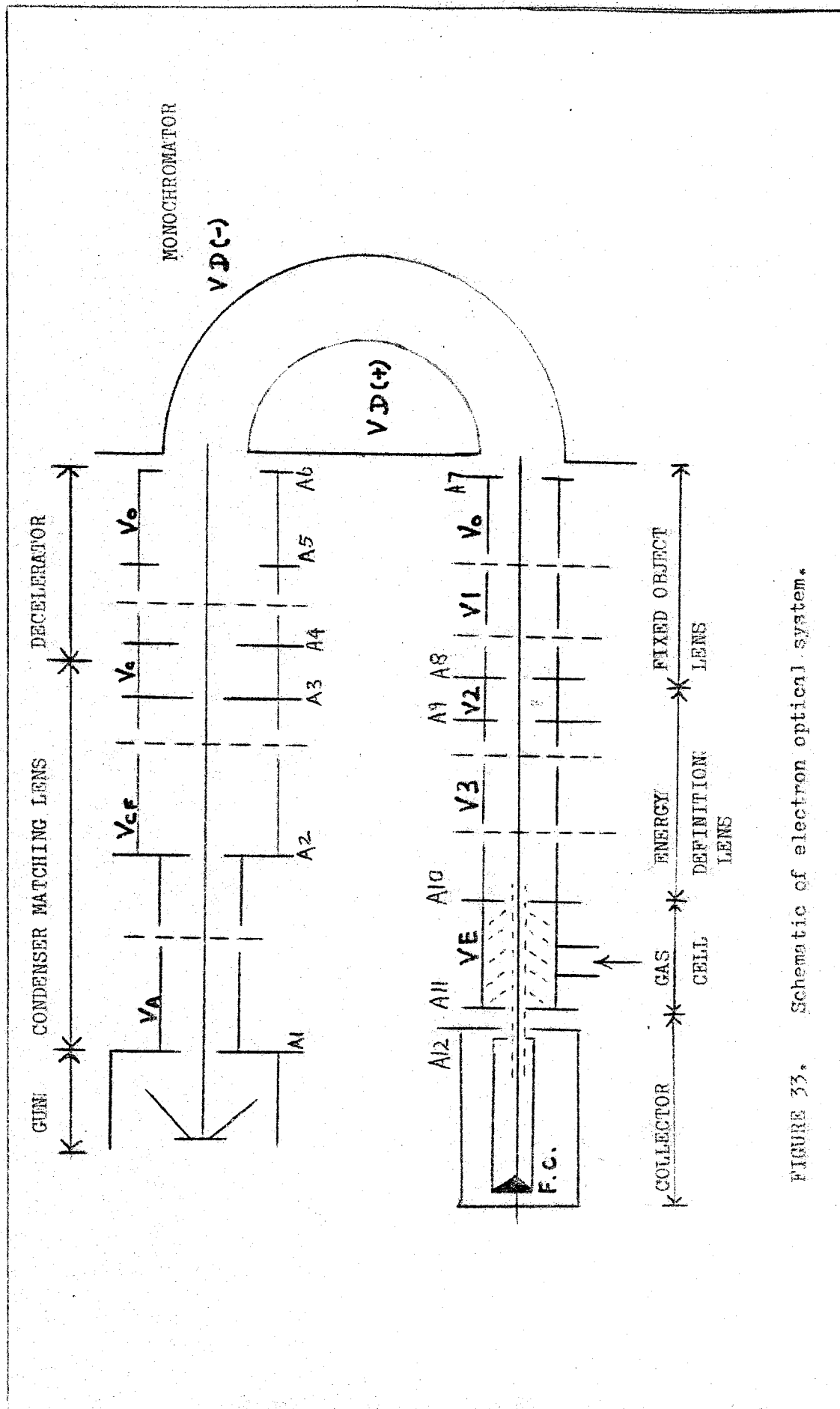


FIGURE 33. Schematic of electron optical system.

only about 3.50" available for the beam forming lenses. Secondly, in case of mechanical misalignment, we had to make certain lens elements long enough to incorporate deflector plates to align the beam. It turned out in practice, however, that deflector plates were not required and that the system operated as required even although not optimised. We will discuss this in the next chapter. In equation (II.1.10) we defined a quantity kI_0 as proportional to the total beam current in the absence of gas. We suggest that this parameter can be monitored by collecting the current at A8. As discussed, the beam size at A8 is always larger than A8, so the current monitored here will be a reasonable measure of changes in I_0 .

A basic diagram of the whole optical system is shown in figure 33.

II.4 Miscellaneous design details.

Mechanical details

In converting electron optical design dimensions to suitable mechanical workshop drawings several additional factors have to be allowed for.

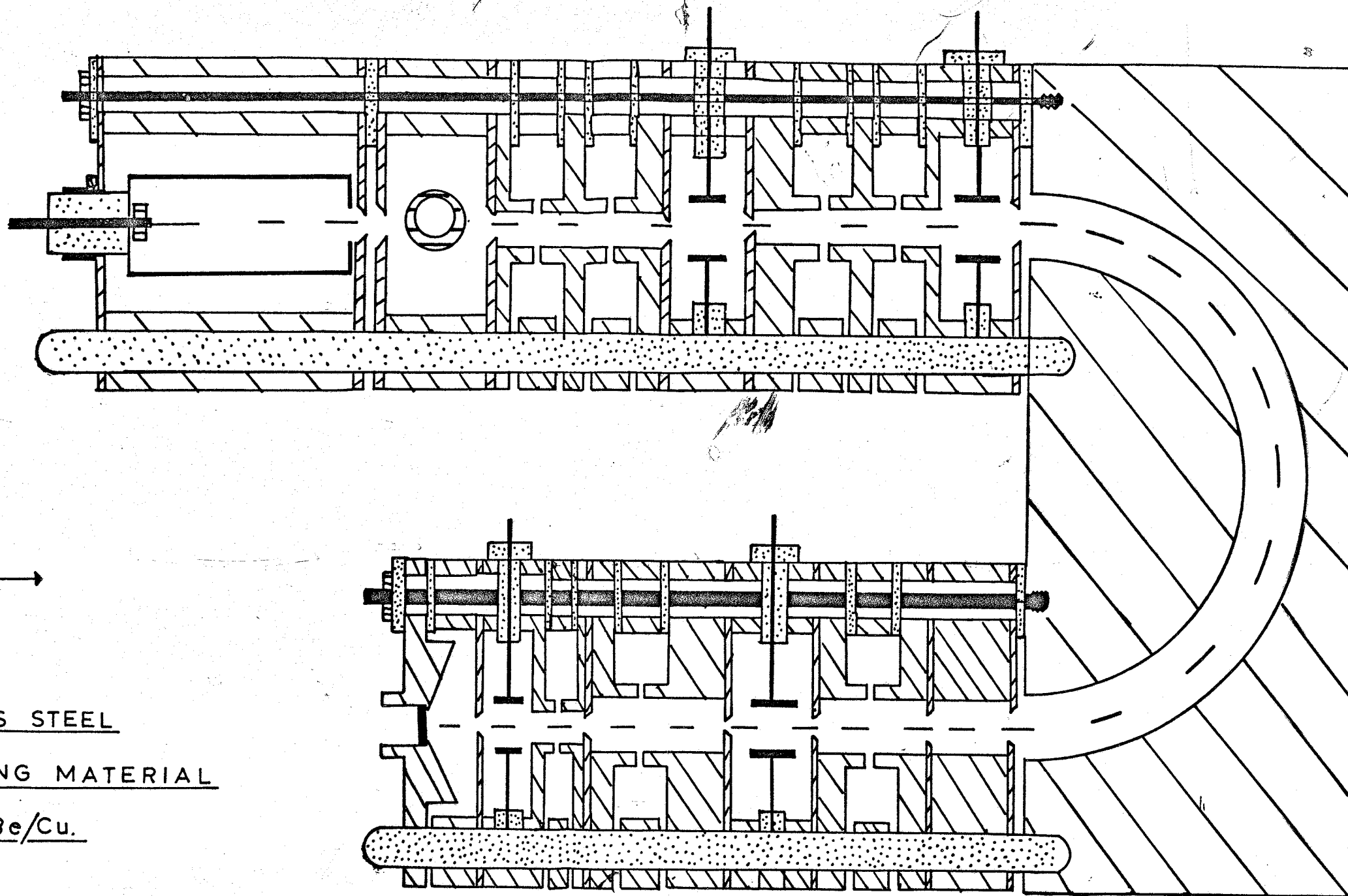
Firstly we must ensure that the material from which we construct our lens elements in no way influences the behaviour of the electron beam. This could occur if the lens element were magnetic to any significant degree or if, due to contact potential effects, which we have already discussed in section I.2, any metal surface seen by the beam does not have a uniform potential everywhere on it. The problem of stray magnetic fields due to the metal composition of the lenses was eliminated by constructing them from a non-magnetic stainless steel (Firth-Vickers "Immaculate V"). The residual magnetism of the metal was checked before and after machining, and found to be less than one milligauss. This is not always so, even with a commercial non-magnetic stainless steel, and one version of the apparatus had to be rejected as it was found to have local magnetic fields as intense as several gauss. At all stages in the production of an electron optical system from this material, it is essential to check for local magnetic fields.

Parker and Warren (1962) investigated the variation in contact potential across various surfaces. They concluded that gold electroplated surfaces had the

least contact potential differences of all the surfaces they investigated. In fact, gold evaporation produces an even better surface. We attempted to gold electroplate all our optical elements. It was found that we could only electroplate pieces of immaculate V stainless steel that had never been under vacuum. So instead of gold plating, we deposited colloidal graphite from an alcoholic suspension on all metal surfaces seen by the beam. (A commercial preparation called DAG 580 was used.) We limited the application strictly to surfaces seen by the beam as graphite could adsorb the residual gases in the vacuum system and cause excessive degassing when evacuating the system. We found this simple treatment quite satisfactory.

It is also essential to work under conditions of extreme cleanliness both during assembly and in the vacuum system. Films of organic solvents, grease or pump oil on a lens surface can become charged by the electron beam and then distort the beam path.

The second factor which we must consider is the control of stray electrons. These can arise either by electrons leaving the beam path due to scattering by a lens aperture or by secondary electron emission when the beam hits a metal surface. To control this we shielded the electron collector carefully and positioned shields at every gap between the lens cylinders. However, complete shielding of scattered electrons can lead to the system becoming difficult to



ELECTRON TRANSMISSION SPECTROMETER.

CHEMISTRY RESEARCH.

STIRLING UNIVERSITY.

evacuate due to trapped gas volumes which can only be pumped through the very small aperture holes. Our present shielding system we find to be a reasonable compromise.

An ideal cylinder lens should consist of thin-walled coaxial cylinders (Read, Adams and Soto-Montiel, 1971). We approximated this by machining the cylinder wall to a thickness of 0.050" within 0.100" of any lens gap. We found that a wall thickness less than this was both difficult to machine and susceptible to damage during the assembly of the system. The aperture holes were drilled rather than spark eroded. We found by experience that, although spark eroding is a very accurate technique, it was difficult to accurately position the hole on the aperture plate. The aperture holes were then knife-edged to reduce scattering at the edges of the holes.

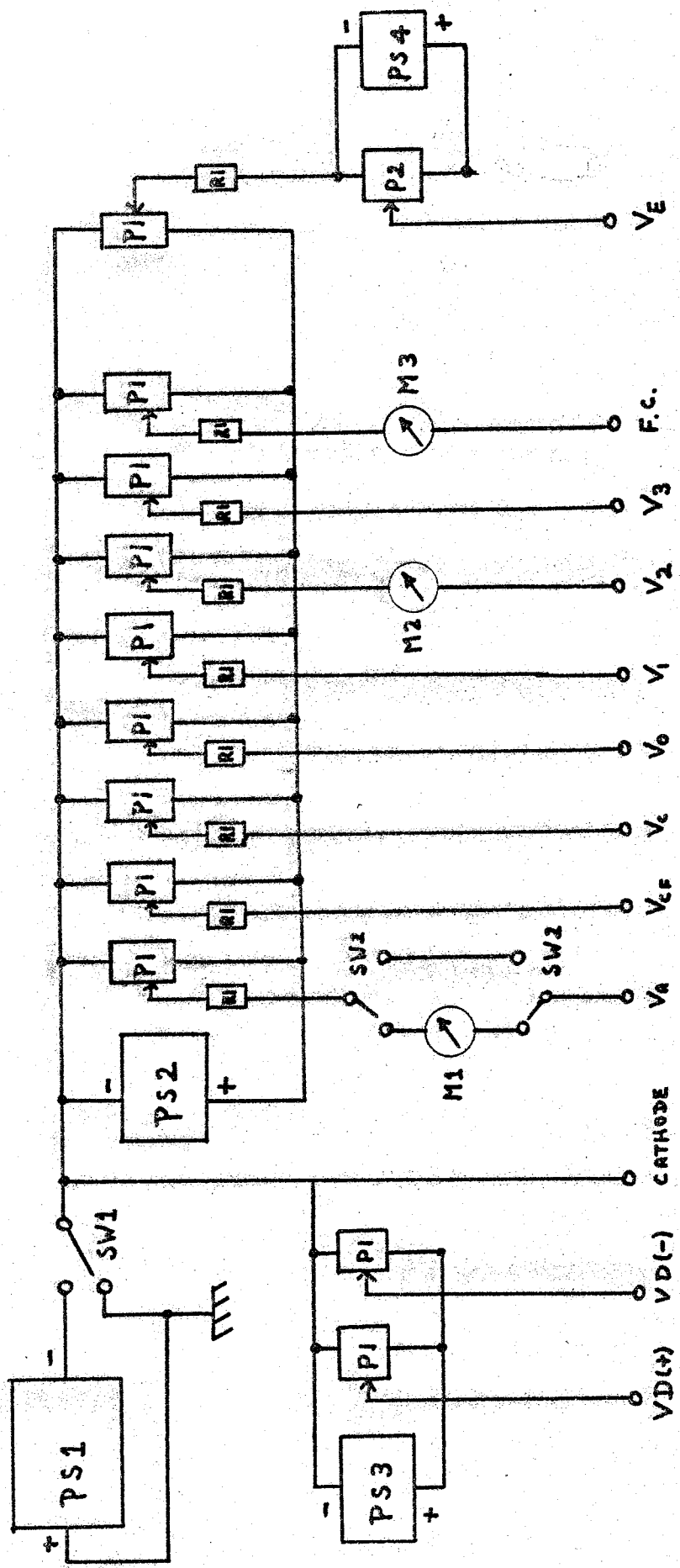
The lens elements were mounted on ceramic rods (Steatite-Porcelain). These were of very accurate diameter ($0.1562" \pm 0.0001"$) and controlled the alignment of the optical systems. The insulators between lens elements at different potentials were of quartz and were all the same thickness (0.040").

A workshop drawing of a cross-section of the assembled optical system is shown in figure 34.

The electrical system.

The purpose of the electrical system is to bias the lens electrodes at the chosen design potentials

FIGURE 35. Electron Optics Control Circuitry.



with respect to the cathode potential and to measure any currents required. A circuit diagram of the system is shown in figure 35.

In this circuit, PS represents a d.c. power supply, P represents a potentiometer, R a resistor and M a current-measuring device.

All the power supplies are commercial high stability d.c. supplies with adjustable output voltages which are not referred to mains earth within the supply ie. floating outputs. PS1 and PS2 are Oltronix Stabpac 30 (type MB120-0.25). These have output voltages variable between 0 volts and 120 volts and voltage stabilities of 0.01%. The meaning of voltage stability can differ for different commercial manufacturers. In this case if the mains supply voltage varies by $\pm 10\%$ the output voltage varies by 0.01%. The maximum ripple and noise is 0.5 mV r.m.s. PS3 and PS4 are Oltronix Stabpac 3 (type MB30-0.1). These have outputs of 0-30 volts, 0.01% stability and a maximum of 0.3 mV r.m.s. noise and ripple.

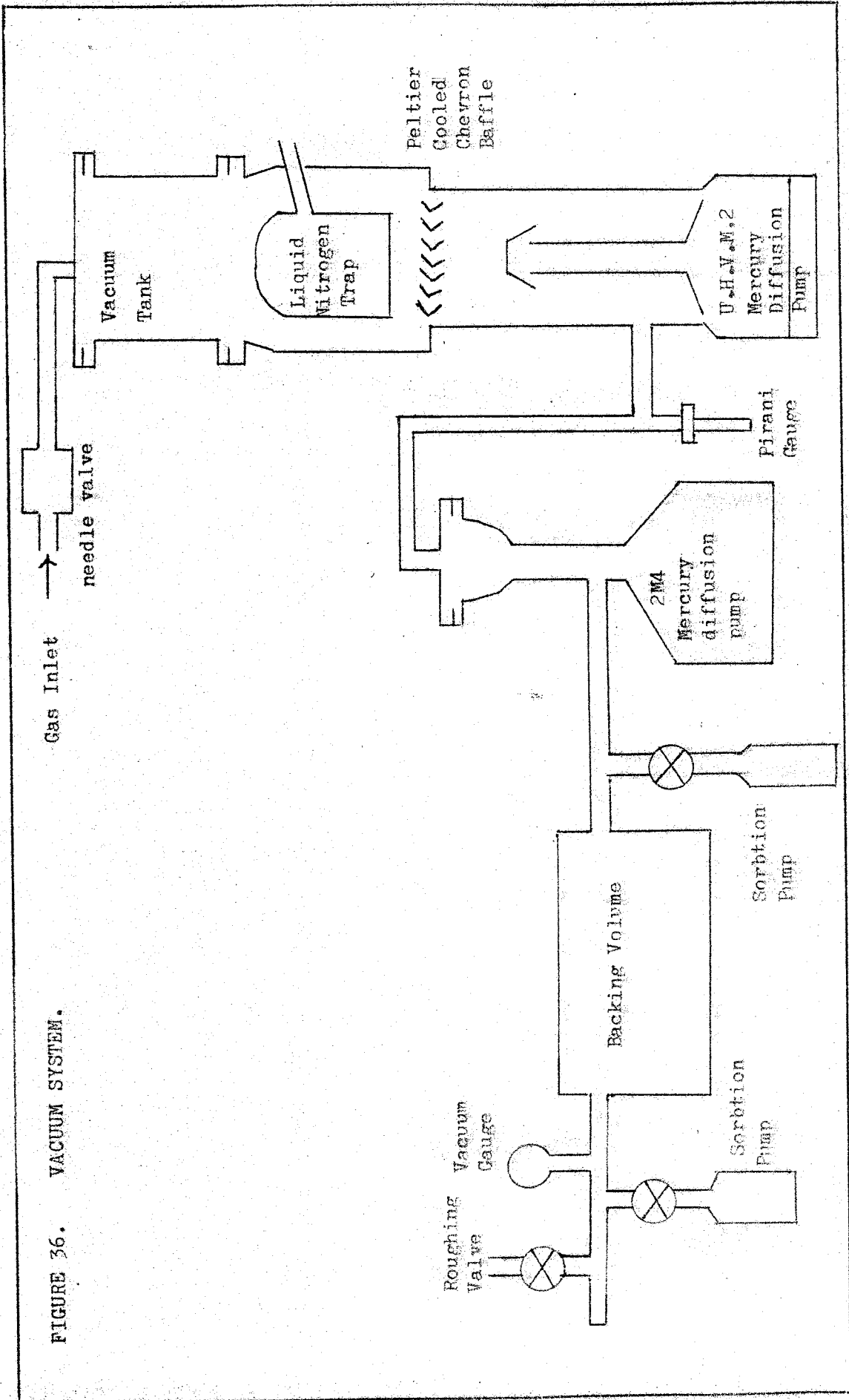
The potentiometers, P1, are all $100k\Omega$ linear potentiometers. Their high resistance value is chosen to minimise the current drawn from the power supplies. The resistors, R1, are all $98k\Omega$ and are used to protect the power supplies against a short circuit in the event of one of the lens elements becoming connected electrically to the cathode. P2 is a motor driven potentiometer ($100k\Omega$).

The meter, M1, is a milliammeter used to monitor the anode current. M2 is a laboratory built electrometer used to monitor the current at aperture A8, as discussed in section II.3. M3 is a Keithley 640 vibrating capacitor electrometer which records the transmitted beam current. This is capable of reading 1.0×10^{-15} A. full scale with a $10^{12} \Omega$ input resistor. It is connected to the Faraday cup collector, F.C., in the electron optical system.

The laboratory built electrometer, M2, was adapted from the design of Garment and Ross (1971). It measures electron currents in the range 10^{-11} - 10^{-5} A, has good long term drift properties and can be operated up to 500 volts above mains earth potential. We added clipping diodes at the input to the operational amplifier in the circuit for extra protection of the amplifier when the input voltages are high. We also found it essential to have the trim potentiometer of the operational amplifier wired as an external control as it is necessary to adjust this frequently.

The switch, SW1, allows us to operate with the cathode either at the system earth potential or at a voltage negative with respect to this earth. The ten-turn potentiometers allow us to vary the voltage on the lenses with reasonable sensitivity. The output voltages are those shown in figure 33. When more sensitivity in selecting voltage is required as, for example, with VD(+) and VD(-), the hemisphere potentials in the monochromator, the subsidiary current involving the low

FIGURE 36. VACUUM SYSTEM.



voltage supply PS3 is used. SW2 removes the anode current meter from the circuit when it is not required.

By varying the setting of the potentiometer P1 and the output voltage of PS4 we can choose the lower and upper limits for scanning the electron beam energy, VE, with the motor driven potentiometer P2.

To record a transmission spectrum we can either connect VE to the x-axis and the analogue voltage output of M3 to the y-axis of an x-y recorder or monitor both these voltages and the analogue voltage output of M2 with a digital voltmeter connected to a data logging system with punched paper tape output. The data tape can then be processed in a computer.

We only have one earth point in the system. This avoids some of the dangers associated with earth loops, which can cause signal noise. This earth is a laboratory noise-free earth and all metal parts of the apparatus are connected to it and not to the mains earth. All electrical connections are made with screened leads with the outer braiding connected to this earth.

The cathode is an indirectly heated Philips BPLA oxide coated cathode. The cathode heater power supply is an Oltronix Stabpac 30 (type MB15-2).

The vacuum system.

A schematic diagram of the vacuum system is shown in figure 36. Mercury pumps were chosen in preference to oil pumps to avoid the risk of oil films discussed earlier in this section. The system gives a

base pressure of 6×10^{-8} torr with a hot cathode after baking. The liquid nitrogen trap is filled automatically from a reservoir dewar. The pumps are protected by an interlocked system which switches the pump heaters off if the vacuum tank pressure, level of liquid nitrogen in the trap or flow rate of the cooling water register values outside preset limits. Like the optical elements the vacuum tank is made of immaculate V stainless steel.

Cancellation of the earth's magnetic field.

The earth's magnetic field can deflect the electron beam from its calculated path. It can be calculated (Trajmar, Rice and Kupperman, 1968) that the earth's magnetic field must be cancelled to better than 1.3×10^{-2} gauss for a 1 eV electron to be unaffected by it in the monochromator. A pair of thin coaxial coils containing the same number of turns, carrying the same current, having the same radius and being separated by a distance equal to the radius, will provide a nearly constant magnetic field vector directed along their axis in a small region about their midpoint. Three mutually perpendicular pairs of coils can be used to cancel the three cartesian components of the earth's magnetic vector.

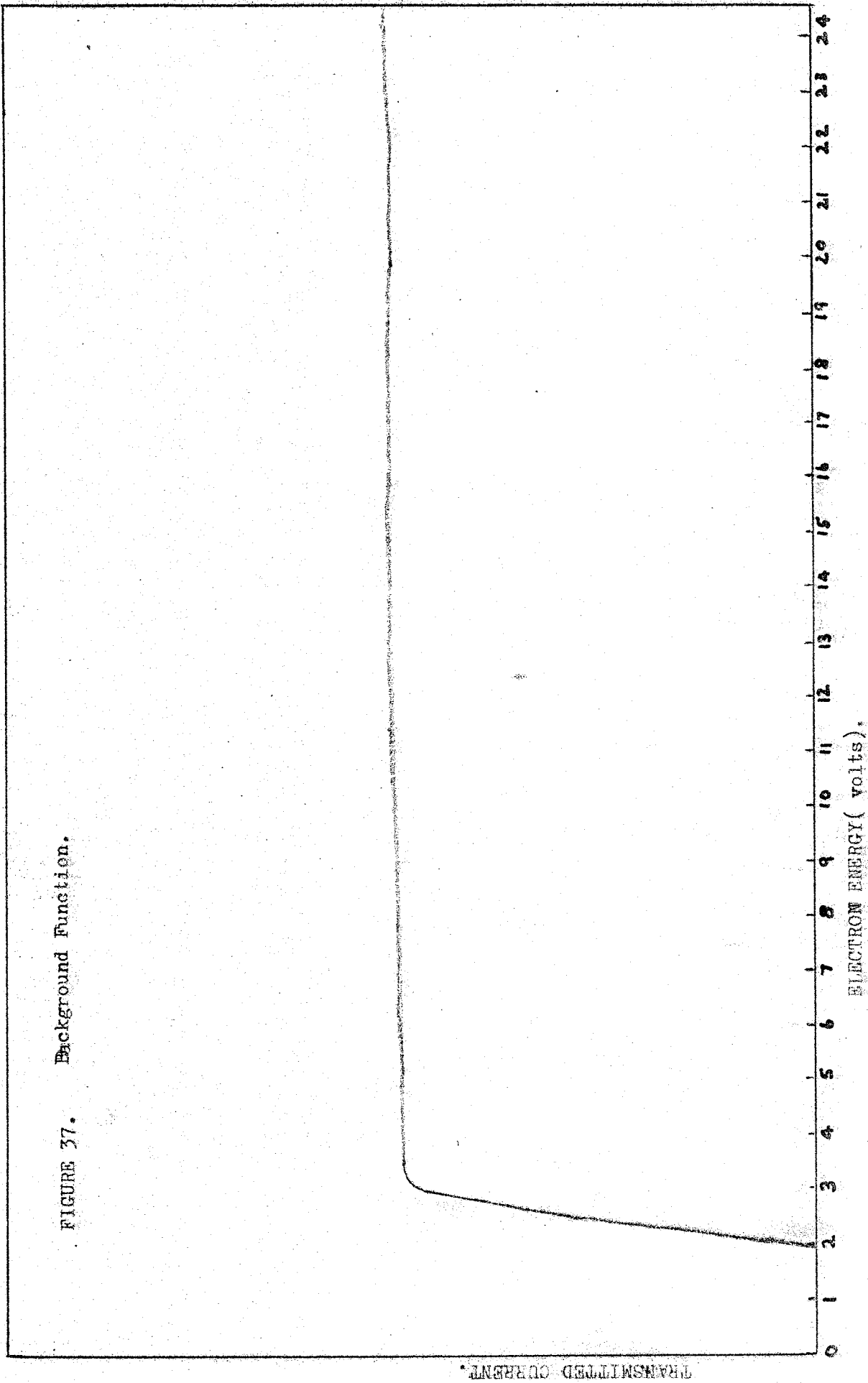
In practice, we used a system of Helmholtz coils of square cross-section. (Alldred and Scollar, 1967). We were able to cancel the earth's magnetic

field to within $\pm 5 \times 10^{-3}$ gauss within a region about 6 in.³ inside the vacuum tank.

In practice, however, we found it preferable to tune the transmitted current to a maximum with the Helmholtz coils. This seems to be common practice in electron spectrometry.

CHAPTER III. THE OPERATION OF THE ELECTRON
TRANSMISSION SPECTROMETER.

FIGURE 37. Background Function.



III.1 The operational characteristics of the spectrometer.

The performance of the spectrometer matched the design requirements, which we discussed in section II.1. The operating characteristics are both stable and reproducible.

Beam currents.

The maximum beam current in the absence of gas is 3×10^{-9} A. When gas is present, the transmitted currents are between approximately 1×10^{-9} A and 1×10^{-11} A. This is well within the range of the electrometer amplifier (cf. section II.4). The background current is almost constant over the whole operational energy range of 2 eV to 100 eV. In some focussing conditions there is a slight increase in current as the electron energy increases, but this is only of the order of 10% at most and is linear with energy. Thus our background current, I_0 in section II.1, is almost constant and is structureless with a sharp onset about 2 eV. The current below 2 eV rises very sharply from a constant onset at zero volts. This is shown in figure 37. It seems unlikely that quantitative work below 2 eV impact energy will be possible with the present system. However, our design specification did not require this very low energy operation. Furthermore, this is sufficiently low an energy to allow comparison of measured total cross-sections with published momentum transfer cross-sections in a number of species.

Energy resolution.

Our design also required that we operate with an energy resolution of about 50 meV in order to observe fine structure in the transmitted current. In fact our energy resolution (F.W.H.M.) at a nominal monochromating energy of 4.0 eV is about 40 meV. This agrees well with the theoretical estimate given in section II.3. This resolution would be improved by operating at a lower monochromator potential, but transmitted currents are then rather low.

Thus the spectrometer operates as required for measuring the total cross-section for electron-gas atom or molecule collisions and for resolving much of the fine structure in the cross-section. Its performance compares well with the only other apparatus employed for measuring total cross-sections at the present time, which is that of D.E. Golden (1966) and his collaborators. This was discussed in detail in section I.2. For fine structure studies it is hoped to improve the sensitivity by modulating the electron beam and observing the differentiated transmitted current, in the manner of Schulz and Sanche (1971). This was also discussed in section I.2. However for the study of many molecular resonance processes, the present performance is quite sufficient.

Optimising the spectrometer.

A beam current in the absence of gas can be observed by setting all potentials to the values suggested in II.3 and adjusting the potential of one of the monochromator hemispheres for maximum transmission. The

FIGURE 38. Gun Electrode Transmission Functions.

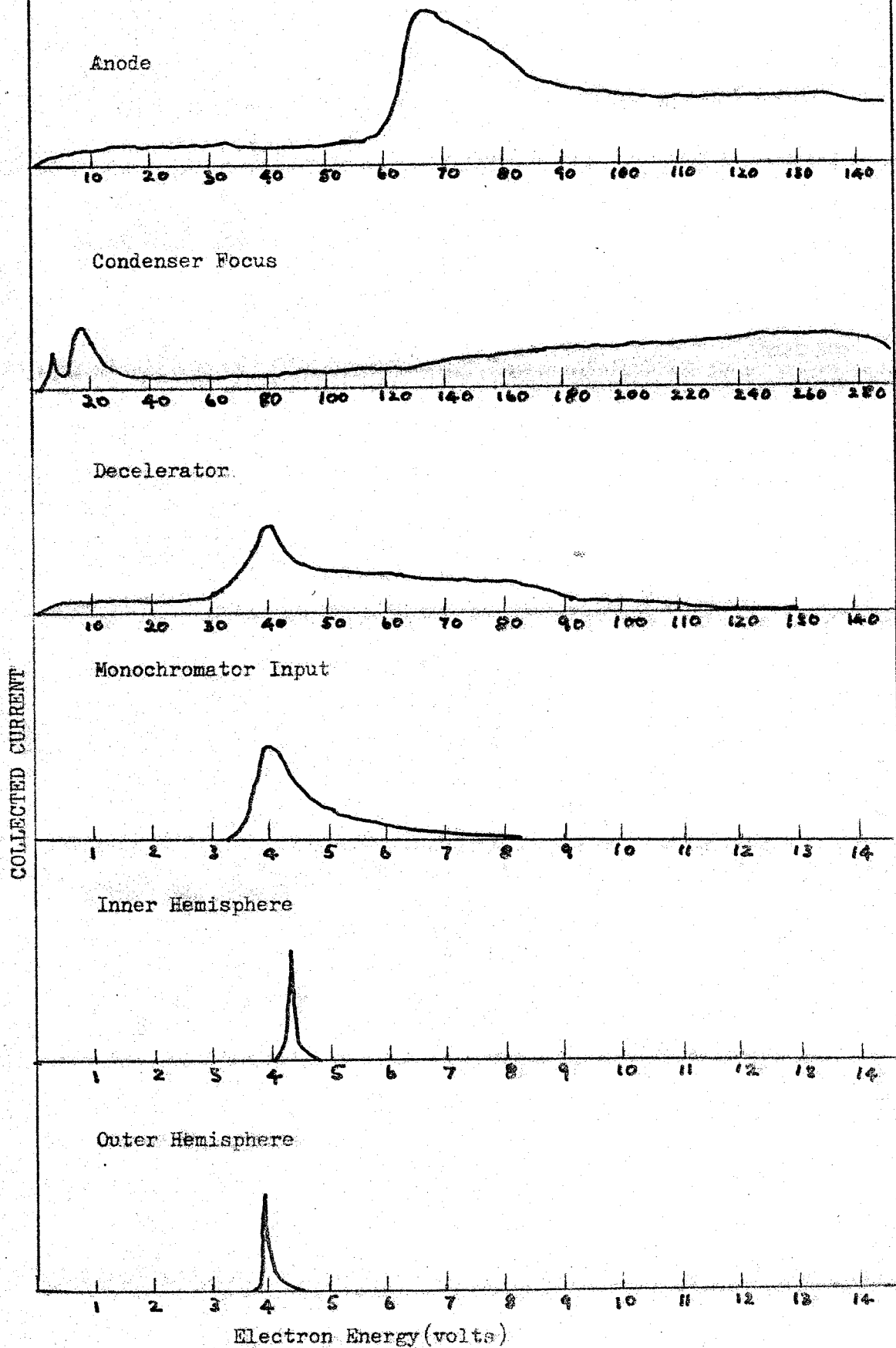
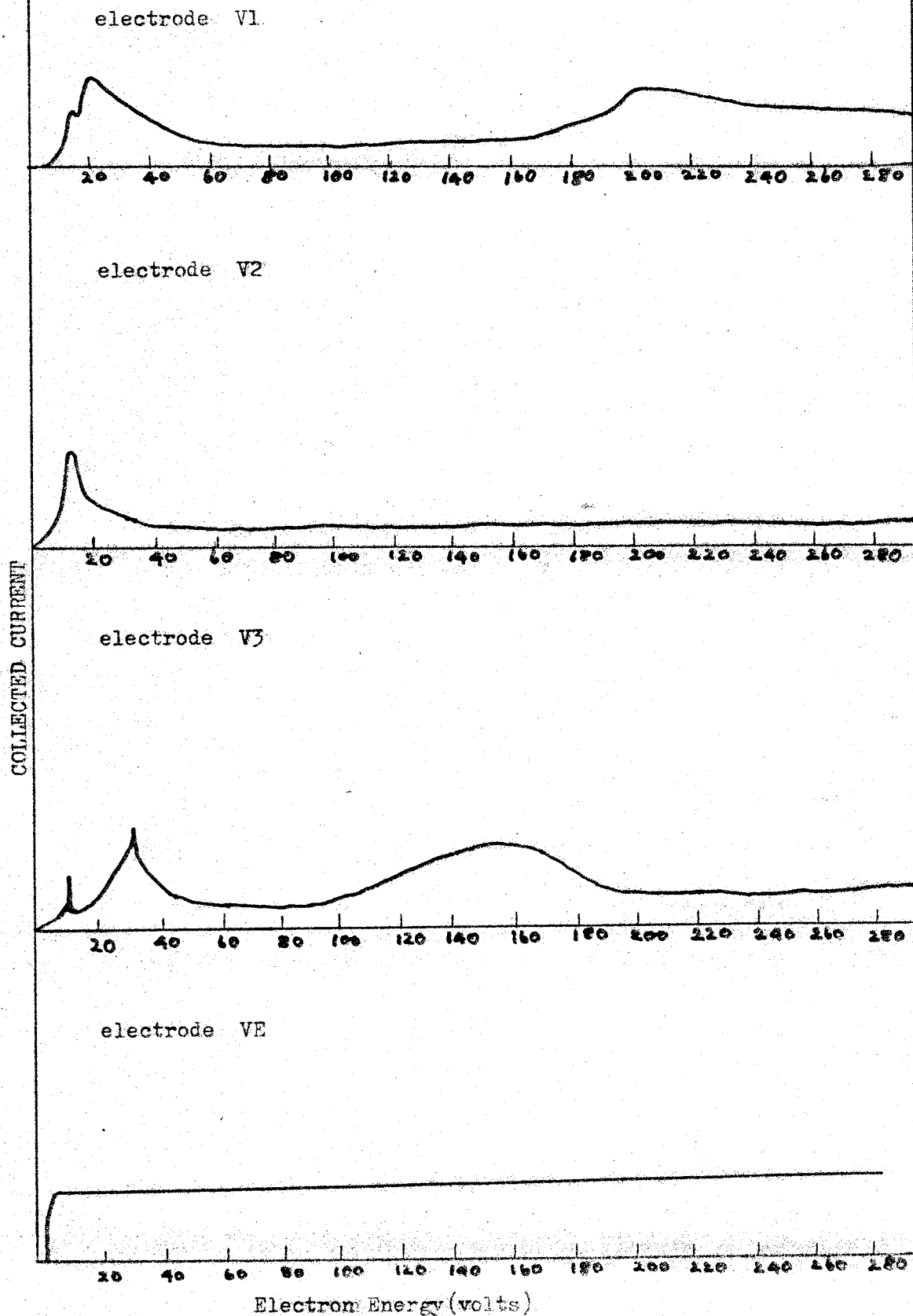


FIGURE 39. Beam Forming Electrode Transmission Functions.



performance of the spectrometer can then be optimised by tuning all potentials, except those of the monochromator for maximum transmission. In practice three of these potentials are more critical than the others. These are the condenser focus voltage in the gun, V_{CF} , the fixed object focus, V_1 , and the energy definition focus, V_3 . These are defined in figures 29, 32, 33. Figure 38 shows the effect on the collected transmitted current of varying the gun voltages and monochromator voltages. Figure 39 is the corresponding diagram for the beam forming output stage. The variation of V_E obviously corresponds to the background transmission function. The preferred technique is to choose V_0 and set +VD and -VD to the calculated potentials. The first stage of the decelerator V_C is then set to $10 V_0$ and the anode to a suitable value, chosen to give the required current. V_{CF} is then tuned for maximum transmission. Figure 38 shows two focussing conditions. We have found that the lower voltage condition is quite satisfactory. Then V_2 is set at a suitable voltage, usually between 6 and 10 volts. This is quite arbitrary as V_1 and V_3 will have focussing conditions for a wide range of values of V_2 . However 6V gives a very good background function. This leaves V_1 and V_3 to control the background function. V_1 is set on its low voltage maximum and V_3 is positioned in the minimum between its two low voltage maxima. The voltage of V_E is then scanned and the background function observed. Minor adjustments to V_3 are required to sharpen the low energy onset. For

FIGURE 41. Logarithm of current versus gas pressure.

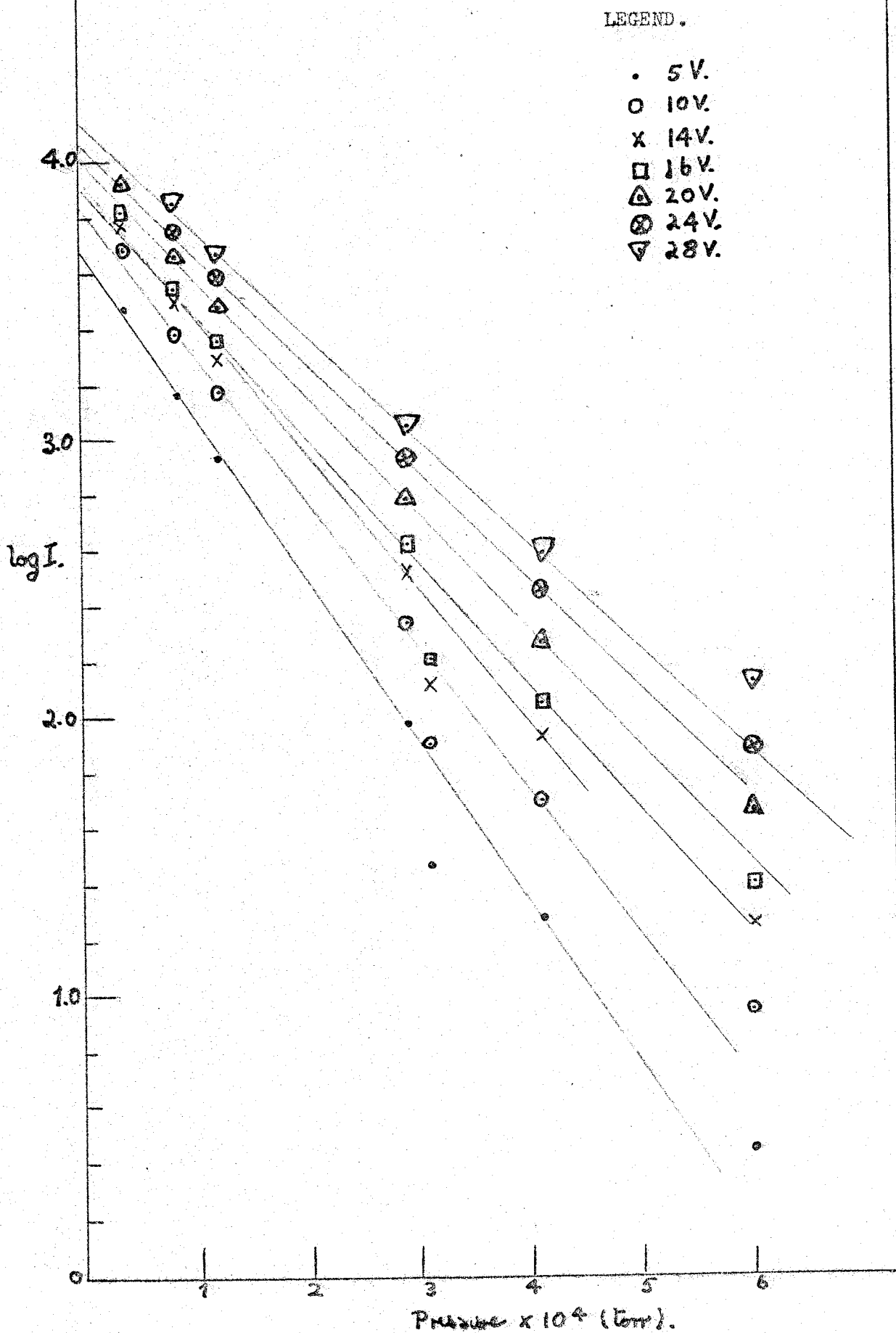
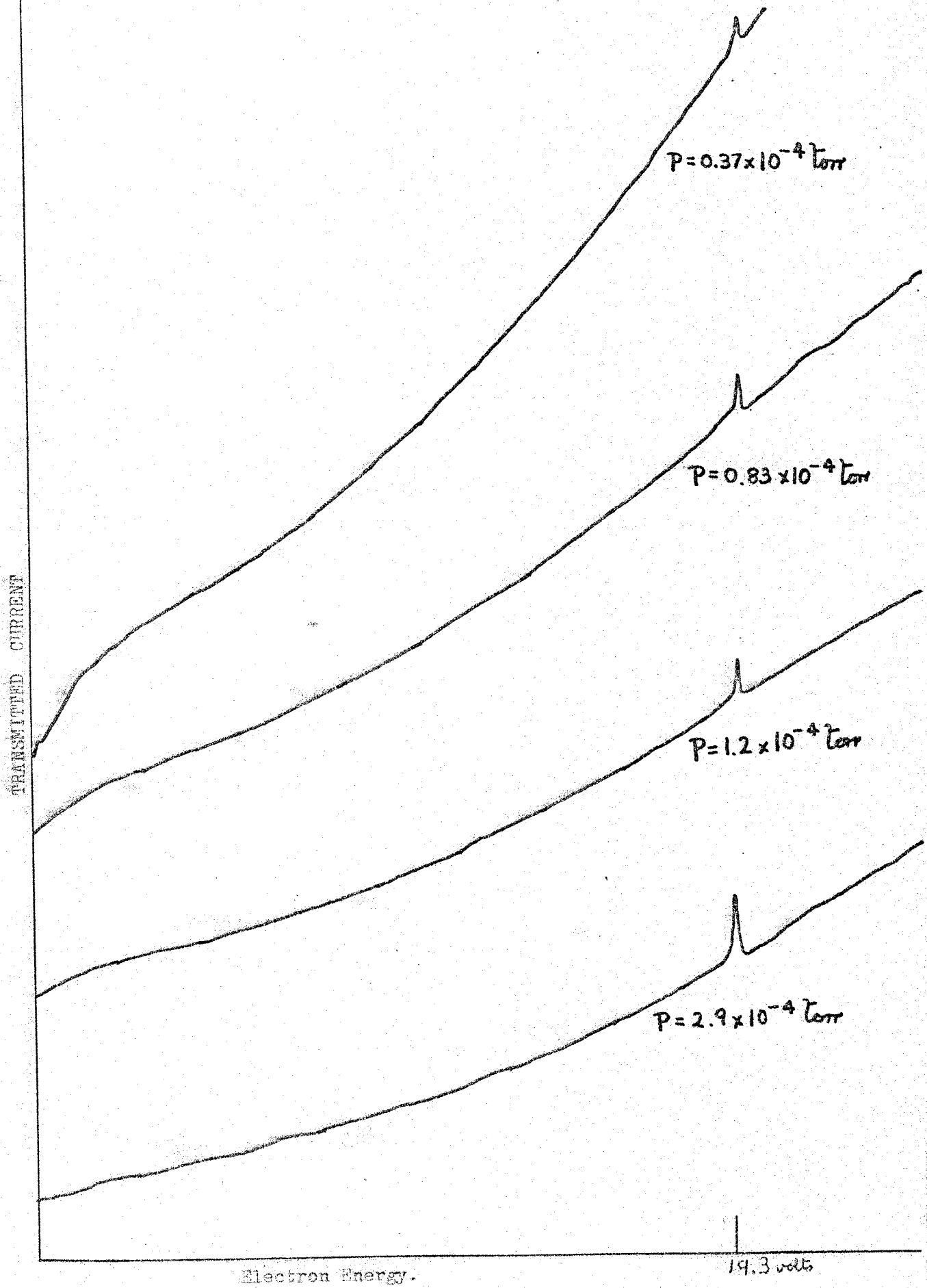


FIGURE 40. Transmission Functions in Helium.



any setting of V_0 and V_2 there will be settings of V_1 and V_3 which will give the characteristic background function of figure 37.

Having set the optical background we then admit gas to the scattering cell, **retuning** the hemispheres for maximum transmission and record the transmitted current as a function of energy at several gas pressures. The current entering the cell I_0 , is monitored on the element of potential V_2 , as discussed in II.4. From the discussion leading to equation (II.1.11) we know that a graph of $\ln(I_0/I)$ versus n should be linear. Where I is the transmitted current and n the gas number density. If I_0 is constant then a graph of $\ln(I)$ versus gas pressure will be sufficient. These graphs are drawn for different electron energies and checked to see if they are in fact linear. If they are, then the total cross-section can be found from the slope.

III.2 The transmission spectrum of helium.

Helium (99.995% minimum purity.B.O.C.) was studied in the energy range 2-30 eV in the manner described in the previous chapter. Figure 40 shows X-Y recorder tracings of the variation of transmitted current with electron energy for various gas pressures. The energy scale is set by using the helium resonance at 19.3eV as a calibration point. Figure 41 shows typical plots of the logarithm of the current versus gas pressure for different electron energies. At higher pressures (6×10^{-4} torr) the point lies off the line. This could be due to multiple scattering effects. The pressures recorded

FIGURE 42. The Total electron-hallium cross-section.

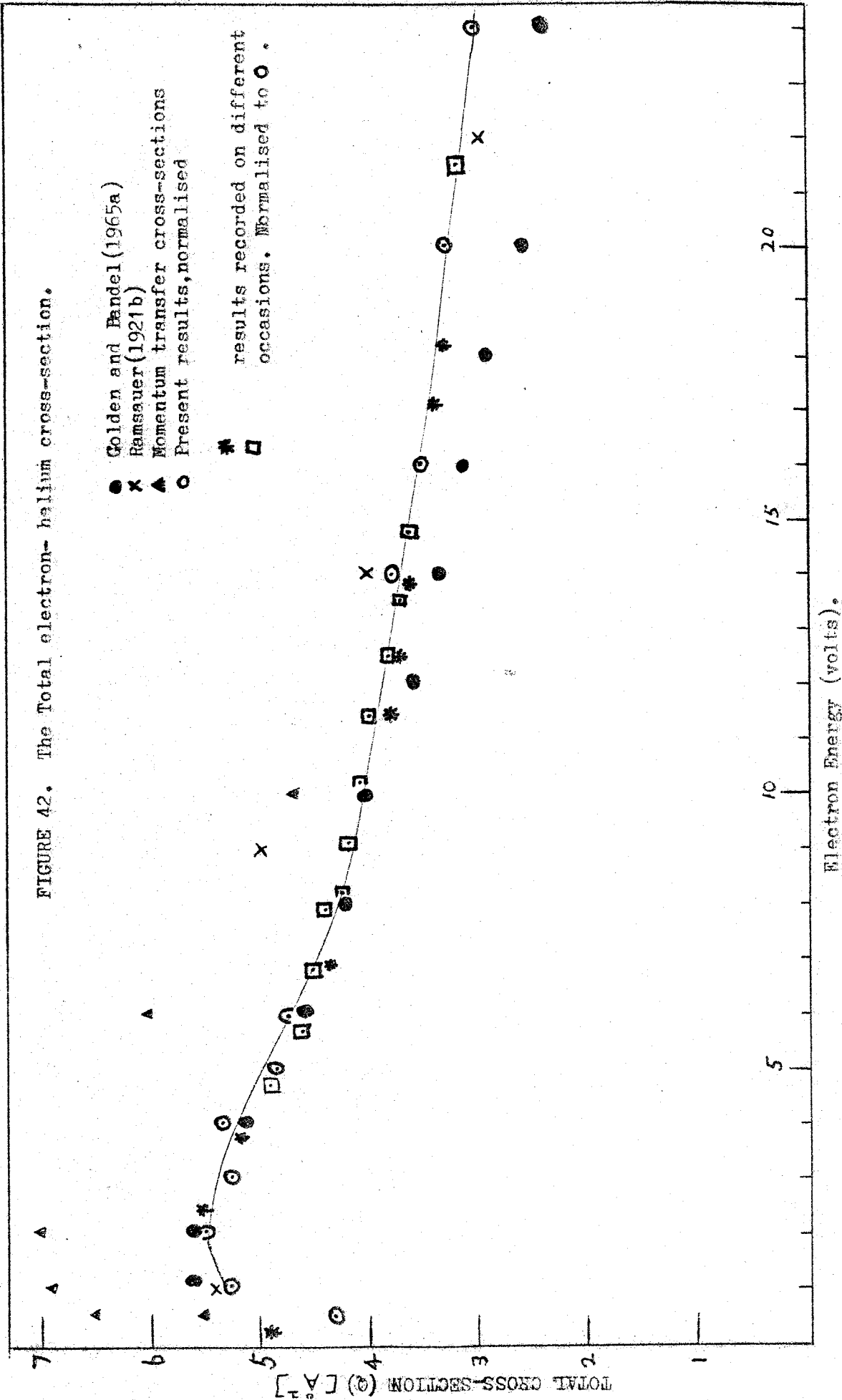
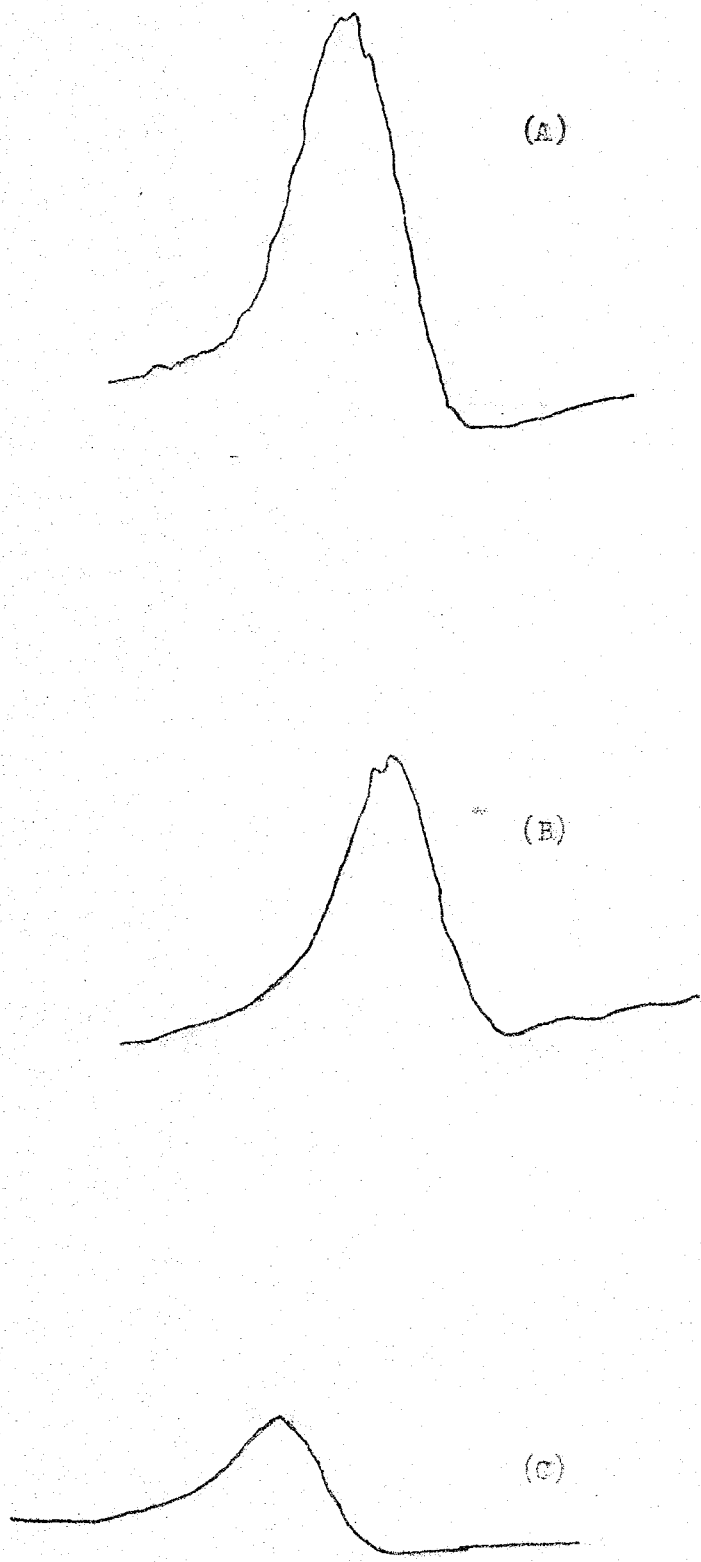


FIGURE 43. The 19.3 eV resonance in helium.

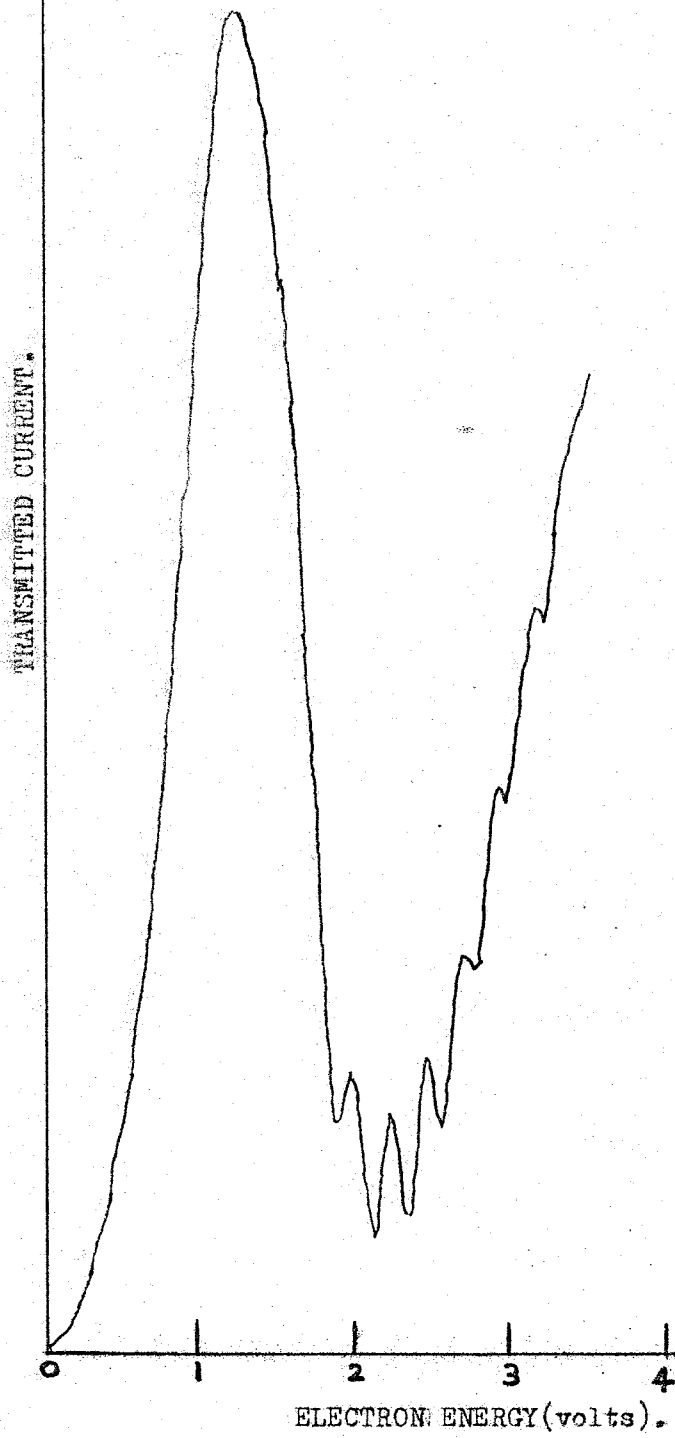
TRANSMITTED CURRENT



ELECTRON ENERGY

here are not the gas cell pressures. They are the vacuum tank pressures, which will be proportional to but considerably less than the gas cell pressures. The points for the pressure 3×10^{-4} torr in this series all lie off the lines and so are regarded as being in error due to some measurement fault. Figure 42 shows total collision cross-sections calculated using data of the type illustrated in figure 41 and normalised to a value of $5.5 \times 10^{-16} \text{ cm}^2$ at 2 eV (Golden and Bandel, 1965a). This curve was compiled from data taken on several different occasions and with the spectrometer tuned to different background functions. Whilst the data are reasonably consistent, normalisation at the low energy end gives cross-sections significantly higher than those of Golden and Bandel at energies above about 10 eV. These discrepancies are discussed more fully in p149-151. Clearly, helium merits further investigation and this we will undertake monitoring the pressure in the collision chamber using a Baratron capacitance manometer. Figure 43 shows the 19.3 eV helium resonance in detail. Monochromator settings, as noted on a digital voltmeter were, 6V (curve A), 4V (curve B) and 3V (curve C). In the presence of helium, contact potentials were about +1.8 eV, so that actual monochromating energies were about 1.8 eV lower than stated above. Allowing for the Doppler broadening of 35 meV at room temperature, we estimate the apparatus energy resolution to be about 40 meV in curve C. In figure 43, 1 cm \equiv 50 meV.

FIGURE 44. The Transmission Function of Nitrogen.



III.3 The transmission spectrum of nitrogen.

In order to assess the instrument behaviour at low incident electron energies, we looked at electron transmission through nitrogen. Figure 44, a recorder trace of the transmission function in nitrogen, illustrates clearly the well-known $2\pi_g N_2^-$ resonance, starting at about 1.8 eV. This resonance appears on a maximum in the total collision cross-section, which accounts for the shape of the function of figure 44. The spacing between minima (cross-section maxima) of figure 44 is 0.25eV. This agrees with spacings obtained by other workers listed in Massey (1969) p. 710.

III.4 Conclusions

The preliminary tests described above indicate that our transmission spectrometer performs in accordance with design specifications. When a suitable gas pressure measuring device is incorporated in the collision region, it should be capable of providing electron-molecule collision cross-sections in a wide range of gaseous molecules. There is a clear need for this kind of data.

Discussion of observed helium total cross-section

The origin of these differences must be some energy-dependent parameter of the apparatuses. The energy-dependent design parameters are angular resolution and incident unattenuated beam current, I_0 , as defined in Section II.1.

The angular resolution of a spectrometer with a static gas target is a complex function of the apparatus geometry in the region of the scattering cell, the detection efficiency of the electron collector and the angular intensity distribution of scattered electrons at a particular energy. This last factor gives us the energy dependence. The angular resolution in the Golden apparatus is not isotropic as it employed rectangular slits, whereas the apparatus described in this thesis has circular symmetry and hence isotropic angular resolution. The purely geometric factor in the angular resolution was discussed by Golden and Bandel (1965) in terms of $f(\theta)$, the fraction of all electrons scattered to the angle θ within the scattering region which are detected. We find that the calculated values of this detection, $f(\theta)$, are very similar to those of Normand (1930) and Brode (1925), which are higher than those of Golden and Bandel (1965) and Ramsauer and Kollath (1929), particularly at small scattering angles. Thus it appears difficult to correlate the differences with the angular resolutions.

The unattenuated beam current, I_0 , which is monitored in the present, experiment and was allowed for in the Ramsauer - Kollath analysis, as described in section I.2, is assumed constant in equation (4) of Golden and Bandel (1965). They discuss several reasons why this assumption is not necessarily valid under all conditions. However Golden and Bandel comment that: "At lower energies it became increasingly difficult to find a combination of accelerating and grid potentials

that would satisfy this condition (ie that F_0 was independent of accelerating voltage) because the range of accelerating voltages over which the Ramsauer signal remains independent of accelerating voltages decreases with decreasing energy."

There are several apparatus factors which could influence the observed total cross-sections. Two important apparatus factors which are energy dependent are the production of secondary electrons in the scattering regions and stray magnetic fields.

Golden does not report any precautions against the production of secondary electrons and no retarding electrodes are included in his apparatus to contain secondary electrons within the collector. In our design we have a suppression voltage of 50 volts between Faraday cup and collector shield and 6 volts between collector shield and a retarding electrode positioned between the gas cell and the collector.

Golden and Bandel (1965) report that some welding on their apparatus was magnetic and that magnetic field measurements were not reproducible to better than 2%. This obviously is a source of error at low energies but as with the other parameters it is impossible to estimate the magnitude of the error.

A theoretical analysis of phase-shifts in electron-helium scattering in the range 3.1 to 19.1eV has been made by Bransden and McDowell (1969), who considered the total cross-section experimental data of Golden and Bandel (1965) and the differential elastic cross-section data of Ramsauer and Kollath (1932) and Gibson and Dolder (1969). Comparing the total collision cross-sections of McDowell, with those of Golden and the present investigation, we find that the energy dependence of the total cross-section is very similar for McDowell and the present work. The change in cross-section between 3eV and 19eV is 50% in the present experiment, 57% for McDowell

and 93% for Golden. Thus it would seem that the present results are in better agreement with the phase-shift analysis than those of Golden. The energy dependence of the discrepancy between the present results and those of Golden depends on the energy at which the present results are normalized.

Additional References

Bransden B.H. and McDowell M.R.C., J. Phys. B 2 (1969), 1187.

Gibson J.R. and Dolder K.T., J. Phys. B. 2 (1969), 1180.

Ramsauer C and Kollath R., Am. Phys. 12 (1932), 529.

References

- Adams, A. and Read, F. H., J. Phys. E. 5 (1972a), 150.
- Adams, A. and Read, F. H., J. Phys. E. 5 (1972b), 156.
- Akesson, N., Lunds. Arsskr N.F. 12 (1916), 29.
- Allred, J. C. and Scollar, I., J. Sci. Instr. 44,
(1967), 755.
- Allis, W. P. and Morse, P. M., Z. Phys. 70 (1931), 567.
- Altshuler, S., Phys. Rev. 107 (1957), 114.
- Baldwin, G. C. and Friedman, S. C., Rev. Sci. Instr.
38 (1967), 519.
- Banford, A. P. "The Transport of charged particle beams".
Spon, London (1966).
- Bardsley, J. N. and Mandl, F., Reports on Progress in
Physics XXXI (1968), 472.
- Becker, A., Ann. der Physik 17 (1905), 381.
- Bederson, B., Perel, J. and Englander, P., Phys. Rev. 128
(1962), 1148.
- Bederson, B., Aberth, W., Sunshine, G., ICPEAC III
(1964), London. p. 53.
- Bederson, B. and Kieffer, L. J., Rev. Mod. Phys. 43
(1971), 601.
- Bernard, M. Y. and Grivet, P., C. R. Acad. Sci. Paris
234 (1952), 606.
- Bernard, M. Y., in "Focussing of charged particles",
Vol I, pp. 3-44, ed. by A. Septier, Academic Press, 1967.
- Bertram, S., Proc. I.R.E. 28 (1940), 418.
- Beuthe, M., Ann. der Physik 84 (1927), 949.
- Boness, M.J.W. and Hasted, J.B., Phys. Lett 21 (1966), 526.
- Boness, M.J.W., Hasted, J.B. and Larkin, I., Proc.
Roy. Soc. 305A (1968) 493.

- Boness, M.J.W. and Schulz, G.J., Phys. Rev. 2 (1970) A2182.
- Brackmann, R. T., Fite, W. L. and Neynaber, R. H.,
Phys. Rev. 112 (1958), 1157.
- Brode, R. B., Phys. Rev. 25 (1925a), 636.
- Brode, R. B., Proc. Roy. Soc. 109 (1925b), 397.
- Brode, R. B. Proc. Roy. Soc. 125 (1929a), 134.
- Brode, R. B., Phys. Rev. 34 (1929b), 673.
- Brode, R. B., Phys. Rev. 35 (1930), 504.
- Brode, R. B., Rev. Mod. Phys. 5 (1933), 257.
- Brose, H. L., Phil. Mag. 50 (1925), 536.
- Brown, S. C., Fundingsland, O. T. and Phelps, A. V.,
Phys. Rev. 84 (1951), 559.
- Brown, S. C., "Basic Data of Plasma Physics", Wiley,
New York (1959).
- Brüche, E., Ann. der Physik 81 (1926), 537.
- Brüche, E., Ann. der Physik 82 (1927a), 25.
- Brüche, E., Ann der Physik 82 (1927b), 912.
- Brüche, E., Ann. der Physik 83 (1927c), 1065.
- Brüche, E., Ann. der Physik 84 (1927d), 279.
- Brüche, E., Ann. der Physik 1 (1929a), 93.
- Brüche, E., Ann. der Physik 2 (1929b), 909.
- Brüche, E., Ann. der Physik 4 (1930a), 387.
- Brüche, E., Ann. der Physik 5 (1930b), 281.
- Buckingham, R. A., Massey, H.S.W., and Tibbs, S.,
Proc. Roy. Soc. A178 (1941) 119.
- Bullis, R. M., Churchill, T. L, W. J. Wiegand and
Schubert, E. K., Vth I.C.P.E.A.C. (1967) Leningrad
(U.S.S.R.), page 263.
- Burhop, E. "Theory of Collisions" in Quantum Theory,
Vol. I, ed. by D. Bates, Academic Press, N.Y. 1961.

- Burrow, P. D. and Schulz, G. J., Phys. Rev. Letters 22 (1969), 1271.
- Coffey, J. M. and Rowlands, G., J. Phys. E 5 (1972), 201.
- Comer, J. and Read, F. H., J. Phys. B. 4 (1971)368.
- Crompton, R. W. and Huxley, L.G.H., in "Atomic and Molecular Processes" (ed. Bates) Academic Press, N.Y. (1962).
- Crompton, R. W., Advan. Electron. Electron Phys. 27 (1969),1
- Cross, J. D., Read, F. H., and Riddle, E. A., J. Sci. Instr. 44 (1967), 993.
- Darrow, K. K., "Electrical Phenomena in Gases". p. 136, Williams and Wilkins, 1932.
- Ehrhardt, H. and Wilman, K., Z. Phys. 204 (1967) 462.
- Ehrhardt, H., Langhans, L. and Linder, F., Z. Phys. 214 (1968), 179.
- Ehrhardt, H., Weingartshofer, A., Hermann, V. and Linder, F., Phys. Rev. 2A (1970), 294.
- Eisner, P. N., 1969 Thesis, New York University.
- El-Kareh, A. B., 10th Symposium of electron, ion and laser beam technology (1969), p. 393.
- El-Kareh, A. B. and El-Kareh, J.C.J., "Electron beams, lenses and optics". Academic Press, London (1970)?
- Epstein, D. W., Proc. I.R.E. 24 (1936), 1005.
- Everhart, E. and Lane, G. H., Phys. Rev. 117 (1960), 920.
- Fano, U. and Cooper, J. W., Phys. Rev. 138A (1965) 400.
- Faxen, H. and Holtsmark, J., Z. Phys. 45 (1927) 307.
- Fermi, E., Nuovo Cimento 11 (1934), 157.
- Firestein, F. and Vine, J., Brit. J. Appl. Phys. 14 (1963),449.

Fisk, J. B., Phys. Rev. 49 (1936), 167.

Fisk, J. B., Phys. Rev. 51 (1937), 25.

Foo, V. Y., Brion, C. E., and Hasted, J. B., Proc. Roy. Soc.
Lond. A322 (1971), 535.

Frost, L. S. and Phelps, A. V., Phys. Rev. 136A (1964), 1538.

Garment, R. and Ross, K. J., J. Phys. E. Scientific Instruments
4 (1971), 707.

Garrett, W. R., Molecular Physics 24 (1971), 465.

Gibson, J. R. and Dolder, K. T., J. Phys. B. 2 (1969), 1180.

Goddard, L. S. , Proc. Camb. Phil. Soc. 42 (1946), 106.

Golant, V. E., Soviet Phys. Tech. Phys. 5 (1961), 1197.

Golden, D. E., Phys. Rev. 151 (1966), 48.

Golden, D. E., Phys. Rev. Letters 27 (1971), 227.

Golden, D. E. and Bandel, H. W., Phys. Rev. 138A (1965a), 14.

Golden, D. E. and Bandel, H. W., Phys. Rev. Letters 14 (1965b)1010.

Golden, D. E. and Bandel, H. W., Phys. Rev. 149 (1966), 58.

Golden, D. E., Bandel, H. W. and Salerno, J. A., Phys. Rev. 146
(1966), 40.

Golden, D. E. and Nakano, H., Phys. Rev. 144 (1966), 71.

Golden, D. E. and Zecca, A., Phys. Rev. A. 1 (1970), 241.

Golden, D. E. and Zecca, A., Rev. Sci. Instr. 42 (1971), 219.

Green, M. C., Phys. Rev. 36 (1930), 239.

Grimm, H. G., Handb. d. Phys. Bd XXIV, S466

Grivet, P., "Electron Optics" Pergamon Press, Oxford, 1965.

Gryzinski, M., Classical Theory of Electronic and Ionic Inelastic
Collisions. Phys. Rev. 115 (1959), 374.

Gryzinski, M., Phys. Rev. 138A (1965a), A305.

Gryzinski, M., Phys. Rev. 138A (1965b), A322.

Gryzinski, M., Phys. Rev. 138A (1965c), A336.

Gryzinski, M., Phys. Rev. Lett 14 (1965d), 1059.

Gryzinski, M., Institute of Nuclear Research, Warsaw, Poland,
Report No. 641/XVIII/PP. July, 1965 (1965e).

Gryzinski, M., Phys. Rev. Lett 24 (1970a), p45.

Gryzinski, M., Institute of Nuclear Research, Warsaw, Poland
Report No. 1217/SLFPG/PP, (1970b).

Gryzinski, M., Electronic and Atomic Collisions VII ICPEAC
p. 907, Amsterdam, July 1971 (1971a)1

Gryzinski, M., Kiraga, A. and Klos, Z., Electronic and Atomic
Collisions VII ICPEAC, p. 910, Amsterdam, July 1971 (1971b).

Hara, S., J. Phys. Soc. Japan 22 (1967) 710.

Hasted, J. B., Boness, M.J.W. and Larkin, I., Proc. Roy. Soc.
305A (1968), 493.

Hasted, J. B. and Awan, A. M., J. Phys. B, 2 (1969), 367.

Hasted, J. B., "Physics of Atomic Collisions", 2nd Ed.
Butterworths, London, (1972).

Heddle, D. W. O., J. Sci. Instr (J. Phys. E.) 2 (1969) 1046.

Heddle, D. W. O., Joint Institute for Laboratory Astrophysics
Report No. 104, October (1970).

Heddle, D. W. O., J. Phys. E. 4 (1971a), 589.

Heddle, D. W. O., J. Phys. E. 4 (1971b), 981.

Heddle, D. W. O. and Kurepa, M. V., J. Phys. E. 3 (1970), 552.

Heidemann, H. G. M., Kuyatt, C. E., and Chamberlain, G. E.,
J.C.P. 44 (1966), 355.

Herzenberg, A., V ICPEAC (1967). Leningrad, p. 264.

Herzog, R., Z. Physik 97 (1935), 596.

Holst, W. and Holtsmark, J., K. norske Vidensk. Selsk. Mus.
Oldsaksaml. Tilv. 4 (1931), 89.

Holtsmark, J., Z. Phys. 66 (1930), 49.

Holtsmark, J., Z. Phys. 55 (1929), 437.

- Imhof, R. E. and Read, F. H., J. Phys. E. 1 (1968), 859.
- Imhof, R. E. and Read, F. H., Chem. Phys. Lett 3 (1969), 652.
- Kennard, E. H., Kinetic Theory of Gases. p. 119,
McGraw-Hill, New York (1938).
- Klemperer, O. and Wright, W. D., Proc. Phys. Soc. B51
(1939), 296.
- Klemperer, O., "Electron Optics", 2nd Edition, Cambridge, 1953.
- Klemperer, O. and Barnett, M. E., "Electron Optics",
3rd Edition, Cambridge, 1971.
- Kollath, R., Physikalische Zeitschrift 31 (1930), 985.
- Kuyatt, C. E., Simpson, J. A. and Mielczarek, S. R.,
Phys. Rev. 138 (1965), A385.
- Kuyatt, C. E. and Simpson, J. A., Unpublished E.O. Notes (1967).
- Kuyatt, C. E., Methods of Experimental Physics vol 7.
Atomic Interactions part A (1968).
- Kuyatt, C. E., Natali, S., and DiChio, D., Journal of
Research N.B.S., 76A (1972a), 27.
- Kuyatt, C. E., Natali, S. and DiChio, D., and Uva, E.,
Rev. Sci. Instr. 43 (1972b), 80.
- Kuyatt, C. E., Natali, S., DiChio, D., Rev. Sci. Instr.
43 (1972c), 84.
- Lenard, P., Ann. de Physik. 56 (1895), 274.
- Lenard, P. Ann. De Physik 12 (1903), 714.
- Larkin, I. W. and Hasted, J. B., Chem. Phys. Lett. 5
(1970), 325.
- Larkin, I. W. and Hasted, J. B., J. Phys. B 5 (1972), 95.
- Margenau, H., Phil. Science 8, (1941), 603.
- Massey, H. S. W., "Theory of Atomic Collisions" in Handbuch
der Physik, Vol XXXVI, Springer-Verlag, Berlin, 1956.
- Massey, H. S. W. and Ridley, R. O., Proc. Phys. Soc.
A69 (1956), 659.

- Massey, H. S. W. and Burhop, E. H. S., *Electronic and Ionic Impact Phenomena*, Vol. I., Oxford, 1969.
- Massey, H. S. W., *Electronic and Ionic Impact Phenomena*, Vol. II, Oxford, 1969.
- Mayer, H. F., *Ann. der Physik* 64 (1921), 451.
- McDaniel, E. W., "Collision Phenomena in Ionised Gases"
J. Wiley and Sons, New York, 1964.
- Morse, P. M., *Rev. Mod. Phys.* 4 (1932), 577.
- Mott, N. and Massey, H. S. W., "Theory of Atomic Collisions", Oxford, 1965.
- Nagahara, S., *J. Phys. Soc. Japan* 9 (1954), 52.
- Neynaber, R. H., Marino, L. L., Rothe, E. W. and Trujillo, S. M., *Phys. Rev.* 123 (1961), 148.
- Normand, C. E., *Phys. Rev.* 35 (1930), 1217.
- O'Malley, T. F., Spruch, L. and Rosenberg, L., *Phys. Rev. Lett.* 5 (1960), 347.
- O'Malley, T. F., Spruch, L. and Rosenberg, L., *J. Math. Physics* 2 (1961), 491.
- O'Malley, T. F., Spruch, L. and rosenberg, L., *Phys. Rev.* 125 (1962), 1300.
- O'Malley, T. F., *Phys. Rev.* 130 (1963), 1020.
- Palmer, R. R., *Phys. Rev.* 37 (1931), 70.
- Parker, J. H. and Warren, R. W., *Rev. Sci. Instr.* 33 (1962), 948.
- Paszkowski, B. "Electron Optics", Iliffe, London, 1968.
- Phelps, A. V., *Rev. Mod. Phys.* 40 (1968), 399.
- Pierce, J. R., "Theory and Design of electron beams"
Van Nostrand, 1954.
- Purcell, E. M., *Phys. Rev.* 54A (1938), 818.

- Ramberg, E. G., J. Appl. Phys. 93 (1942), 582.
- Ramsauer, C., Ann. der Physik 45 (1914), 1000.
- Ramsauer, C., Ann. der Physik 64 (1921a), 513.
- Ramsauer, C., Ann. der Physik 66 (1921b), 545.
- Ramsauer, C., Ann. der Physik 72 (1923), 345.
- Ramsauer, C. Ann. der Physik 83 (1927), 1129.
- Ramsauer, C. and Kollath, R., Ann. der Physik 73 (1929), 536.
- Ramsauer, C. and Kollath, R., Ann. der Physik 4 (1930), 91.
- Read, F. H., J. Sci. Instr. (J. Phys. E.) 2, (1969a), 165.
- Read, F. H., J. Phys. E. 2 (1969b), 679.
- Read, F. H., J. Phys. E. 3 (1970), 127.
- Read, F. H., J. Computational Physics 6 (1970), 527.
- Read, F. H., J. Phys. E. 4 (1971), 562.
- Read, F. H., Adams, A. and Soto-Montiel, J. R., J. Phys. E.
4 (1971), 625.
- Rudd, M. E., in "Low Energy Electron Spectrometry" by
K. D. Sevier, Wiley (1972).
- Rusch, M., Physik Zeitscher 26 (1925), 748.
- Rusch, M., Ann. der Physik, 80 (1926), 707.
- Salop, A. and Nakano, H. H., Phys. Rev. 2A (1970), 127.
- Sanche, L. and Schulz, G. J., Phys. Rev. A 5 (1972a), 1672.
- Sanche, L. and Schulz, G. J., Phys. Rev. 6 (1972b), 69.
- Schiff, L. I., "Quantum Mechanics", 2nd Edition,
McGraw-Hill, 1955.
- Schmeider-Oppau, F., Z. Elektrokern 36 (1930), 700.
- Schulz, G. J. and Phelps, A. V., Rev. Sci. Instr. 28
(1957), 1051.
- Schulz, G. J., Third International Conference on Physics of
Atomic and Electronic Collisions, London, July 1963,
p. 124.

- Schulz, G. J., Phys. Rev. 135 (1964), A988.
- Schulz, G. J., Phys. Rev. 136 (1964), 650.
- Schulz, G. J. and Sanche, L., Phys. Rev. Lett. 26,
(1971), 943.
- Silbermann, L, Heidelberg Disc., 1910.
- Simpson, J. A., Atomic Collision Processes, London (1963),
p.128.
- Simpson, J. A. and Mielczarek, S. R., Bull. Am. Phys.
Soc. 9 (1964), 89.
- Simpson, J. A., Kuyatt, C. E. and Mielczarek, S. R.,
Phys. Rev. Lett 12 (1964), 293.
- Simpson, J. A., Kuyatt, C. E. and Mielczarek, S. R.
J.C.P. 44 (1966), 437.
- Simpson, J. A. and Kuyatt, C. E., Rev. Sci. Instr. 38
(1967), 103.
- Skinker, M. F., Phil. Mag, 44 (1922), 994.
- Skinker, M. R. and White, J. V., Phil. Mag. 46 (1923), 630.
- Spangenberg, K., and Field, L. M., Elec. Commun. 20,
(1942), 305.
- Spangenberg, K. and Field, L. M., Elec. Commun. 21
(1943), 194.
- Spangenberg, K., "Vacuum Tubes", McGraw-Hill, 1948.
- Stamatovic, A. and Schulz, G. J., Rev. Sci. Instr.,
39 (1968), 1752.
- Stier, H. C., Z. Phys. 76 (1932), 439.
- Sunshine, G., Aubrey, B. B. and Bederson, B., Phys.
Rev. 154 (1967), 1.
- Takayanagi, K and Itikawa, Y., J. Phys. Soc. Japan 24,
(1968) 160.

Townsend, J. S. and Bailey, V. A., Phil. Mag. 42 (1921), 873.

Townsend, J. S. and Bailey, V. A., Phil. Mag. 43 (1922), 593.

Townsend, J. S. and Bailey, V. A. Phil. Mag. 46 (1923), 657.

Trajmar S., Rice, J. K. and Kupperman, A., NASA
Technical Memorandum 33-373 (March, 1968), Jet
Propulsion Laboratory, Pasadena, California.

Verster, J. L., Phillips Research Reports 18 (1963), 465.

Weiss, A. W. and Krauss, M., J. C. P. 52 (1970), 4363.

Wei, P. S. P., Bell Telephone Laboratories Memorandum
38140-15 (1969).

Zworykin, V. K., Morton, G. A., Ramberg, E. G., Hillier, J.
and Vance, A. W., "Electron Optics and the Electron
Microscope", 1945.

ACKNOWLEDGEMENTS

I wish to record my gratitude to Dr. Isobel Walker for initiating and supervising this research, and for her continual advice and encouragement; and to Mr. Don Dance for his experienced assistance and advice in many stages of this work. I also wish to thank Mr. V. Raible and other members of the experimental and theoretical Physics departments for useful discussions; Messrs. Brian Povey and Bill Stirling for their technical advice and cooperation and the staff of Shared Technical Services of the University of Stirling, in particular Messrs. John Dyer, William Grant, Campbell Chesterman and Roy Scott. Finally, I record my appreciation to Professors R. P. Bell and W. Parker for financial support and laboratory facilities and the Science Research Council for a maintenance grant.

Hamish Porter